



HAL
open science

Mediterranean tephrostratigraphy and peri-Tyrrhenian explosive activity revaluated in light of the 430-365 ka record from Fucino Basin (central Italy)

Lorenzo Monaco, Danilo Palladino, Mario Gaeta, Fabrizio Marra, Gianluca Sottili, Niklas Leicher, Giorgio Mannella, Sébastien Nomade, Alison Pereira, Eleonora Regattieri, et al.

► To cite this version:

Lorenzo Monaco, Danilo Palladino, Mario Gaeta, Fabrizio Marra, Gianluca Sottili, et al.. Mediterranean tephrostratigraphy and peri-Tyrrhenian explosive activity revaluated in light of the 430-365 ka record from Fucino Basin (central Italy). *Earth-Science Reviews*, 2021, 220, pp.103706. <10.1016/j.earscirev.2021.103706>. <hal-03265320>

HAL Id: hal-03265320

<https://hal.science/hal-03265320v1>

Submitted on 7 Jun 2023

HAL is a multi-disciplinary open access archive for the deposit and dissemination of scientific research documents, whether they are published or not. The documents may come from teaching and research institutions in France or abroad, or from public or private research centers.

L'archive ouverte pluridisciplinaire HAL, est destinée au dépôt et à la diffusion de documents scientifiques de niveau recherche, publiés ou non, émanant des établissements d'enseignement et de recherche français ou étrangers, des laboratoires publics ou privés.



HAL Authorization

Mediterranean tephrostratigraphy and peri-Tyrrhenian explosive activity reevaluated in light of the 430-365 ka record from Fucino Basin (central Italy)

Lorenzo Monaco^a, Danilo M. Palladino^a, Mario Gaeta^a, Fabrizio Marra^b, Gianluca Sottili^a, Niklas Leicher^c, Giorgio Mannella^d, Sébastien Nomade^e, Alison Pereira^f, Eleonora Regattieri^g, Bernd Wagner^c, Giovanni Zanchetta^{d,b,i}, Paul G. Albert^h, Ilenia Arienzoⁱ, Massimo D'Antonio^j, Paola Petrosino^j, Christina J. Manning^k, Biagio Giaccio^{l-b,*}

a Dipartimento di Scienze della Terra, Sapienza-Università di Roma, Rome, Italy

b Istituto Nazionale di Geofisica e Vulcanologia, Rome, Italy

c Institute of Geology and Mineralogy, University of Cologne, Cologne, Germany

d Dipartimento di Scienze della Terra, University of Pisa, Pisa, Italy

e Laboratoire de Sciences du Climat et de l'Environnement, UMR 8212, CEA-UVSQ, IPSL and Université de Paris-Saclay, Gif-sur-Yvette, France

f Université Paris-Saclay, CNRS, UMR 8148 GEOPS, Orsay, 91405, France

g Istituto di Geoscienze e Georisorse, IGG-CNR, Pisa, Italy

h Department of Geography, Swansea University, Swansea, UK

i Istituto Nazionale di Geofisica e Vulcanologia, Osservatorio Vesuviano, Naples, Italy

j Dipartimento di Scienze della Terra, dell'Ambiente e delle Risorse, Università degli Studi di Napoli Federico II, Naples, Italy

k Department of Earth Sciences, Royal Holloway, University of London, Egham, Surrey, UK

l Istituto di Geologia Ambientale e Geoingegneria, IGAG-CNR, Rome, Italy

** Corresponding author: biagio.giaccio@cnr.it*

ABSTRACT

Accurately reconstructing the scale and timing of dynamic processes, such as Middle-Late Pleistocene explosive volcanism and rapid climatic change, requires rigorous and independent chronological constraints. In this framework, the study of distal volcanic ash layers, or tephra, transported and deposited over wide regions during explosive volcanic eruptions, is increasingly being recognised as a fundamental chronostratigraphic tool for addressing these challenging issues. Here we present a high-resolution distal tephra record preserved in the lacustrine sedimentary succession of the Fucino Basin, central Italy. The investigated record spans the 430-365 ka time interval, covering the entirety of Marine Isotope Stage 11 (MIS 11), and provides important insights into peri-Tyrrhenian potassic explosive volcanism from sources located in central Italy against a backdrop of Mediterranean palaeoclimate records. The succession of ash fall events of this time interval is reconstructed through a detailed lithostratigraphic, geochemical and ⁴⁰Ar/³⁹Ar geochronological characterization of the deposits preserved as discrete layers in the Fucino F4-F5 sediment core. This work is complemented by similarly detailed characterization of selected proximal pyroclastic units from the peri-Tyrrhenian potassic volcanoes. Geochemical fingerprinting of the tephra deposits by means of their major, minor and trace elements and Sr isotope compositions indicates that all the thirty-two investigated ash layers derived from the peri-Tyrrhenian potassic volcanoes. The stratigraphically continuous succession of the Fucino tephra layers allowed the development of a fully independent, ⁴⁰Ar/³⁹Ar age-constrained, Bayesian age-depth model for the investigated time interval. The age-model allows us to establish modelled ages for the tephra layers within the succession that are not directly dated. The resulting dated tephra record clearly reveals a highly time resolved and previously unparalleled chronicle of explosive activity from the Vulcini, Vico, Sabatini, Colli Albani and Roccamonfina volcanic complexes. Our study provides a benchmark and valuable geochemical and geochronological dataset to be used as a reference for any future development and application of the tephrostratigraphic methods across the central Mediterranean area both during the investigated 430-365 kyr time interval, and deeper in time. This contribution underlines the importance of

50 integrating proximal and distal sedimentary records to more accurately establish long-term and comprehensive
51 volcanic eruption records.

52

53 1. Introduction

54 Reconstructing the history of explosive volcanism, including the dynamics, timing, and recurrence intervals of
55 eruptions, is a fundamental requirement for understanding the temporal evolution of the volcanic systems and
56 for assessing the related hazards (e.g., [Gehrels et al., 2006](#)). The required stratigraphic, chronological and
57 volcanological data are commonly acquired in near-vent (proximal) volcanic areas, where the geological record
58 provides key data for evaluating eruptive and emplacement dynamics, as well as the evolution of the volcanic
59 edifices. Furthermore, the presence of coarse-grained K-rich crystals in proximal deposits from volcanoes fed
60 by highly potassic evolved magmas enables direct and precise radiometric dating using the $^{40}\text{Ar}/^{39}\text{Ar}$
61 technique. However, due to the intense volcano-tectonic and sedimentary processes occurring in near-source
62 volcanic regions, many proximal deposits are often buried, inaccessible, or partially eroded. In contrast,
63 intermediate and distal archives, usually located downwind with respect to volcanic sources, can offer a more
64 continuous record of volcanic ash layers (or “tephra”) derived from sustained columns and co-ignimbrite ash
65 clouds, thus enabling the reconstruction of the eruptive history and dynamics of individual volcanic systems
66 and regions (e.g., [Paterne et al., 1986, 1988](#); [Newnham et al., 1999](#); [de Fontaine et al., 2007](#); [Dugmore et al.,](#)
67 [2013](#); [Giaccio et al., 2014](#); [Leicher et al., 2016, 2019](#); [Albert et al., 2018, 2019](#); [Larsen et al., 2020](#); [Wulf et al.,](#)
68 [2020](#)).

69 The relevance of tephrostratigraphy extends beyond volcanological applications, as these instantaneously
70 deposited layers are also outstanding chronological, stratigraphic and correlation tools for addressing
71 numerous issues in Quaternary sciences (e.g., [Lowe et al., 2011](#)). Through diagnostic geochemical,
72 stratigraphic, and chronological features, the volcanic ash, widely dispersed during explosive eruptions and
73 deposited on regional to global scale ([Ponomareva et al., 2015](#)), can be recognized and correlated to eruptive
74 events or distal tephra of known ages. This provides an effective and reliable way through which sedimentary
75 archives with co-located tephra can be accurately and precisely dated and correlated over wide regions.
76 Indeed, when combined with high-precision and accurate radiometric $^{40}\text{Ar}/^{39}\text{Ar}$ dating and detailed multiproxy
77 series, long and continuous distal tephra successions become the cornerstones for reconstructing both the
78 paleoclimatic change and the history of explosive volcanism (e.g., [Thorarinson, 1981a, b](#); [Paterne, 1986, 1988](#);
79 [Dugmore, 1989](#); [Narcisi and Vezzoli, 1999](#); [Wastergard, 2002](#); [Wulf et al., 2004, 2008, 2012](#); [Lane et al., 2013](#);
80 [Giaccio et al., 2015a](#); [Kousis et al., 2018](#); [Leicher et al., 2019](#); [Mannella et al., 2019](#); [Regattieri et al., 2019](#)).

81 Tephrostratigraphy is most successfully applied when long and continuous sedimentary successions
82 containing well-preserved tephra layers are in a suitable range of distances from sources of recurrent explosive
83 activity. These requirements are fulfilled in the Mediterranean area, particularly in central-southern Italy.
84 Indeed, the recurrent and continuous explosive activity of the peri-Tyrrhenian volcanism, fed by potassic to
85 ultrapotassic magmas (e.g., [Peccerillo, 2017](#)), as well as the presence of numerous Quaternary tectonic basins
86 hosting thick sedimentary successions, constitute a unique combination which has allowed the retrieval of
87 extremely rich tephra repositories and, consequently, eruption event stratigraphies. An increasing number of
88 studies on marine ([Keller et al., 1978](#); [Paterne et al., 2008](#); [Bourne et al., 2010, 2015](#); [Tamburrino et al., 2012](#);
89 [Insigna et al., 2014](#); [Morabito et al., 2014](#); [Matthews et al., 2015](#); [Petrosino et al., 2015, 2016](#); [D’Antonio et al.,](#)
90 [2016](#)), lacustrine ([Wulf et al., 2004, 2008](#); [Petrosino et al., 2014a](#); [Giaccio et al., 2015a](#); [Di Roberto et al., 2018](#);

91 [Leicher et al., 2019](#); [Regattieri et al., 2019](#)) and sub-aerial ([Giaccio et al., 2012a](#); [Gatta et al., 2016](#); [Donato et](#)
92 [al., 2016](#); [Zanchetta et al., 2018](#); [Bini et al., 2020](#)) sedimentary environments of the Mediterranean region have
93 documented this potential. However, despite these recent advances, the tephrostratigraphic framework of the
94 central Mediterranean area is still fragmentary and unexplored, especially for the Middle Pleistocene (~780-
95 130 ka).
96

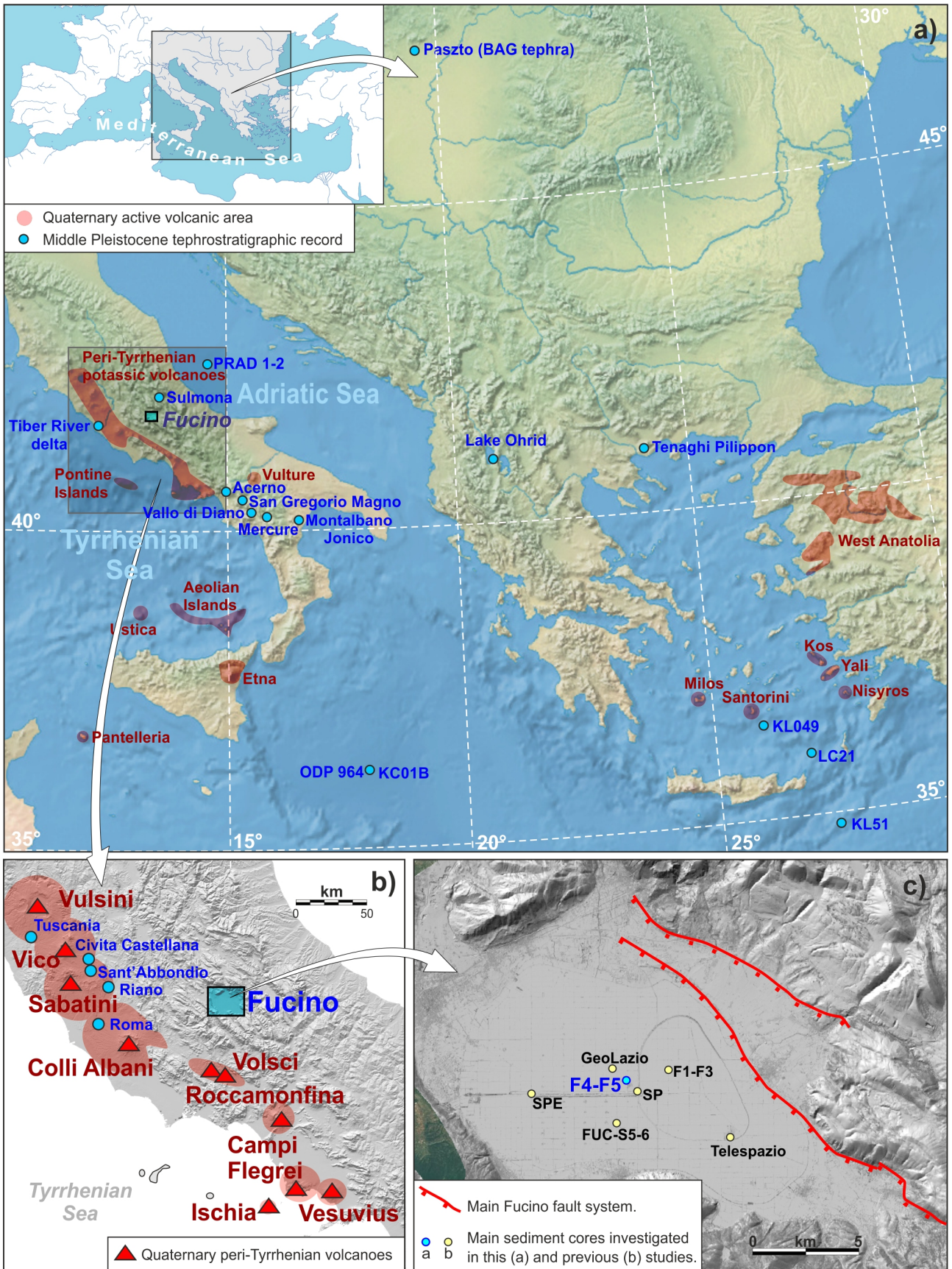


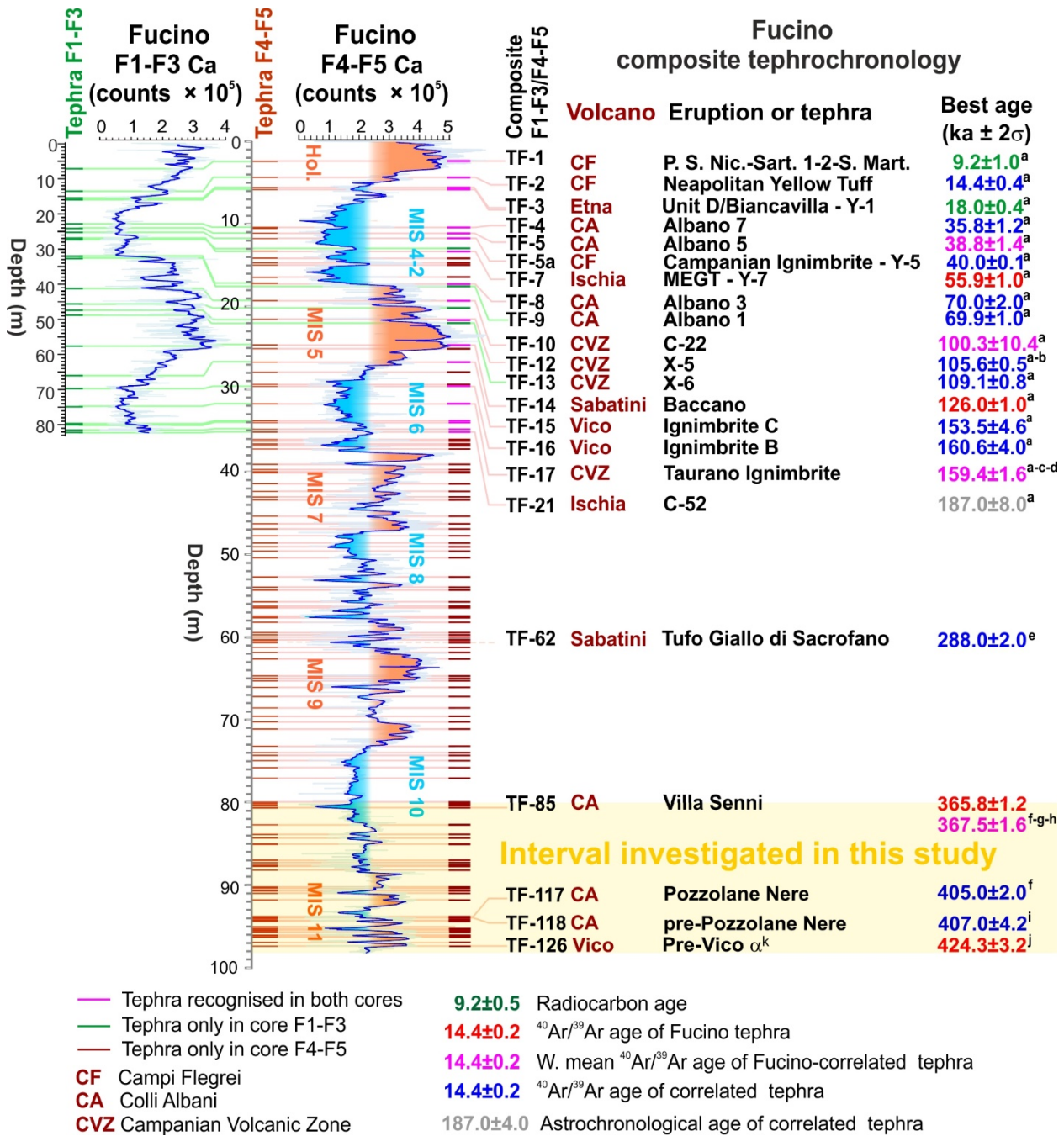
Figure 1. Reference maps. **a)** The Fucino Basin and the peri-Tyrrhenian potassic volcanoes in the context of the Mediterranean Quaternary volcanism and the Middle Pleistocene tephrostratigraphic records (blue dots) cited in the text. **b)** Magnification of the area highlighted in **a)** showing in detail the location of Fucino Basin relative to the peri-Tyrrhenian potassic volcanic systems of central-southern Italy. **c)** DEM map of Fucino Basin highlighting the location of the F4-F5 core, along with other cores from this lacustrine basin.

97
98
99
100
101
102

103 Among the lacustrine successions hosted in the Pliocene-Quaternary inter-mountain tectonic basins of the
104 central-southern Apennines (Italy), Fucino's is the most continuous and temporally resolved, with ~900 m of
105 seemingly uninterrupted sedimentary infill, documenting the sediment accumulation since the Lower
106 Pleistocene up to historical times (Cavinato et al., 2002; Giaccio et al., 2015b) and a rich tephra record (Giaccio
107 et al., 2017, 2019; Di Roberto et al., 2018; Mannella et al., 2019; Del Carlo et al., 2020). Three factors make
108 the Fucino Basin unique for reconstructing the eruptive history of the Italian peri-Tyrrhenian potassic to ultra-
109 potassic volcanic activity and improving the central Mediterranean Middle Pleistocene tephrostratigraphic
110 framework: (i) its relatively short distance from the peri-Tyrrhenian volcanoes of central Italy (~70 to ~150 km,
111 Fig. 1a); (ii) its downwind location with respect to these volcanoes, i.e., along the preferential ash dispersal
112 axes (Fig. 1b); (iii) the occurrence of tephra with K-rich minerals, which facilitates the laser fusion single crystals
113 $^{40}\text{Ar}/^{39}\text{Ar}$ dating approach.

114 Recently, Giaccio et al. (2019) reported the presence of ~130 volcanic ash layers in a composite ~98 m-long
115 sediment core (F4-F5) from Fucino Basin spanning the last 430 kyr (Fig. 2) confirming the great potential of
116 this succession to become one of the cornerstones in the tephrostratigraphic network of the entire
117 Mediterranean region. However, so far less than a quarter of these ~130 tephra layers have been
118 stratigraphically, geochemically, and chronologically characterized (Giaccio et al., 2017, 2019). In this paper,
119 we present detailed lithostratigraphic, geochemical and chronological data for the lowermost 28 tephra layers
120 from the F4-F5 core, along with proximal deposits from 5 selected volcanic units of the peri-Tyrrhenian
121 volcanoes, all constrained within the Marine Isotope Stage (MIS) 11 period (i.e., ~430-365 ka). The MIS 11
122 period is particularly important both in terms of volcanological and tephrochronological investigations. Indeed,
123 it marks the onset of activity at Vico volcano (e.g., Perini et al., 2004; Pereira et al., 2020), thus adding a further
124 volcanic source to the already rich central Mediterranean Middle Pleistocene tephrostratigraphic framework
125 (Fig. 3). Furthermore, currently only very few tephrostratigraphic records spanning the MIS 11 period in the
126 Mediterranean region have been investigated (Leicher et al., 2019; Vakhrameeva et al., 2018, 2021; Fig. 1a).
127 The results of this study are discussed in the general context of the Middle Pleistocene Mediterranean
128 tephrostratigraphy and that of the central Italy peri-Tyrrhenian explosive volcanism, providing a major
129 contribution towards improved framework of the regional to extra-regional tephrochronology and of the
130 explosive volcanism history. They also provide the basis for developing a robust and independent age-model
131 for the multi-proxy paleoclimate information of the Fucino succession during MIS 11, a key period in the Late
132 Quaternary climatic history, whose analogies with the Holocene have long been debated (e.g., McManus et
133 al., 2003; Tzedakis, 2010).

134



135
136
137
138
139
140
141
142
143
144
145
146
147
148
149
150
151
Figure 2. Stratigraphic interval of the F4-F5 Fucino Basin sediment core investigated in this study (modified from [Giaccio et al., 2019](#)). ⁴⁰Ar/³⁹Ar ages are recalculated relatively to an age of 1.1891 Ma for the Alder Creek sanidine monitor standard ([Niespolo et al., 2017](#)), with the uncertainty expressed at 2σ. ⁴⁰Ar/³⁹Ar ages data source: ^a [Mannella et al. \(2019 and references therein\)](#); ^b [Petrosino et al. \(2016\)](#); ^c [Amato et al. \(2018\)](#); ^d [De Vivo et al. \(2001\)](#); ^e [Sottili et al. \(2010\)](#); ^f [Marra et al. \(2009\)](#); ^g [Marra et al. \(2019\)](#); ^h [Giaccio et al. \(2012a, 2012b\)](#); ⁱ [Pereira et al. \(2018\)](#); ^j [Giaccio et al. \(2019\)](#).

2. Geological and volcanological setting

2.1. The Fucino Basin

The Fucino Basin (42° 00' 00" N; 013° 30' 00" E) is one of the larger inter-Apennine tectonic basins that developed during the extensional phase related to the geodynamic evolution of the Tyrrhenian Basin and central-southern Apennine chain (e.g., [Doglioni et al., 1996](#)). Extensional tectonics, mainly acting along E-W, NE-SW and NW-SE oriented high-angle faults, caused the stretching of the mountain chain (e.g., [D'Agostino et al., 2001](#)). The opening and evolution of these intermountain basins started from the Late Pliocene-Lower

152 Pleistocene period (Galadini and Galli, 2000; Boncio et al., 2004; Giaccio et al., 2012a; Amato et al., 2014).
153 The Plio-Quaternary tectonic and sedimentary evolution of the Fucino Basin was driven by the *Fucino Fault*
154 *System* (FFS, Galadini and Galli, 2000; Fig. 1c), which depicts a semi-graben architecture with a thickness of
155 the Plio-Quaternary sedimentary infilling increasing up to ~900 m from west to east toward the depocenter
156 (Cavinato et al., 2002; Patacca et al., 2008).

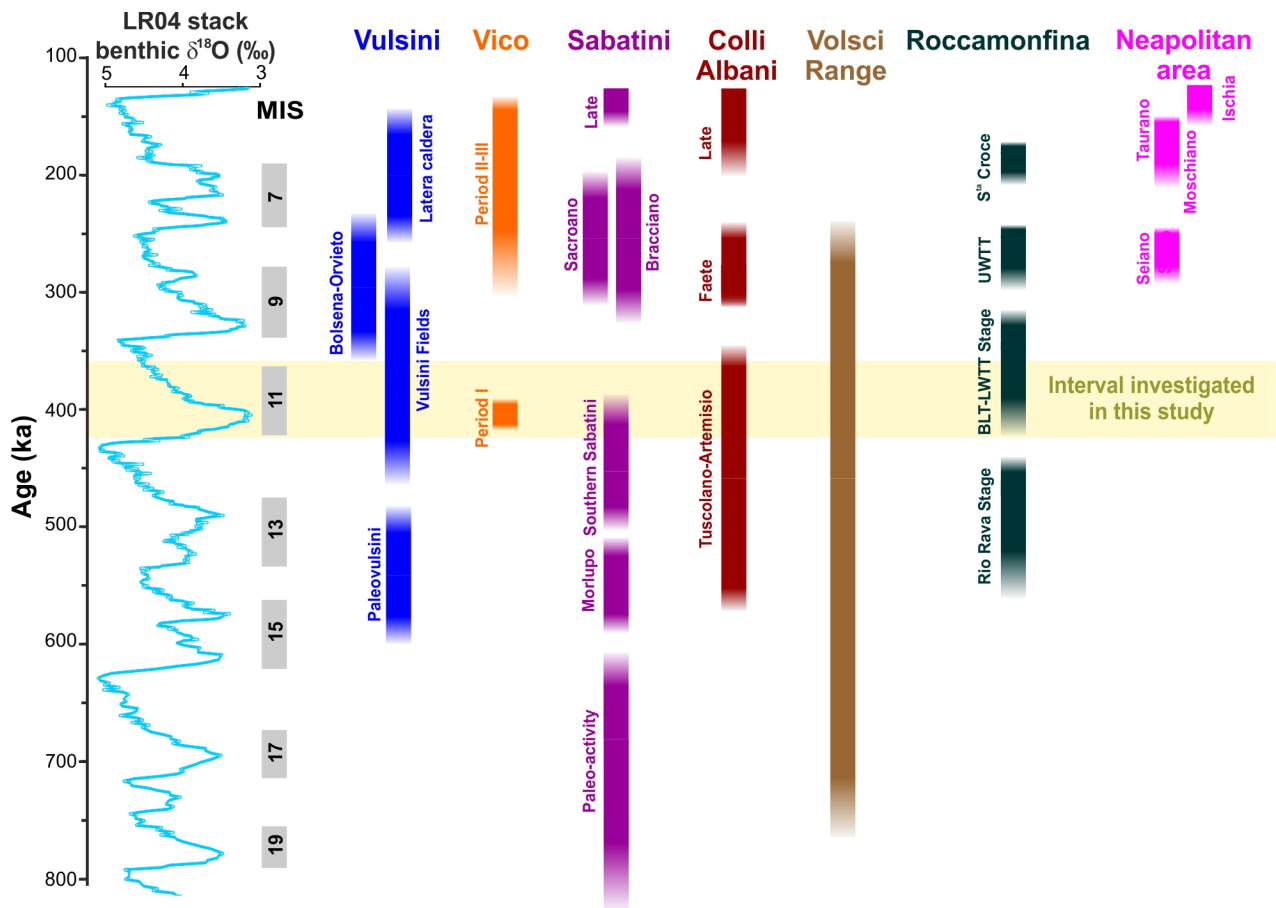
157 The Fucino Basin, unlike other intra-Appennine basins, has likely undergone continuous sedimentation (~0,45
158 mm/yr in average in the central-eastern sector of the basin; Giaccio et al., 2017, 2019; Mannella et al., 2019)
159 since the Plio-Pleistocene and to recent historical times, i.e., potentially covering the last ~2.0 Ma (Giaccio et
160 al., 2015). Indeed, the basin hosted a lake, *Lacus Fucinus*, which was first partially reclaimed during Emperors
161 Claudius and Adrian reigns (1st-2nd century CE), and then completely drained by the Torlonia family at the end
162 of the 19th century.

163

164 **2.2. The peri-Tyrrhenian potassic volcanic systems**

165 The Quaternary peri-Tyrrhenian volcanic systems of central-southern Italy (hereafter peri-Tyrrhenian potassic
166 volcanoes) belong to the *Roman Comagmatic Region* of Washington (1906), which comprises the volcanic
167 centers and areas fed by potassic and ultrapotassic magmas extending from southern Tuscany, through
168 Latium and Campania, i.e., from north-west to south-east (Fig. 1a and 1b): Vulsini, Vico, Sabatini and Colli
169 Albani (grouped in the *Roman Province* s.s. by Peccerillo, 2017), Volsci and Roccamonfina (*Ernici-*
170 *Roccamonfina Province*; Peccerillo, 2017) and the active volcanoes of the so-called *Campanian Volcanic Zone*
171 (Rolandi et al., 2003) or *Campanian Province* (Peccerillo, 2017), including Campi Flegrei, Ischia, Procida and
172 Somma-Vesuvius, also known as the *Neapolitan* volcanoes. Volcanism in the region started at the beginning
173 of the Middle Pleistocene, but the volcanic centers have been active during different time intervals (Fig. 3).
174 Direct evidence, i.e., near-vent deposits, of the oldest activity is documented within the Volsci Volcanic Field
175 (Cardello et al., 2020; Marra et al., 2021), which covers the 760-230 ka interval (Boari et al., 2009; Centamore
176 et al., 2010; Marra et al., 2021). Possible evidence of similarly old activity at Sabatini is provided by distal
177 tephra layers found in Tiber River delta, dated between 750 and 810 ka (Marra et al., 2014). During the ~600-
178 415 ka interval, the Vulsini, Sabatini, Colli Albani, Volsci and Roccamonfina volcanic complexes were all
179 simultaneously active (e.g., Sottili et al., 2004; Rouchon et al., 2008; Boari et al., 2009; Palladino et al., 2010;
180 Soligo and Tuccimei, 2010). Around ~415 ka, volcanic activity also started at Vico volcano (Pereira et al.,
181 2020). Finally, the onset of volcanic activity at Neapolitan volcanoes occurred around ~300 ka (Rolandi et al.
182 2003), although there is growing evidence from distal settings which reveal significantly older activity in this
183 region, extending as far back as at least 560 ka or perhaps more (e.g., Giaccio et al., 2014; Petrosino et al.,
184 2015; Wagner et al., 2019).

185 In summary, all the Latium (i.e., Vulsini, Vico, Sabatini, Colli Albani and Volsci) and Roccamonfina volcanoes
186 were active during the interval investigated in this study (i.e., 430-365 ka), consequently there is quite a degree
187 of complexity when trying to establish the volcanic source of distal ash layers deposited during this interval
188 (Fig. 3).



189
190
191
192
193
194
195
196

Figure 3. Temporal distribution of the Middle Pleistocene volcanic activity from the peri-Tyrrhenian potassic volcanic systems, plotted against the LR04 benthic stack record (Lisiecki and Raymo, 2005) Data source: Vulsini volcanic district: Palladino et al. (2010), Marra et al. (2020a); Vico: Perini et al. (2004), Pereira et al. (2020); Monti Sabatini volcanic district: Sottili et al. (2010), Marra et al. (2014, 2020b); Colli Albani: Marra et al. (2009); Volsci Volcanic Field: Boari et al. (2009), Centamore et al. (2010), Marra et al. (2021); Roccamonfina: Giannetti (1996a, 1996b), Giannetti and De Casa (2000), Rouchon et al. (2008), Scaillet et al. (2008); Neapolitan area: De Vivo et al. (2001), Rolandi et al. (2003), Belkin et al. (2016), Sbrana et al. (2018).

197
198
199
200
201
202
203
204
205
206
207
208
209
210
211
212

3. Materials and methods

3.1. Investigated tephra from F4-F5 cores and Roman volcanic province

A summary of the here investigated tephra from Fucino and the Roman volcanic area in this study, and those available in the literature, is reported in Table 1.

Two cores were recovered at the F4-F5 drill site in the central area of the basin (Fig. 1c) and combined to a composite profile 98 meters long. Drilling site selection strategy and recovery procedure are reported in Giaccio et al. (2019). The F4-F5 composite record contains at least 130 tephra (Giaccio et al., 2019; Fig. 2). Based on correlations with tephra layers from the nearby F1-F3 record covering the last 190 kyr (Fig. 2; Giaccio et al., 2017), the geochemical fingerprinting of 11 relevant tephra markers, one direct $^{40}\text{Ar}/^{39}\text{Ar}$ age determination, and the recognition of a climatic proxy variability linked to glacial-interglacial cyclicity, the sediment succession from F4-F5 was ascribed to the last 430 kyr (Fig. 2; Giaccio et al., 2019). In this paper, we focus on the lowermost ~17-meter-thick interval (between ~80 and ~98 m composite depth) of the F4-F5 core, spanning a ~60 kyr time interval. The interval includes the lowermost tephra layer labelled TF-126, which is directly dated by $^{40}\text{Ar}/^{39}\text{Ar}$ method at 424.3 ± 3.2 ka (Giaccio et al., 2019), and up to TF-85, correlated to the Villa Senni eruption (i.e., Tufo Lionato) from the Colli Albani volcano (Giaccio et al., 2019), which is dated at 367.6 ± 1.6 ka (Marra et al., 2009; Giaccio et al., 2012b; Fig. 2). This interval contains 32 ash layers, out of which 28 are

213 investigated and presented in this study, while 4 (i.e., TF-85, TF-117, TF-118 and TF-126) were already studied
 214 and reported in [Giaccio et al. \(2019; Table 1\)](#).

215

216

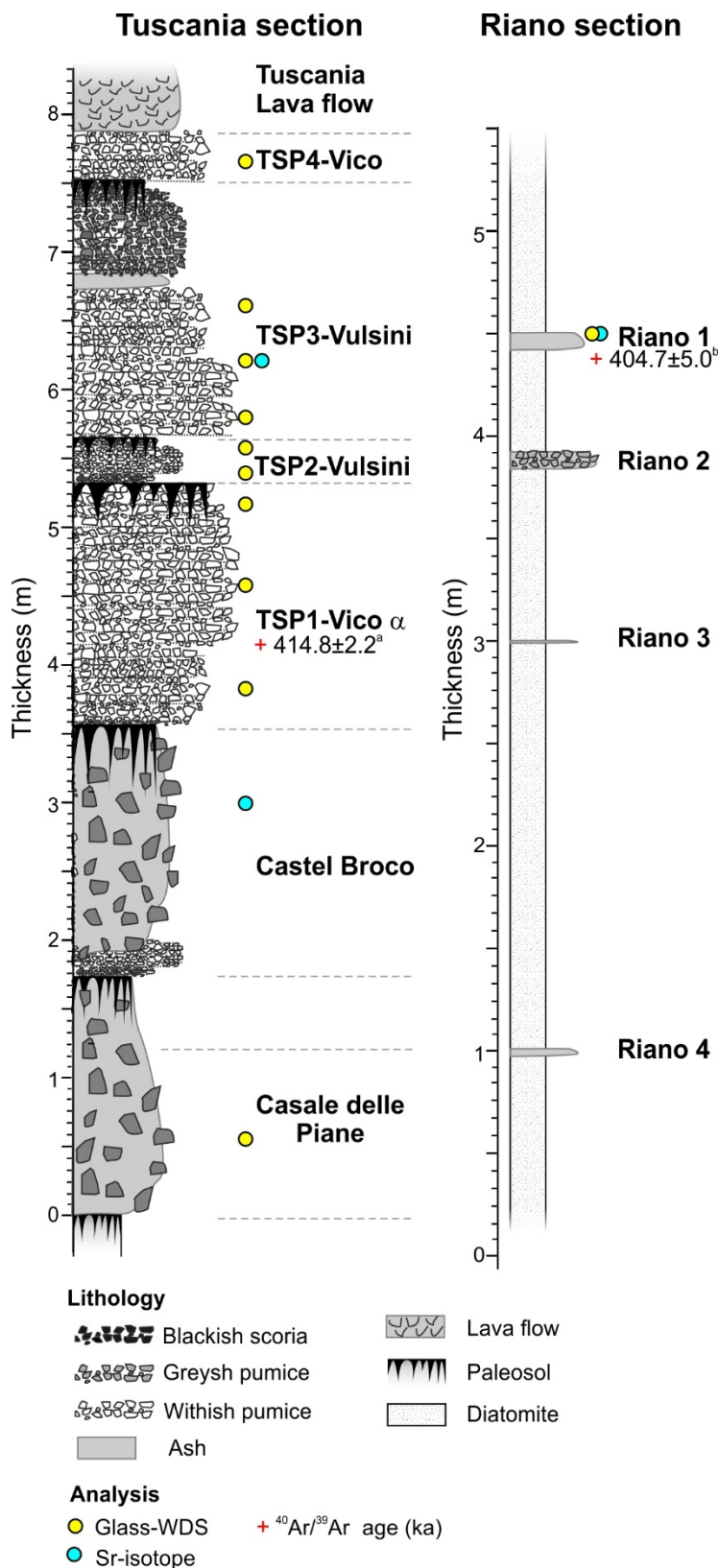
Table 1. Data acquired in this study and available from literature for each investigated Fucino tephra or proximal volcanic unit.

Tephra	Site/Section	Type of analysis			
		Glass-WDS (EMPA)	Trace elements (LA-ICP-MS)	Sr isotopes (TIMS)	⁴⁰ Ar/ ³⁹ Ar
TF-85	F4-F5	Yes ^a	No	Yes ^b	Yes ^b
TF-88	F4-F5	Yes ^b	No	No	No
TF-89	F4-F5	Yes ^b	No	No	No
TF-90	F4-F5	Yes ^b	No	No	No
TF-93	F4-F5	Yes ^b	No	No	No
TF-94	F4-F5	Yes ^b	No	No	No
TF-96	F4-F5	Yes ^b	No	No	No
TF-97	F4-F5	Yes ^b	No	No	No
TF-98	F4-F5	Yes ^b	No	No	No
TF-99	F4-F5	Yes ^b	No	No	No
TF-100	F4-F5	Yes ^b	No	No	No
TF-102	F4-F5	Yes ^b	No	No	No
TF-103	F4-F5	Yes ^b	No	No	No
TF-104	F4-F5	Yes ^b	No	No	No
TF-106	F4-F5	Yes ^b	No	No	No
TF-107	F4-F5	Yes ^b	Yes ^b	Yes ^b	No
TF-108	F4-F5	Yes ^b	No	No	No
TF-109	F4-F5	Yes ^b	No	No	No
TF-110	F4-F5	Yes ^b	No	No	No
TF-111	F4-F5	Yes ^b	Yes ^b	Yes ^b	No
TF-114	F4-F5	Yes ^b	No	No	No
TF-115	F4-F5	Yes ^b	No	No	No
TF-116	F4-F5	Yes ^b	Yes ^b	No	No
TF-117	F4-F5	Yes ^a	No	No	Yes ^b
TF-118	F4-F5	Yes ^a	No	No	No
TF-120	F4-F5	Yes ^b	No	No	No
TF-121	F4-F5	Yes ^b	No	No	No
TF-122	F4-F5	Yes ^b	No	No	No
TF-123	F4-F5	Yes ^b	No	No	No
TF-124	F4-F5	Yes ^b	No	No	No
TF-125	F4-F5	Yes ^b	Yes ^b	No	No
TF-126	F4-F5	Yes ^a	Yes ^b	Yes ^b	Yes ^a
Casale delle Piane	Tuscania	Yes ^b	No	No	No
Castel Broco	Tuscania	Yes ^a	Yes ^b	Yes ^b	No
Vico α (TSP-1)	Tuscania	Yes ^b	No	No	No
TSP-2	Tuscania	Yes ^b	No	No	No
TSP-3	Tuscania	Yes ^b	No	Yes ^b	No
TSP-4	Tuscania	Yes ^b	No	No	No
Riano R-1	Riano	Yes ^b	Yes ^b	Yes ^b	Yes ^c
Pozzolane Nere	Rome	Yes ^d	No	Yes ^f	Yes ^b
Vico β	Vignanello	Yes ^e	Yes ^b	No	Yes ^e
Vico α type locality	Viterbo	Yes ^e	Yes ^b	No	Yes ^e

217

218

^a [Giaccio et al. \(2019\)](#); ^b This study; ^c [Marra et al. \(2018\)](#); ^d [Marra et al. \(2009\)](#); ^e [Pereira et al. \(2020\)](#); ^f [Gaeta et al. \(2006\)](#).



219
220
221
222
223
224

Figure 4. Reference stratigraphic successions outcropping at Tuscania-San Pietro (southern Vulsini) and Riano (eastern Sabatini) (see Fig. 1b for locations). The stratigraphic position of the samples used for geochemical analyses in this study are also shown. ⁴⁰Ar/³⁹Ar dating: ^a Pereira et al. (2020); ^b Marra et al. (2018).

225 In order to improve the reference geochemical dataset required for establishing reliable tephra correlations of
226 the Fucino tephra, we re-examined the key pyroclastic succession at Tuscania-San Pietro (southern Vulsini;

227 Cioni et al., 1987; Palladino et al., 1994, 2010; 42° 24' 43.32" N, 011° 52' 45.13" E; Fig. 1b; Fig. 4) and
228 performed new analyses on four pumice fall units (TSP#). Of these, TSP-1 is correlated to the Vico α Plinian
229 fall marker (Cioni et al., 1987), while TSP-2 and TSP-3 are referred to the Plinian activity of the Vulsini Fields
230 (although with undefined source locations). TSP-3 in particular is tentatively correlated to the Pumice Fall 0
231 (PF-0) of Turbeville (1992, 1993) dated at 399.8 ± 18.0 ka (Turbeville, 1992; age recalculated according to the
232 Alder Creek sanidine at 1.1891 Ma). We stress that this attribution is just putative until it can be corroborated
233 by stratigraphic and geochemical characterization of proximal PF-0 products collected in the type locality.
234 Finally, the Plinian fall horizon TSP-4 is attributed to Vico Plinian activity, although with an uncertain correlation.
235 The TSP succession also includes the Casale delle Piane and Castel Broco major pyroclastic flow deposits
236 (investigated also in the present study, see below) and is topped by the Tuscania lavas (Palladino et al., 1994,
237 2010), which are broadly coeval with the Quarticciolo lavas (356 ± 15 ka; Funicello et al., 2012) outcropping in
238 other nearby localities.

239 To supplement the major element datasets for Vico volcano presented in Pereira et al., (2020), we provide
240 trace element glass analyses of selected proximal Vico α and β samples collected from Viterbo (Vico α ; Lower
241 fall [VT-Base Vico α] and Upper fall [VT-1A, VT-1B and VT-1C]) and Vignanello (Vico β ; [VIG-3]) sections.

242 With the same aim, we also analysed the Riano R-1 tephra (Fig. 4), found within a lacustrine (diatomite)
243 succession outcropping along the Flaminia road (42° 05' 24.06" N, 012° 31' 57.43" E), north of Rome (Fig.
244 1b), and dated at 404.7 ± 5.0 ka by Marra et al. (2018). The Riano R-1 tephra is a 10-cm-thick, coarse to fine
245 blackish ash layer, likely representing a relatively distal occurrence of a major fall deposit, of uncertain, Sabatini
246 or external (i.e., from another Latium volcano), source area. The Riano diatomite succession contains three
247 additional tephra layers (R-2, R-3, and R-4; Fig. 4). However, while R-2 is a 10-cm-thick layer of dense scoria
248 lapilli, likely deriving from a minor local (i.e., Sabatini) Strombolian eruption, the ash layers R-3 and R-4 did
249 not yield fresh glass suitable for geochemical analyses.

250 Finally, in order to acquire a new $^{40}\text{Ar}/^{39}\text{Ar}$ age for the Colli Albani Pozzolane Nere caldera-forming eruption,
251 we sampled an exposure in Rome City (41° 50' 44.74" N, 012° 28' 40.56" E). Indeed, since we could not
252 establish which of the two different monitor standards was used for determining the previous set of $^{40}\text{Ar}/^{39}\text{Ar}$
253 ages for this deposit (Karner and Renne, 1998), the existing age of 407 ± 2 ka can not be recalculated with
254 respect to the current monitor standard improved ages, and thus does not allow direct comparisons.

255

256 3.2. EPMA-WDS

257 Major and minor element compositions were determined on micro-pumice fragments and/or glass shards of
258 the 28 tephra layers from the F4-F5 record (Table 1), which were labelled following the same criteria adopted
259 in previous studies of the F1-F3 and F4-F5 cores (Giaccio et al., 2017, 2019), and for the above described five
260 proximal samples (Table 1). To have a good statistical expression of the tephra composition and their
261 geochemical variability, we aimed at analysing at least 10-15 shards/micro-pumices from each tephra.
262 However, in some cases (i.e., TF-96, TF-100, TF-103, TF-104, TF-123 and TF-124), the dense microlithic
263 texture of the juvenile clasts or the incipient alteration of the glass prevented us to acquire such a satisfactory
264 number of analyses. Nevertheless, also in those cases, the relatively homogeneity and/or geochemical
265 consistency of the analysed glasses indicate a satisfactory reliability and representativity of the compositional
266 data for tephrochronological purposes. A synthesis of all acquired data for each of the 28 tephra and 4 proximal

267 pyroclastic units can be found in [Table 1](#), along with information relative to previously investigated tephra from
268 F4-F5 core and proximal volcanics.

269 Polishing and carbon coating of the epoxy slides were performed for electronprobe microanalyser wavelength
270 dispersive spectroscopy (EPMA-WDS) analysis at the *Istituto di Geologia Ambientale e Geoingegneria* of the
271 Italian National Research Council (IGAG-CNR, Rome). Major and minor elements quantitative analyses were
272 performed with a CAMECA SX-50 EPMA equipped with five-wavelength dispersive spectrometers (WDS),
273 operating at 15 kV accelerating voltage, 15 nA beam current, 10 μm defocused beam diameter - to limit Na
274 mobilization and loss - and 20 s element counting time for all elements. Wollastonite (Si and Ca), corundum
275 (Al), periclase (Mg), magnetite (Fe), rutile (Ti), orthoclase (K), jadeite (Na), phlogopite (F), potassium chloride
276 (Cl), barite (S), F-apatite (P) and metals (Mn) were used as calibration standards. The Kakanui augite and
277 Rhyolite RLS132 glasses from the United States Geological Survey were measured prior to each analytical
278 run to evaluate the accuracy of the electron-microprobe analysis. Obtained mean values are shown in
279 [Supplementary Dataset-4 \(SD-4\)](#), along with the % difference between each oxide with respect to the
280 recommended values. The mean values show $\sim 0.5\%$ difference for SiO_2 , ranging in concentrations from 50
281 wt% to 77 wt%, $<0.2\%$ for oxides in the 15-16 wt% concentration range, 3.3-1.8% for oxide concentrations
282 between 5 and 12 wt%, 4.2-0.1% for oxides in the 2-5 wt% range, up to 5.7% for the oxides ranging from 0.2
283 wt% to 2 wt% and up to 39% for minor elements (i.e., oxides with concentrations <0.2 wt%).

284 In order to test the quality and reproducibility of our data, we also performed a series of analysis on the MPI-
285 DING glass standards of [Jochum et al. \(2006\)](#) and a rhyolitic Lipari obsidian (i.e., ID3506; [Kuehn et al., 2011](#)).
286 The results show $<1.1\%$ difference for SiO_2 , ranging between 46 wt% and 77 wt% range, 2.8-0.2% for oxides
287 ranging from 15 wt% to 27 wt%, 4.0-1.0% for oxides in the 5-13 wt% range, 5.2-0.6% for oxides ranging from
288 2 wt% to 5 wt%, 8.1-1.5 for oxides in the 0.2-2 wt% range and up to 62% for minor elements (SD-4).

289 Data reduction was carried out using the PAP correction, while data processing was performed in Microsoft
290 Excel. We adopted 93 wt% as a threshold for the measured total: analysis with total values lower than 93 wt%
291 were discarded. All compositional data are shown as oxide weight percentages (wt%) in the Total Alkali vs
292 Silica (TAS; [Le Maitre et al., 2002](#)) classification diagram - as well as bi-plots diagrams - with total iron (FeOt)
293 expressed as FeO and normalized to 100% on a volatile-free basis (i.e., excluding Cl, SO_3 and F volatiles) for
294 correlation purposes. Collected data are all reported in [Supplementary Dataset-1 \(SD-1\)](#), along with secondary
295 standards and MPI-DING measured values.

296

297 **3.3. LA-ICP-MS**

298 Trace element analyses were conducted on volcanic glasses from five Fucino tephra units, i.e., TF-107, TF-
299 111, TF-116, TF-125, and TF-126, and four proximal-medial pyroclastic deposits, i.e., the Castel Broco unit,
300 from the above described Tuscania-San Pietro section at Vulsini ([Fig. 4](#)), Vico α and β , and the Riano R-1
301 Tephra (unknown source) ([Table 1](#)). These samples have been selected (i) to test if compositions of the trace
302 elements and/or the ratios of incompatible trace elements allow distinguishing of tephra layers with similar
303 major element composition (e.g., TF-107, TF-111, TF-126, Castel Broco, Riano R-1), and (ii) to obtain the
304 complete geochemical composition of the products from the two major eruptions of Vico Period I (i.e., Vico α
305 and Vico β), likely dispersed over wide areas of the central Mediterranean and thus representing potential
306 tephra markers for this region. The analysis was performed using an Agilent 8900 triple quadrupole ICP-MS
307 (ICP-QQQ) coupled to a Resonetics 193nm ArF excimer laser-ablation at the Department of Earth Sciences,

308 Royal Holloway, University of London. Full analytical procedures used for volcanic glass analysis are reported
309 in Tomlinson et al. (2010). Spot sizes of 25 and 34 μm were used depending on the sample vesicularity and/or
310 size of glass surfaces available for analysis. The repetition rate was 5 Hz, with a count time of 40 s on the
311 sample, and 40 seconds on the gas blank to allow the subtraction of the background signal. Typically, blocks
312 of eight or nine glass shards and one MPI-DING reference glass were bracketed by the NIST612 glass adopted
313 as the calibration standard. The internal standard applied was ^{29}Si (determined by EPMA-WDS analysis). In
314 addition, MPI-DING reference glasses were used to monitor analytical accuracy (Jochum et al., 2006). LA-
315 ICP-MS data reduction was performed in Microsoft Excel, as outlined in Tomlinson et al. (2010). Accuracies
316 of LA-ICP-MS analyses of the MPI-DING reference glasses, ATHO-G and StHs6/80-G, were typically $\leq 5\%$
317 for most elements measured. These measurements are provided in Supplementary Dataset-2 (SD-2), along
318 with those of selected proximal eruption units and the full Fucino dataset.

319

320 **3.4. Isotopic composition of strontium**

321 Strontium (Sr) isotope compositions were determined on glass shards/pumices and mineral phases (i.e.,
322 feldspar, leucite, and pyroxene) from six selected samples, as summarised in Table 1. The rationale underlying
323 the selection of these samples is similar to that for LA-ICP-MS analysis, i.e., obtaining a further geochemical
324 characterization of the tephra from some major eruptions of the peri-Tyrrhenian volcanoes during MIS 11
325 period, in order to have, if any, an additional fingerprinting tool for strengthening their recognition/discrimination
326 in distal settings. The variable fractions were handpicked under a binocular microscope. When possible, the
327 cleanest crystals were selected, avoiding the presence of glass rinds attached. Before chemical dissolution,
328 glass shards and pumices were acid leached three to five times to reduce alteration effects. Leaching was
329 carried out each time by placing the beakers containing samples and high-purity 6 N HCl on a hot plate for 10
330 min. Feldspar and pyroxene separates coated by a thin film of glass were leached with high-purity 7% HF for
331 10 min in an ultrasonic bath. After leaching, samples were rinsed with Milli Q[®] H₂O and dissolved with high-
332 purity HF–HNO₃–HCl mixtures. Sr was separated from the matrix through conventional ion-exchange
333 procedures at the clean chemistry laboratory of the *Istituto Nazionale di Geofisica e Vulcanologia, Osservatorio*
334 *Vesuviano*. Sr blank was on the order of 0.3 ng during chemistry processing.

335 Sr isotopic compositions were determined by thermal ionization mass spectrometry (TIMS) at DiSTAR (Naples,
336 Italy), using a Thermo Scientific Triton Plus mass spectrometer equipped with one fixed and eight adjustable
337 Faraday cups. $2\sigma_{\text{mean}}$, i.e., the standard error with $N = 150$, was better than ± 0.000008 for all Sr
338 measurements. Measured $^{87}\text{Sr}/^{86}\text{Sr}$ ratios were normalized for within-run isotopic fractionation to $^{88}\text{Sr}/^{86}\text{Sr} =$
339 8.37521 . During the period of isotopic data collection, replicate analyses of NIST–SRM 987 (SrCO_3)
340 international reference standard were carried out to check for external reproducibility at 2σ level (where σ is
341 the standard deviation of the standard results, according to Goldstein et al., 2003). No correction has been
342 applied to the measured $^{87}\text{Sr}/^{86}\text{Sr}$ values, since the mean measured value of $^{87}\text{Sr}/^{86}\text{Sr}$ for NIST–SRM 987
343 standard was 0.710248 ± 0.000006 (2σ , $N = 17$), which is indistinguishable from the recommended value of
344 $^{87}\text{Sr}/^{86}\text{Sr} = 0.710248$ (Thirlwall, 1991).

345

346 **3.5. $^{40}\text{Ar}/^{39}\text{Ar}$ geochronology**

347 In order to improve the chronology of the investigated interval of the F4-F5 record, three new $^{40}\text{Ar}/^{39}\text{Ar}$ dating
348 were performed on TF-85 and TF-117 samples, correlated to the Villa Senni and Pozzolane Nere eruptions,

349 respectively (Giaccio et al., 2019), and on a sample of the proximal Pozzolane Nere (PN) unit collected from
350 the above-mentioned outcrop in Rome City (Table 1). Samples were sieved and cleaned in distilled water,
351 while undesirable magnetic crystals were removed by magnetic separation. Approximately thirty crystals were
352 selected from each sample and loaded into an aluminium disk in three individual pits. All crystals from the
353 individual samples were irradiated for 120 min in the Cd-lined, in-core CLICIT facility of the Oregon State
354 University TRIGA reactor (IRR CO002). Interference corrections were based on the nucleogenic production
355 ratios given in Renne et al. (2015). After irradiation, samples were transferred into a copper sample holder and
356 loaded individually into a differential vacuum Cleartan© window. All measurements were done in the LSCE
357 $^{40}\text{Ar}/^{39}\text{Ar}$ facility (France). Detailed analytical procedures can be found in Nomade et al. (2010). Single crystals
358 were fused individually using a 25 Watts Synrad CO₂ laser at about 10 to 15 % of the nominal power. Extracted
359 gas was then purified for 10 min by two hot GP 10 and two GP 50 getters (ZrAl). Argon isotopes (^{40}Ar , ^{39}Ar ,
360 ^{38}Ar , ^{37}Ar and ^{36}Ar) were successively measured using a VG 5400 mass spectrometer equipped with an
361 electron multiplier (Balzer SEV 217 SEN) coupled with an ion counter. Each argon isotope measurement
362 consisted of 20 cycles of peak-hopping. Neutron fluence J for each sample was calculated using co-irradiated
363 Alder Creek sanidine standard (ACs at 1.1891 Ma; Niespolo et al., 2017) and the K total decay constant of
364 Renne et al. (2011). This calibration produces ages independent of the astronomical tuning. J-values are the
365 followings: TF-85 (Villa Senni) = $0.00053020 \pm 0.00000053$, TF-117 (Pozzolane Nere) = $0.00052950 \pm$
366 0.00000053 and PN = $0.00053260 \pm 0.00000059$. Mass discriminations were monitored by analysis of air
367 pipette throughout the analytical period, and relative to a $^{40}\text{Ar}/^{36}\text{Ar}$ ratio of 298.56 (Lee et al., 2006). Procedural
368 blank measurements were achieved after every two or three unknown samples. For 10 min times of isolation
369 typical backgrounds are about $2.5\text{-}4.0 \times 10^{-17}$ and $5.0 \text{ to } 7.0 \times 10^{-19}$ moles for ^{40}Ar and ^{36}Ar , respectively.

370 371 **3.6. Age-depth modelling**

372 The age model and corresponding 95%-confidence interval were both obtained using the Bacon software
373 (Blaauw and Christen, 2011) written in the open-source statistical environment R (R Core Team, 2016).
374 To accommodate large differences in the sedimentation rate occurring during the investigated interval, we split
375 the record into three sedimentary zones A to C. Zone boundaries are defined through a preliminary evaluation
376 of changes in sedimentary facies and on the availability of the dated points. The definition of sedimentary
377 facies is based on the analysis of the composite profile derived by stacking consecutive core images acquired
378 by the ITRAX core scanner (Giaccio et al., 2019). For each interval, the mean sedimentation rate is estimated
379 by dividing the thickness of the interval for the time span elapsed between the deposition of the youngest and
380 oldest dated tephra layers bracketing the interval, or at least, a large part of it. In the case of multiple dated
381 layers in close stratigraphic position, we choose those featuring the most accurate dating. Sedimentary
382 intervals and estimated mean sedimentation rates are as follows:

- 383
- 384 • Zone A: 80.520 – 91.810 m, 33.33 cm/kyr
 - 385 • Zone B: 91.810 – 95.950 m, 30.30 cm/kyr
 - 386 • Zone C: 95.950 – 98.100 m, 4.76 cm/kyr
- 387

388 These zones do not represent homogeneous sedimentary facies; however, they represent the most accurate
389 approximation of long term (>4 kyr) changes in mean sedimentation rate that can be made based on currently
390 available tephrochronological information.

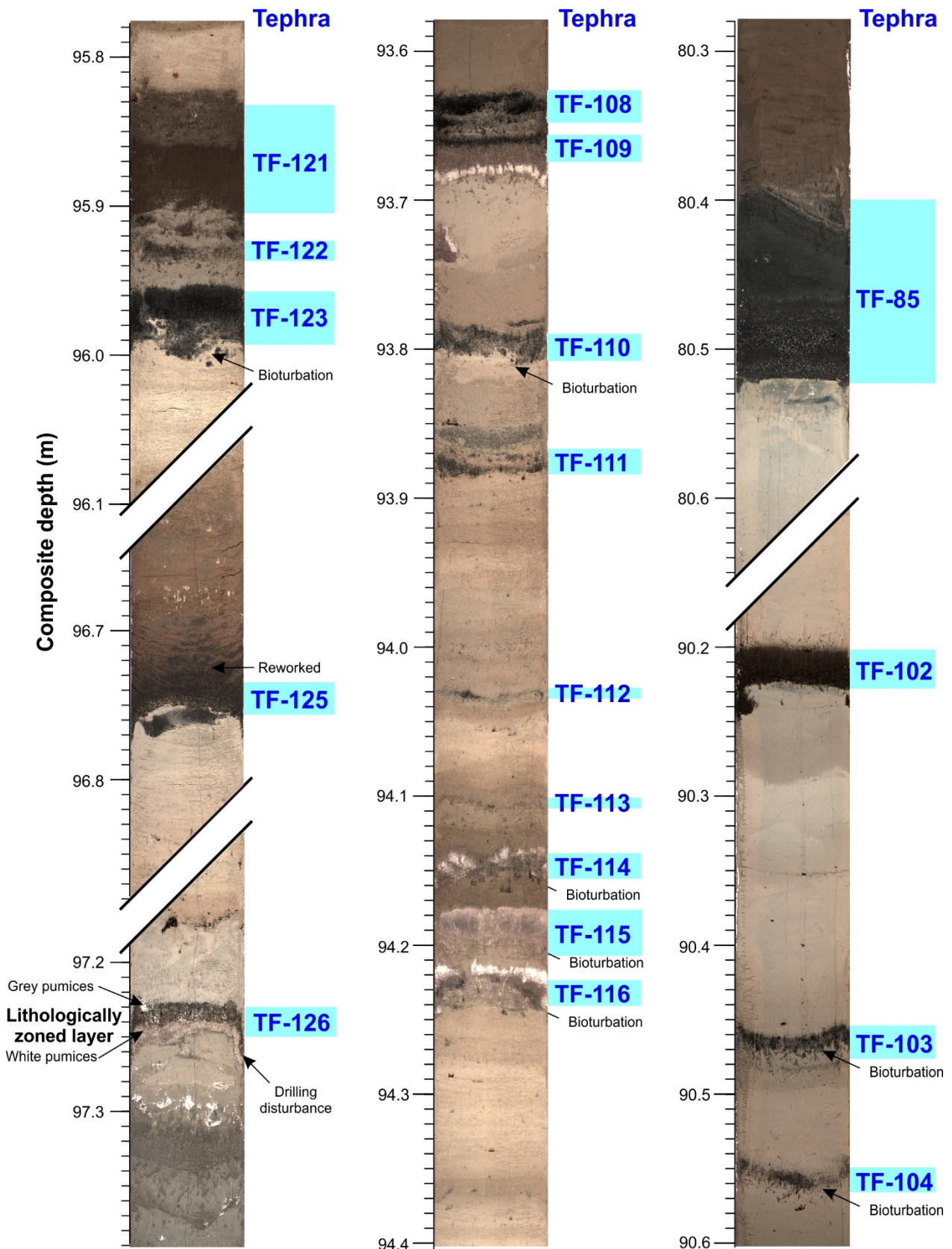
391

392 **4. Results**

393 ***4.1. Depositional and sedimentological features of the Fucino tephra succession***

394 Tephra horizons in the Fucino lacustrine succession occur as discrete layers of ash with variable thickness
395 (Table 2) and grain-size, well separated from each other by fine lake sediments (marl) (Fig. 5). Despite a slight
396 bioturbation and/or mechanic disturbance related to the drilling operation (Fig. 5), each tephra layer shows
397 distinctive lithological (i.e., grain-size, shape, colour, vesicularity pattern and textural features of the juvenile
398 clasts, type, and assemblage of the crystal and lithic components) and geochemical (glass-WDS major
399 element composition) features. These circumstances are verified also in the case of closely clustered tephra
400 layers, i.e., each layer forming the cluster presents its own distinctive lithological and geochemical
401 characteristics with respect to the adjacent ones. In some cases, tephra layers are also characterised by a
402 sharp lower boundary and by an upsection lithological zonation (e.g., TF-126; Fig. 5). These features
403 undoubtedly indicate that tephra layers are undoubtedly primary fallout deposits and that post-depositional
404 processes are negligible and did not affect the integrity of the tephra succession.

405



406
 407 **Figure 5.** Representative, selected intervals of Fucino core sections, showing the general sedimentological and lithological features of the
 408 investigated tephra.
 409

410 **4.2. Tephra lithology and glass composition**

411 4.2.1. *Data summary*

412 The thickness and main lithological features of the 32 Fucino tephra and proximal volcanic units are
 413 summarized in [Tables 2 and 3](#), respectively. Full glass compositions are provided in [Supplementary Dataset-](#)
 414 [1 \(SD-1\)](#), while their classification according to the total alkali vs silica (TAS) diagram ([Le Maitre et al., 2002](#))
 415 is shown in [Figure 6](#). Description of the geochemistry (i.e., major, minor and trace elements and Sr-isotopes)
 416 of the volcanic glasses is given in the following sections.

417
 418 **Table 2.** Main lithological, mineralogical, and geochemical features of the 365-430 ka F4-F5 Fucino tephra.

Tephra	Thickness (cm)	Composite depth (m)	Core section and depth (cm)	CG	Lithology			Rock type
					Juvenile clasts	Minerals	Lithic content	
TF-85*	14.00	80.520	F5-49 74-88	ND	Black-brown scoria	Lc>bmca>cpx	Poor	K-f
TF-88	1.25/2.00	83.770	F4-51 131-133/ F5-51 65-66	CG-2	White pumice and grey-brown scoria	Kfs>cpx>bmca	Poor	ph-tr
TF-89	2.00	84.168	F5-51 107-109	CG-2	Grey scoria	Kfs>cpx>bmca	Poor	ph
TF-90	2.00	84.388	F5-51 130-131	CG-2	Black-grey scoria	Kfs>cpx>bmca	Rich	tr
TF-93	0.90	86.140	F4-53 51.3-52.2/ F5-52 149-150	CG-2	White pumice	Kfs>cpx	No	tph-ph
TF-94	0.75	86.853	F4-53 53.6-54.6	CG-2	White pumice	Kfs	No	ph-tr
TF-96	1.20	87.166	F4-53 85-86.2	CG-2	White pumice and grey scoria	Kfs>cpx	Poor	ph
TF-97	2.50	87.470	F4-53 110-112	CG-2	Grey scoria	Kfs>bmca	Poor	lat
TF-98	1.00	87.575	F4-53 119-120	CG-2	Grey scoria and whitish pumice	Kfs>bmca	Poor	lat-tph-ph-tr
TF-99	1.00	87.677	F4-53 128-129	CG-3	Highly vesicular white pumice and brown scoria	Kfs>bmca	Poor	K-tr-rhy
TF-100	6.75	88.045	F5-54 0-4.5	CG-1	Dense black scoria	Lc	Poor	K-f
TF-102	2.00	90.230	F4-55 58-60/ F5-54 125-126	CG-2	Poorly vesicular black scoria	Kfs>Lc>bmca	Poor	t-pht
TF-103	3.00	90.485	F4-55 83-86/ F5-54 133-134.2	CG-2	Poorly vesicular black scoria	Kfs>Lc>bmca	Poor	pht-tph
TF-104	2.00	90.560	F4-55 92-93/ F5-54 142-144	CG-2	Poorly vesicular grey scoria	Kfs>Lc>bmca	Poor	pht-tph
TF-106	1.40	90.860	F4-55 123-124.4	CG-2	Poorly vesicular grey scoria	Kfs>Lc>bmca	Rich	trb-pht-tph-sho
TF-107	2.00	91.620	F4-56 29-31/ F5-55 57.2-59	CG-2	Moderately vesicular whitish pumice and poorly vesicular greyish scoria	Kfs>bmca>cpx	Rich	ph-tr
TF-108	3.00	93.650	F5-56 110-113	CG-1	Dense, leucite-bearing black scoria	Lc	No	K-f
TF-109	3.00	93.690	F5-56 114-117	CG-3	Highly vesicular white pumice and greyish scoria	Kfs>bmca	Poor	K-ph-tr-rhy
TF-110	2.00	93.810	F5-56 126-128	CG-2	Highly vesicular white pumice and greyish scoria	Kfs>bmca	Poor	ph-tr
TF-111	3.00	93.885	F4-57 47-50	CG-2	Highly vesicular white pumice	Kfs>bmca	Very poor	ph-tr
TF-114	2.00	94.166	F4-57 77-79	CG-3	Highly vesicular white pumice and greyish scoria	Kfs>bmca>cpx	Poor	K-tr-rhy
TF-115	2.00	94.211	F4-57 81-83	CG-3	Highly vesicular white pumice	Kfs>bmca>cpx	Poor	K-tr-rhy
TF-116	2.00	94.251	F4-57 85-87	CG-3	Highly vesicular white pumice	Kfs>bmca>cpx	Poor	K-ph-tr-rhy
TF-117*	9.00	95.130	F4-57 151-152/ F5-57 0-7	ND	Poorly vesicular leucite-bearing black scoria	Lc>cpx	Poor	K-f
TF-118*	5.50	95.290	F5-57 16-23	ND	Poorly vesicular leucite-bearing black scoria	Lc	Poor	K-f
TF-120	2.00	95.540	F5-57 45-47	CG-2	Highly vesicular white pumice	Kfs>bmca	Very poor	ph-tr
TF-121	8.00	95.910	F5-57 77-85	CG-2	Poorly vesicular greyish-brownish scoria	bmca>Kfs>Lc	Poor	tph-ph-tr
TF-122	1.00	95.930	F5-57 85-86	CG-2	Dense, leucite-bearing brown scoria	Kfs>bmca>Lc	Poor	tph-ph-lat-tr
TF-123	5.50	96.005	F5-57 87-94	CG-2	Poorly vesicular black scoria	Lc>cpx>Kfs>bmca	Very rich	pht-tph
TF-124	0.75	96.155	F5-57 107-110	CG-2	Poorly vesicular black scoria and whitish pumice	Lc>cpx>bmca	Rich	sho
TF-125	3.50	96.775	F5-58 16-19.5	CG-3	Highly vesicular white pumice	Kfs>bmca>cpx>op	Poor	K-ph-tr-rhy
TF-126*	2.00	97.250	F5-58 64-66	ND	Highly vesicular white (base) and honey (top) pumice	Kfs>bmca>cpx>op	Poor	ph-tr

419
 420 *=EPMA data in [Giaccio et al. \(2019\)](#); ND=Not determined in this study. Rock type abbreviations: K- = potassium- (suffix); f = foidite; ph
 421 = phonolite; tr = trachyte; tph = tephriphonolite; lat = latite; rhy = rhyolite. Mineral abbreviations: Kfs = K-feldspar; bmca = black mica; cpx
 422 = clinopyroxene; Lc = leucite; op = opaques. CG = compositional group (see [Fig. 6](#)).
 423

424 **Table 3.** Geochemical and mineralogical data summary of the investigated proximal units.

Outcrop/Location	Coordinates	Unit	Volcanic source	Lithology		Rock type
				Juvenile clasts	Minerals	

		Casale delle Piane	Vulsini	Highly vesicular dark grey, Kfs+bmca-bearing scoria	Kfs>bmca	Ph
		Vico α	Vico	Highly vesicular white, Kfs+bmca-bearing pumice and grey scoria	Kfs>bmca>cpx	K-tr-rhy
Tuscania-San Pietro	42° 24' 43.32" N – 11° 52' 45.13" E	TSP-2	Vulsini	Moderately vesicular grey Kfs-bearing pumice	Kfs>cpx	Ph
		TSP-3 (PF-0?)	Vulsini	Highly vesicular white, Kfs+bmca-bearing pumice	Kfs>bmca>cpx	Ph
		TSP-4	Vico	Reddish (thermally altered) Kfs-bearing pumice	Kfs>cpx	K-tr-rhy
Riano	42° 05' 24.06" N – 12° 31' 57.43" E	Riano R-1	ND (Sabatini?)	Blackish ash	Kfs>cpx>lc	Ph-tph-lat
Rome	41° 50' 44.74" N – 12° 28' 40.56" E	Pozzolane Nere	Colli Albani	Lc-bearing black scoria	Lc>cpx>bmca	K-f

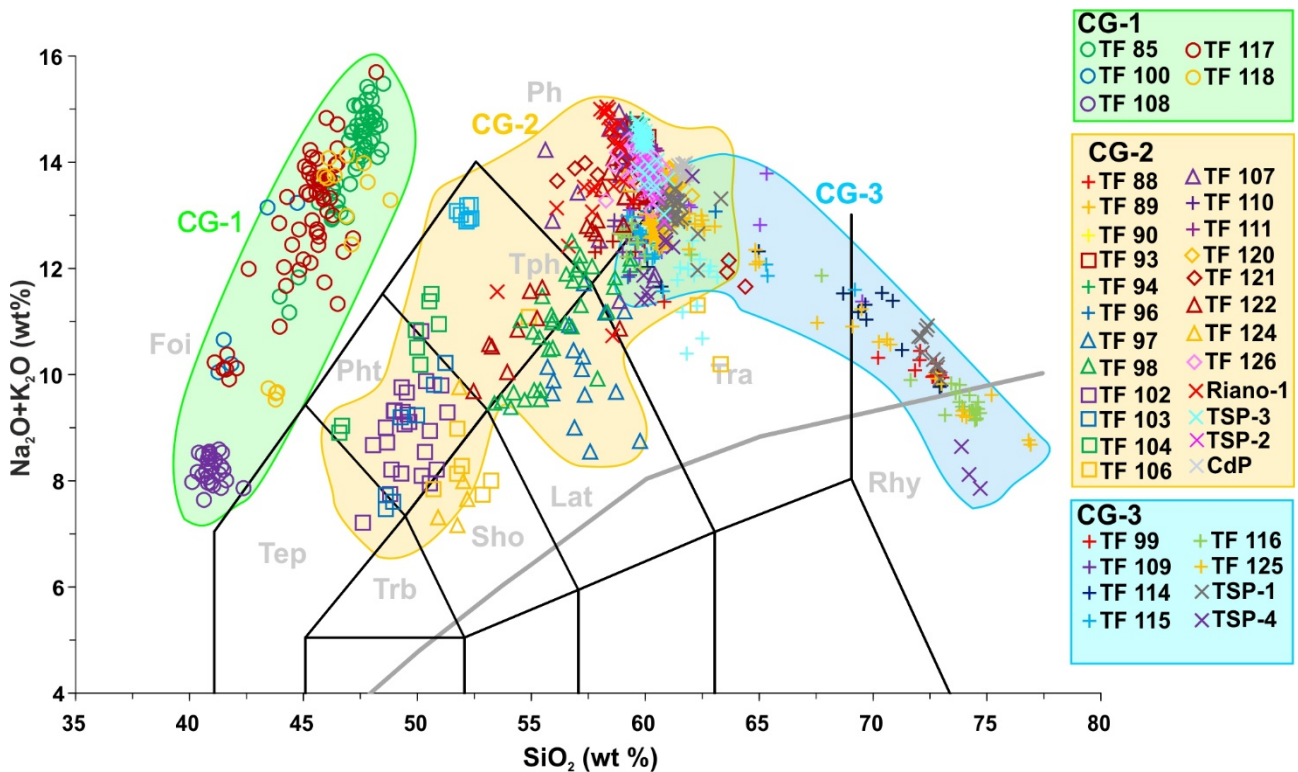
ND=undetermined. Rock type abbreviations: K- = potassium- (suffix); f = foidite; ph = phonolite; tr = trachyte; tph = tephriphonolite; lat = latite; rhy = rhyolite. Mineral abbreviations: Kfs = K-feldspar; bmca = black mica; cpx = clinopyroxene; lc = leucite.

425
426
427

4.2.2. Major and minor elements

428
429 In the TAS diagram, the analysed tephra layers can be conveniently divided into three compositional groups
430 (CGs; see also Table 2 for a classification summary). CG-1 (green area in Fig. 6) comprises of two tephra
431 layers (i.e., TF-100 and TF-108), plus the previously investigated TF- 85, TF-117 and TF-118 layers (Giaccio
432 et al., 2019), all displaying a K-foiditic composition. CG-2 (light-orange area) includes twenty-one F4-F5 tephra,
433 plus two proximal units (TSP-2 and TSP-3), and the Riano R-1 tephra, and are classified as potassic
434 phonotephrites, tephriphonolites, phonolites, latites and trachytes, each being often variable in composition
435 and covering two or more fields of the TAS diagram (Fig. 6). Finally, CG-3 (blue area) includes six F4-F5
436 tephra (i.e., TF-99, TF-109, TF-114, TF-115, TF-116 and TF-125), and two proximal units (TSP-1/Vico α and
437 TSP-4), which are phonolites-trachytes-rhyolites, trachytes-rhyolites, and rhyolites. Although partially
438 overlapping with CG-2 (Fig. 6), CG-3 tephra layers are clearly distinguishable owing to their distinctive rhyolitic
439 components.

440



441
442
443
444

Figure 6. Total alkali vs silica (TAS) classification diagram (Le Maitre et al., 2002). The thirty-two F4-F5 MIS11 tephra and the proximal pyroclastic units plot in three compositional groups (CG-1, CG-2 and CG-3). Data source: glass-WDS of TF-85, TF-117, TF-118 and TF-126: Giaccio et al. (2019); glass-WDS compositions of all others Fucino tephra and proximal pyroclastic units: this study. Foi=foidite;

445 Pht=phonotephrite; Tph=Tephriphonolite; Ph=phonolite; Rhy=rhyolite; Tra=Trachyte; Lat=latite; Sho=Shoshonite; Trb=trachybasalt;
446 Tep=tephrite; CdP=Casale delle Piane unit (Tuscania-San Pietro section).
447

448 4.2.3. Trace elements

449 The full trace element glass dataset of the tephra samples can be found in [Supplementary Dataset-2 \(SD-2\)](#).
450 Phonolite tephra layers TF-107 and TF-111 (CG2) display relatively heterogeneous, yet largely overlapping
451 trace element concentrations. For instance, Th contents range from 67-91 ppm and 66-95 ppm, respectively
452 ([Fig. 7a](#)). Despite the variability in absolute incompatible trace element concentrations, ratios of High Field
453 Strength Element (HFSE) to Th in both TF-107 (Nb/Th = 0.39 ± 0.02 ; Ta/Th = 0.021 ± 0.001 ; Zr/Th = 5.5 ± 0.5
454 [2 s.d.]) and TF-111 (Nb/Th = 0.39 ± 0.03 ; Ta/Th = 0.021 ± 0.001 ; Zr/Th = 5.6 ± 0.3 [2 s.d.]) remain constant,
455 and indistinguishable from one another, possibly implying a common volcanic source.

456 TF-116 belongs to CG3 and comprises phonolitic-trachytic to rhyolitic glasses. However, our trace element
457 analyses derive from glass shards relating to the phonolite-trachyte end-member only. These TF-116 glasses
458 are heterogeneous in terms of their trace element contents (e.g., 82-139 ppm Th; 31-55 ppm Nb; 469-718 ppm
459 Zr) and are more enriched in incompatible trace element than the overlying phonolitic tephra layers (TF-107
460 and TF-111) ([Fig. 7a](#)). Ratios of HFSE to Th in these glasses remain constant, including Nb/Th ratio ($0.41 \pm$
461 0.04 [2 s.d.]), Ta/Th (0.020 ± 0.001 [2 s.d.]) and Zr/Th (5.3 ± 0.4 [2 s.d.]) which all remain largely consistent
462 with the overlying tephra (TF-107 and TF-111) ([Fig. 7b](#)).

463 TF-125 also belongs to CG3, ranging from phonolitic-trachytic (mainly trachytic) to rhyolitic glasses, and this
464 major element variability is captured by a large degree of trace element heterogeneity (e.g., 57-184 ppm Th;
465 1462-151 ppm Sr; 522-879 ppm Rb). Incompatible trace element concentrations observed in the phonolite-
466 trachyte end-member glasses are consistent with TF-107 and TF-111 glasses. The TF-125 phonolite-trachyte
467 glasses are more enriched in Sr, Ba and Eu relative to the rhyolitic end-member glasses, illustrating their
468 compatibility during K-feldspar fractionation. Ratios of HFSE to Th in TF-125 glasses also differ between the
469 phonolitic-trachytic (Nb/Th = 0.39 ± 0.2 ; Zr/Th = 5.5 ± 0.3 ; Hf/Th = 0.13 ± 0.005 [2 s.d.]) and rhyolitic (Nb/Th =
470 0.30 ± 0.3 ; Zr/Th = 2.7 ± 0.7 ; Hf/Th = 0.07 ± 0.01 [2 s.d.]) end-members. Moreover, HFSE to Th ratios in the
471 rhyolitic glasses show more variability than those of the phonolite-trachyte glasses, particularly in terms of
472 Zr/Th, where Zr becomes depleted, probably driven by zircon fractionation ([Fig. 11a](#)).

473 TF-126, previously reported in [Giaccio et al. \(2019\)](#), has a phonolite-trachyte composition and plots in CG-2.
474 Incompatible trace element concentrations reveal a relatively homogeneous composition (e.g., 79 ± 7 ppm Th;
475 29 ± 1 ppm Nb; 393 ± 29 ppm Zr [2 s.d.]), and as such the ratios of HFSE to Th, show very limited variability,
476 consistent with the homogeneous major element composition of the tephra (e.g., Nb/Th (0.37 ± 0.01 ; Ta/Th =
477 0.020 ± 0.001 ; Zr/Th = 4.9 ± 0.5 [2 s.d.]).

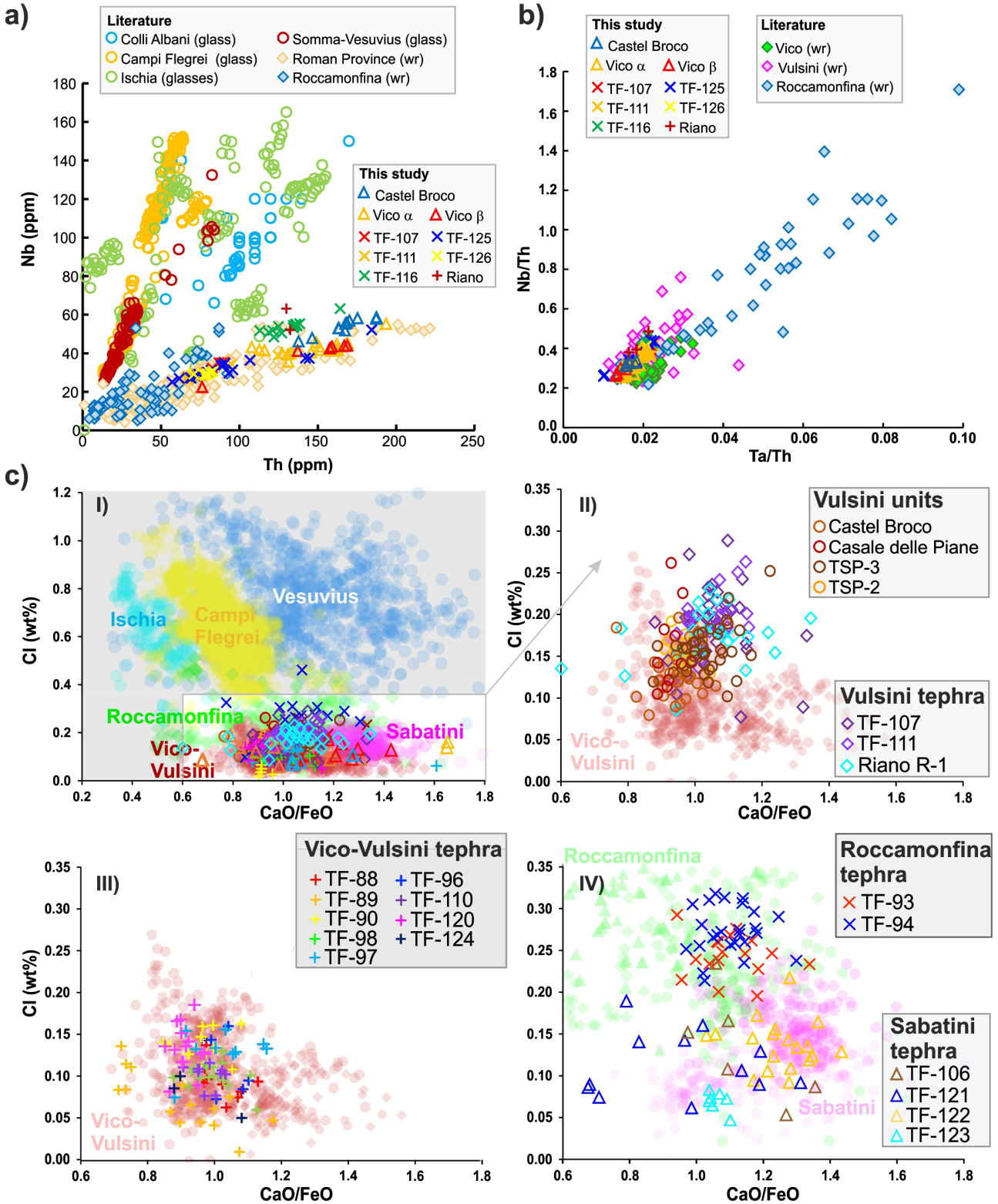
478 Concerning the proximal pyroclastic deposits, the Castel Broco phonolitic glasses show a slight heterogeneity
479 and are enriched in certain incompatible trace elements (e.g., 138-188 ppm Th [[Fig. 7a](#)]; 627-750 ppm
480 Zr; 30-42 ppm Y). Ratios of HFSE to Th remain constant within these glasses (Nb/Th = 0.32 ± 0.02 ; Zr/Th =
481 4.1 ± 0.5 [2 d.]).

482 Vico α trace element glass compositions are extremely heterogeneous (75-194 ppm Th; 1303-87 ppm Sr; 248-
483 955 ppm Rb), consistent with their major element variability ranging from phonolite-trachytes to rhyolites
484 ([Pereira et al., 2020](#)). The less evolved phonolite-trachyte glasses are more enriched in Sr, Ba and Eu relative
485 to the rhyolitic end-member glasses, where these elements clearly behave compatibly during K-feldspar

486 fractionation. Ratios of HFSE to Th in these glasses also differ between the phonolitic-trachytic (Nb/Th ~ 0.38;
 487 Zr/Th ~ 5.6) and rhyolitic (Nb/Th ~ 0.29; Zr/Th = 1.9-5.6) end-members.

488 Vico β analyses focused on the predominantly rhyolitic sub-unit (VIG-3; [Pereira et al., 2020](#)); these rhyolitic
 489 glasses are relatively heterogeneous in the case of some incompatible elements (e.g., 137-169 ppm Th; 948-
 490 995 ppm Rb). Sr, Ba and Eu contents are more depleted in the rhyolitic glasses of Vico β than in Vico α .

491
 492



493

494 **Figure 7.** Discrimination diagrams for F4-F5 tephra. **a)** Th vs Nb bi-plot of the investigated tephra compared with literature data for the
495 glasses of Neapolitan (i.e., Campi Flegrei, Somma-Vesuvius and Ischia) and Colli Albani volcanoes, which are characterized by a higher
496 Nb/Th ratio than Roman/Latium (Vulsini, Sabatini, Vico) and Roccamonfina volcanoes; the compositions of the four tephra are compatible
497 with either a Latium or Roccamonfina origin. **b)** Ta/Th vs Nb/Th discrimination diagram for Roccamonfina and Latium Volcanoes; the four
498 tephra here investigated are characterized by a ratio compatible with either a Vulsini or Vico origin. Data source: TF-107, TF-111, TF-116
499 and TF-126: this study; literature data of whole rock (wr) compositions of products from Latium volcanoes and Roccamonfina: [Lustrino et al. \(2011\)](#)
500 and references therein; glass composition of products from Colli Albani: [Cross et al., 2014](#); Ischia: [Tomlinson et al., 2014](#); Campi
501 Flegrei: [Smith et al., 2011](#), [Tomlinson et al., 2012](#); Somma-Vesuvius: [Tomlinson et al., 2015](#). **c)** CaO/FeO vs Cl discriminating diagram of
502 the volcanic sources of the Italian potassic trachyte-phonolite and tephriphonolite tephra (modified after [Giaccio et al., 2017](#)) for the F4-
503 F5 and Riano R-1 tephra here shown in the Vulsini group for comparison. The compositions of the Vico and Vulsini pyroclastic units
504 collected at Tuscania-San Pietro section, are also shown.
505

506 Only two successful analyses were obtained from the phonolitic Riano R-1 tephra, but the compositions are
507 internally consistent for most incompatible elements, with the noticeable exception being the variable Nb
508 content leading to a Nb/Th ratio of 0.39-0.48. Levels of incompatible trace element enrichment in the R-1
509 glasses (of unknown source area) appear more akin to those of Vulsini (e.g., Castel Broco), rather than Vico
510 ([Fig. 7b](#)). Unfortunately, available trace element data for Sabatini are scant and cannot be considered here for
511 comparison.

512 Ratios of HFSE to Th are seemingly useful when evaluating the origin of the five tephra layers characterised
513 here in the context of peri-Tyrrhenian potassic volcanism, particularly given the limited trace element glass
514 data available for some regional volcanic sources, and thus a reliance on whole-rock datasets, which are not
515 always directly comparable to volcanic glass data (e.g., [Tomlinson et al., 2012](#)). The Nb/Th ratios of the five
516 Fucino layers analysed (TF-107, TF-111, TF-116, TF-125 and TF-126) clearly preclude an origin from the
517 Neapolitan volcanic zone (e.g., Campi Flegrei, Ischia, Vesuvius), where Nb values are far higher at overlapping
518 Th content, and Nb/Th ratios are typically > 1.5 (glass datasets; [Fig. 7a](#)).

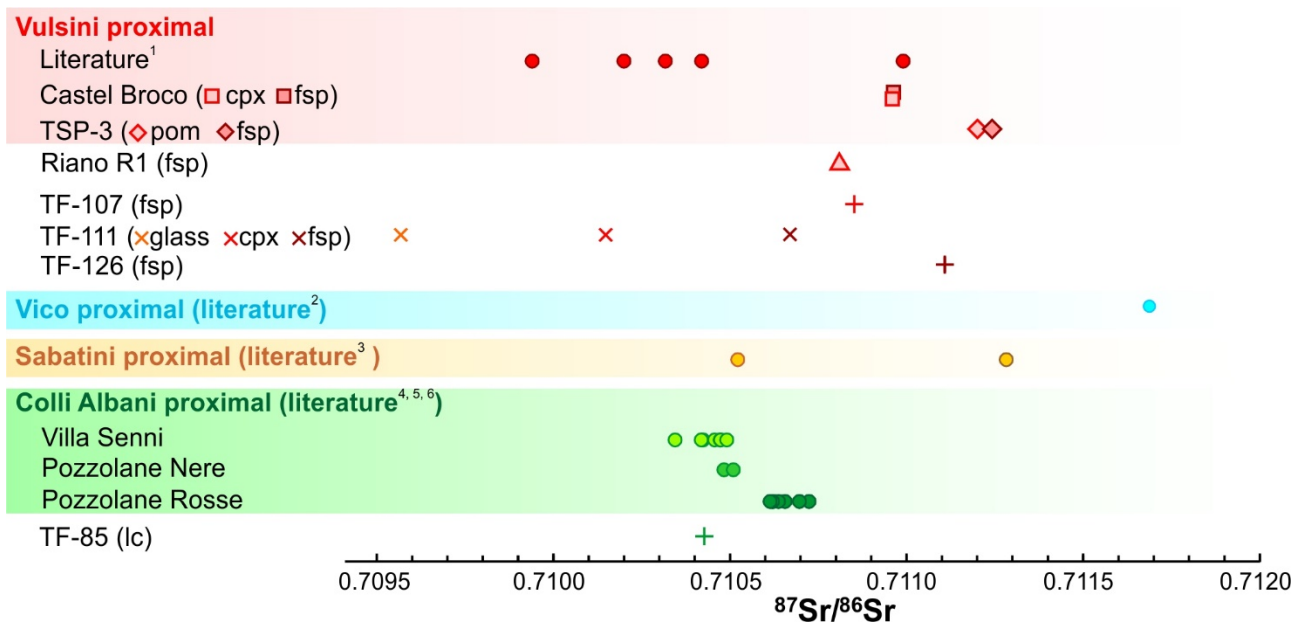
519 TF-107, TF-111, TF-116, TF-125 and TF-126 all have incompatible trace element concentrations and ratios of
520 HFSE to Th compatible with the published analyses of the Latium and Roccamonfina volcanics ([Fig. 7a](#)).
521 However, Roccamonfina appears an unlikely source of the five Fucino tephra layers owing to its typically higher
522 Ta/Th ratios ([Fig. 7b](#)). In the investigated timespan, Colli Albani exclusively erupted K-foidites (CG-1) and can
523 easily be discounted as the possible volcanic source of these Fucino layers, thus leaving the remaining Latium
524 (Vulsini, Sabatini and Vico) volcanoes as the most obvious candidates. Indeed, ratios of HFSE to Th observed
525 in TF-107, TF-111, TF-116, TF-125 and TF-126 are broadly consistent with those from published whole-rock
526 (e.g., [Lustrino et al., 2011](#)) and our preliminary glass (reported above) data from Vulsini and Vico (although
527 similarities to Sabatini products cannot be excluded owing to a paucity of data).
528

529 4.2.4. Strontium (Sr) Isotopes

530 Results for each analysed sample, along with associated uncertainty (2σ), are presented in [Table 4](#), while a
531 comparison with values from the literature of proximal Vulsini, Vico, Sabatini and Colli Albani rock samples,
532 erupted in the time interval 430-350 kyr, is shown in [Figure 8](#). In literature there are very few Sr-isotopic data
533 (i.e., just one from [Perini et al., 2004](#)) for the Vico activity in the investigated 430-365 ka time interval, thus
534 making it challenging to identify eruptive units from this volcano based on Sr-isotope signature. This knowledge
535 gap should be filled in the future to better constrain the attribution of several TF tephra layers.

536 $^{87}\text{Sr}/^{86}\text{Sr}$ values were measured on either pyroxene or feldspar minerals on each sample, except for TSP-3,
537 for which a matrix (pumice) measurement was obtained as well. For sample TF-85 a mineral fraction enriched
538 in leucite crystals was analysed. The lowest value (0.7095) was measured on pumice fragments from the TF-
539 111. Pyroxenes and feldspar from TF-111 are featured by $^{87}\text{Sr}/^{86}\text{Sr}$ ratio of 0.710149 and 0.710671,

540 respectively. The highest value (0.71120) was measured on feldspars of TSP-3. Therefore, all the measured
 541 ratios suggest a Roman province origin for the investigated tephra (Fig. 8). Minerals from TF-85=Villa Senni
 542 have an $^{87}\text{Sr}/^{86}\text{Sr}$ ratio of 0.71043, which agrees with literature data (Gaeta et al., 2016). Measured values of
 543 proximal units from Vulsini (i.e., TSP-3 and Castel Broco) range up to 0.71125 (TSP-3 fsp), thus slightly
 544 extending the literature range for Vulsini (Fig. 8). The Riano R-1 tephra value of 0.71081 is broadly compatible
 545 with either a Sabatini or Vulsini source (rather than Vico). Finally, TF-126 has $^{87}\text{Sr}/^{86}\text{Sr}$ ratio of 0.71111 that
 546 would support the attribution of this tephra to a Vulsini eruption, as already suggested by Giaccio et al. (2019).
 547 Overall, the measured $^{87}\text{Sr}/^{86}\text{Sr}$ values do not provide sufficient evidence to be used as correlation tool for the
 548 Latium volcanoes, except for perhaps Vico: indeed, the amount of literature data on proximal samples is still
 549 too limited to allow solid attributions to a specific volcano. Nevertheless, the Latium volcanics, as previously
 550 known and confirmed by our data, show similar $^{87}\text{Sr}/^{86}\text{Sr}$ ranges, which are different from the products of other
 551 Italian volcanoes (e.g., Peccerillo, 2017). Thus, $^{87}\text{Sr}/^{86}\text{Sr}$ ratio can support an ascription of a tephra of unknown
 552 origin to the Latium volcanism, narrowing down the list of possible sources.
 553



554
 555 **Figure 8.** $^{87}\text{Sr}/^{86}\text{Sr}$ ratio values of selected tephra layers and literature proximal references for the 430-350 ka time interval. Abbreviations:
 556 cpx=clinopyroxene; fs=feldspar; pom=pumice. Data source: TF-85, TF-107, TF-111, TF-126, Castel Broco, TSP-3, Riano R-1: this study;
 557 literature data: ¹ Peccerillo (2017); ² Perini et al. (2004); ³ Sottili et al. (2019); ⁴ Gaeta et al. (2006; 2016); ⁵ Giaccio et al. (2013a).
 558

559
 560 **Table 4.** $^{87}\text{Sr}/^{86}\text{Sr}$ ratio values of the selected four Fucino tephra and three proximal units.

Tephra/sample	Setting	Volcano	Glass composition	Analysed material	$^{87}\text{Sr}/^{86}\text{Sr}$	2 σ
TF-85	distal	Colli Albani	K-foidite	lc	0.710430	± 0.000007
TF-107	distal	unknown	phonolite	fsp	0.710851	± 0.000006
				pum	0.709507	± 0.00006
				fsp	0.710671	± 0.000006
TF-111	distal	Vulsini-Vico	phonolite	cpx	0.710149	± 0.000007
				fsp	0.711105	± 0.000007
TF-126	distal	Vulsini	phonolite	cpx	0.710960	± 0.000006
				fsp	0.710965	± 0.000006
TSP-3	proximal	Vulsini	phonolite	pum	0.711199	± 0.000007
				fsp	0.711245	± 0.000006
Riano R-1	mid-proximal	Vulsini	phonolite	K-fsp	0.710810	± 0.000007

561 Abbreviations: K-fsp=K-feldspar; fsp=feldspar; cpx=clinopyroxene; pum=pumice.
 562

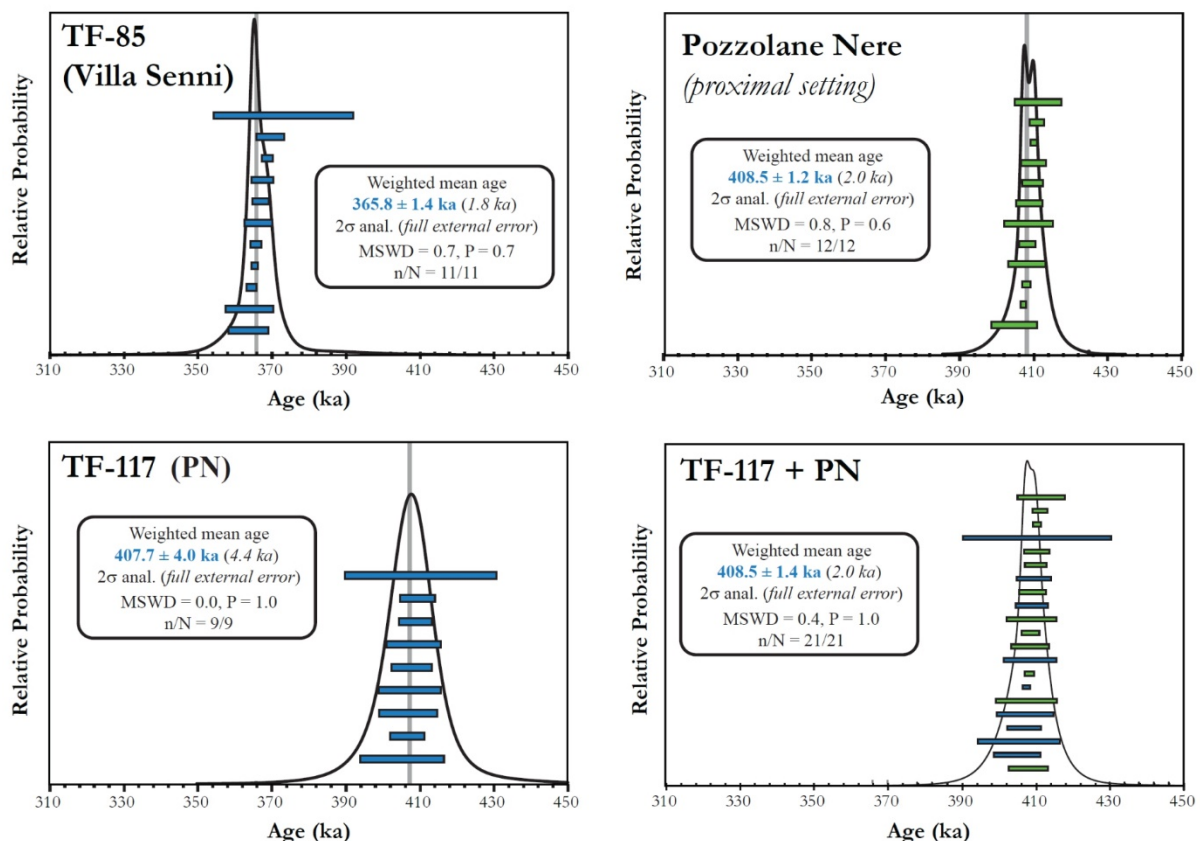
563 **4.3. $^{40}\text{Ar}/^{39}\text{Ar}$ age of TF-85, TF-117 and Pozzolane Nere**

564 The results for each dated deposit are presented as probability diagrams in Figure 9. Reported uncertainties
565 are analytical at a 95.5% of confidence limit (J-value included), as well as fully propagated ones. Detailed
566 analytical data are available in Supplementary Dataset-3 (SD-3).

567 **TF-85 (Villa Senni):** A total of eleven leucite single crystals were dated. All crystals yielded an
568 undistinguishable age, allowing us to calculate a meaningful weighted mean age of $365.8 \pm 1.4/1.8$ ka (MSWD
569 $=0.7$, $P=0.7$).

570 **TF-117 (Pozzolane Nere):** Nine leucite crystals were individually dated. All crystals yielded an
571 undistinguishable age, allowing the straightforward calculation of a weighted mean age of $407.7 \pm 4.0/4.4$ ka
572 (MSWD $=0.04$, $P=1.0$).

573 **Pozzolane Nere (Rome proximal setting):** Twelve leucite crystals were dated. They all share a similar age
574 within uncertainties, allowing us to calculate a statistically meaningful weighted mean age of $408.5 \pm 1.2/2.0$
575 ka (MSWD $=0.8$, $P=0.6$). In Figure 9 we also combined the 21 single leucite ages obtained on the Pozzolane
576 Nere from both the proximal deposits (PN) and distal equivalent (TF-117), allowing us to propose a new, more
577 precise weighted mean age of $408.5 \pm 1.4/2.0$ ka (MSWD $=0.4$, $P=1.0$) for the Pozzolane Nere regional marker.
578



579

580 **Figure 9.** $^{40}\text{Ar}/^{39}\text{Ar}$ on single grain results (leucite crystals), presented as probability diagrams, for TF-85 (Villa Senni), TF-117 (Pozzolane
581 Nere) and Pozzolane Nere (Rome proximal setting). A combined weighted mean age of TF-117/Pozzolane Nere is then proposed. Ages
582 are calibrated according to [Renne et al. \(2011\)](#) total ^{40}K decay constant and from the optimization calibrated age of 1.1891 Ma for the flux
583 standard ACs-2 ([Niespolo et al., 2017](#)). Individual crystal error bars are at 1σ of uncertainties.
584
585

5. Discussion

586 **5.1. Volcanic sources of tephra layers from core F4-F5**

587 **5.1.1. K-foidites (CG-1)**

588 The K-foidite compositions of the two tephra layers from CG-1 (Fig. 6) are distinctive within the context of
589 Quaternary Italian volcanism, being limited to a few eruptive sources (e.g., Peccerillo, 2017). Among these,
590 the Colli Albani volcanic district has produced and dispersed several K-foiditic tephra (e.g., Marra et al., 2009)
591 from moderate to major eruptions that have been traced in both medial and distal settings (e.g., Giaccio et al.,
592 2013a, 2014; Petrosino et al., 2014b, Leicher et al., 2016). Consequently, Colli Albani should be regarded as
593 the most likely source of TF-100 and TF-108.

594

595 **5.1.2. Potassic phonotephrites, tephriphonolites, phonolites, trachytes, trachyte-phonolites and latites (CG2)**

596 The glass geochemical compositions of tephra from CG-2 (i.e., potassic phonotephrites, tephriphonolites,
597 phonolites, trachytes, trachyte-phonolites and latites) are quite common and shared by almost all peri-
598 Tyrrhenian potassic volcanoes of central-southern Italy (e.g., Peccerillo, 2017). However, considering the time
599 interval investigated here (430-365 ka), we can confidently exclude the Neapolitan volcanoes (i.e., Ischia,
600 Procida, Campi Flegrei and Somma-Vesuvius) as possible sources of any of the twenty-one CG-2 tephra
601 layers, since the so-far oldest known eruption from these volcanoes is significantly younger (i.e., the $\sim 289.6 \pm$
602 1.9 ka Seiano Ignimbrite; De Vivo et al., 2001; Rolandi et al., 2003; Belkin et al., 2016; Fig. 3). Nevertheless,
603 a geochemical fingerprinting approach remains essential, as there is always the possibility that Neapolitan
604 volcanism may be extended deeper in time with future investigations, particularly since some distal archives
605 seem to suggest older activity in the region (e.g., Giaccio et al., 2014; Petrosino et al., 2015).

606 To discriminate the source of this large group of tephra, we employed the CaO/FeO vs Cl classification diagram
607 (Giaccio et al., 2017), which defines quite distinct fields for the individual sources of the Latium and Neapolitan
608 pyroclastic rocks with a SiO₂ content ranging from 52 wt% to 67 wt% (Fig. 7c-I). This confirms the lack of
609 products from the Neapolitan volcanoes and points to the Latium or Roccamonfina volcanoes as the only
610 plausible sources of 17 out of 21 - i.e., those with $52 < \text{SiO}_2 \text{ wt\%} < 67$ - CG-2 Fucino tephra (Fig. 7c-I).
611 Furthermore, the trace element compositions of all the phonolite and trachyte glass shards from the CG-2 (and
612 CG-3) tephra layers also clearly precludes the Neapolitan volcanoes as possible eruptive sources (Fig. 7a-b).

613

614 **Vulsini** – In the CaO/FeO vs Cl diagram TF-107 and TF-111 plot at the boundary between Vulsini-Vico
615 (northern Latium) and Roccamonfina fields (Figs. 7c-II and 7c-IV), making the attribution to one of these
616 sources not straightforward. However, a slight difference in Cl content between Vulsini-Vico and
617 Roccamonfina tephra, clustering between 0.05 wt% up to 0.20 wt% and 0.25-0.33 wt%, respectively (cfr. Fig.
618 7c-II with 7c-IV), makes the distinction between the two volcanic sources still tenable. More importantly, in this
619 diagram, TF-107 and TF-111 overlap the composition of the Vulsini proximal pyroclastic units analysed in the
620 present study (especially TSP-3 Pumice fall from Tuscania-San Pietro section; Fig. 7c-II), suggesting that
621 Vulsini is the most probable source of these tephra layers. More detailed, individual tephra correlations are
622 discussed below (see section 5.2.3.3.) and fully support this volcanic source attribution. Finally, despite the
623 paucity of the proximal reference dataset, ⁸⁷Sr/⁸⁶Sr ratios also support a Vulsini origin for these two tephra
624 layers (Fig. 8), while the trace elements confirm an origin from northern Latium (Vulsini or Vico) volcanoes
625 (Fig. 7b).

626 The Riano R-1 tephra (404.7 ± 5.0 ka; [Marra et al., 2018](#)), for which a clear stratigraphic/compositional
 627 correlation is still lacking, also matches the compositions of the Vulsini units analysed in this study. It is
 628 therefore compatible with a possible distal origin from Vulsini, rather than from the nearest Sabatini source.

629
 630 **Vulsini-Vico** – Cl contents and CaO/FeO ratios of TF-88, TF-89, TF-90, TF-96, TF-97, TF-98, TF-110, TF-
 631 120 and TF-124 are consistent with either Vico or Vulsini compositions, and thus do not allow a further
 632 discrimination between these two potential sources ([Fig. 7c-III](#)). However, a discrimination is possible based
 633 on further oxides composition as discussed in section 5.2.3.4.

634
 635 **Sabatini** – According to the CaO/FeO vs Cl diagram, TF-106 and TF-122 can be related to the Sabatini
 636 Volcanic District based on the high (i.e., >1.15) CaO/FeO ratio ([Fig. 7c-IV](#)). TF-106 forms along with TF-102,
 637 TF-103 and TF-104 a well-defined cluster of tephra that share a similar phonotephritic composition ([Fig. 6](#);
 638 [SD-1](#)) and lithology ([Table 2](#)). Therefore, though the CaO/FeO vs Cl discrimination diagram cannot be applied
 639 to TF-102, TF-103 and TF-104 because of their SiO₂ content being lower than 52 wt%, ([Giaccio et al., 2017](#)),
 640 they can be reliably regarded as part of a cluster of eruptions from Sabatini. Although showing a more scattered
 641 composition in the CaO/FeO vs Cl diagram ([Fig. 7c-IV](#)), TF-121 can be attributed to the Sabatini as well,
 642 because of its close geochemical similarity with the directly underlying TF-122 layer ([Fig. 5](#)). Finally, TF-123
 643 can be also likely attributed to the Sabatini, because of its homogenous composition in the CaO/FeO vs Cl
 644 diagram that matches a second well-defined compositional cluster of the Sabatini rock types ([Fig. 7c-IV](#)).

645
 646 **Roccamonfina** – TF-93 and TF-94 can be confidently attributed to the Roccamonfina volcano, based on the
 647 relatively high Cl content (i.e., >0.25 wt%), and thus their clear position in the Roccamonfina field of the
 648 CaO/FeO vs Cl diagram ([Fig. 7c-IV](#)), which is quite distinctive with respect to the Latium volcanoes ([Fig. 7c-
 649 IV](#)).

650
 651 **5.1.3. K-rhyolites (CG-3)**

652 The six tephra layers forming CG-3 (TF-99, 109, 114, 115, 116, 125; [Fig. 6](#)) show K-rich rhyolitic and trachy-
 653 rhyolitic compositions, which is quite unusual within the context of the peri-Tyrrhenian Quaternary Italian
 654 volcanism, and peculiar to Vico Volcano (e.g., [Perini et al., 1997, 2000, 2003, 2004](#); [Perini and Conticelli, 2002](#);
 655 [Pereira et al., 2020](#)), hence the most probable source of the Fucino CG-3 tephra layers.

656
 657 In summary, based on distinctive chemical compositions, stratigraphic clues and lithological features and
 658 affinities, we propose an attribution of the Fucino tephra layers to the peri-Tyrrhenian potassic volcanoes, as
 659 summarized in [Table 5](#).

660
 661 **Table 5.** Volcanic sources of the investigated Fucino tephra, inferred from glass chemical composition and lithological features.

Volcano	Fucino tephra
Vulsini	TF-107, TF-111
Vico	TF-99, TF-109, TF-114, TF-115, TF-116, TF-125
Vulsini or Vico	TF-88, TF-89, TF-90, TF-96, TF-97, TF-98, TF-110, TF-120, TF-124
Sabatini	TF-102, TF-103, TF-104, TF-106, TF-121, TF-122, TF-123
Colli Albani	TF-100, TF-108
Roccamonfina	TF-93, TF-94

662

663 **5.2. Individual tephra correlation**

664 5.2.1. Tephra from Colli Albani (CG-1).

665 **TF-100 and TF-108** - These two K-foiditic tephra layers (CG-1), ascribed to the Colli Albani activity, occur
666 between TF-85 and TF-117 (Fig. 2), which were attributed to the Villa Senni (365.8 ± 1.4 ka) and Pozzolane
667 Nere (408.5 ± 1.4 ka) eruptions, respectively (Giaccio et al., 2019). The $^{87}\text{Sr}/^{86}\text{Sr}$ composition determined in
668 this study for TF-85 further supports its attribution to the Villa Senni eruption. Indeed, $^{87}\text{Sr}/^{86}\text{Sr}$ ratios of the
669 Colli Albani products show a strong time-dependent variability (Gaeta et al., 2006, 2016; Giaccio et al., 2013a)
670 and the $^{87}\text{Sr}/^{86}\text{Sr}$ value obtained for TF-85 precisely matches that of Villa Senni (Fig. 8).

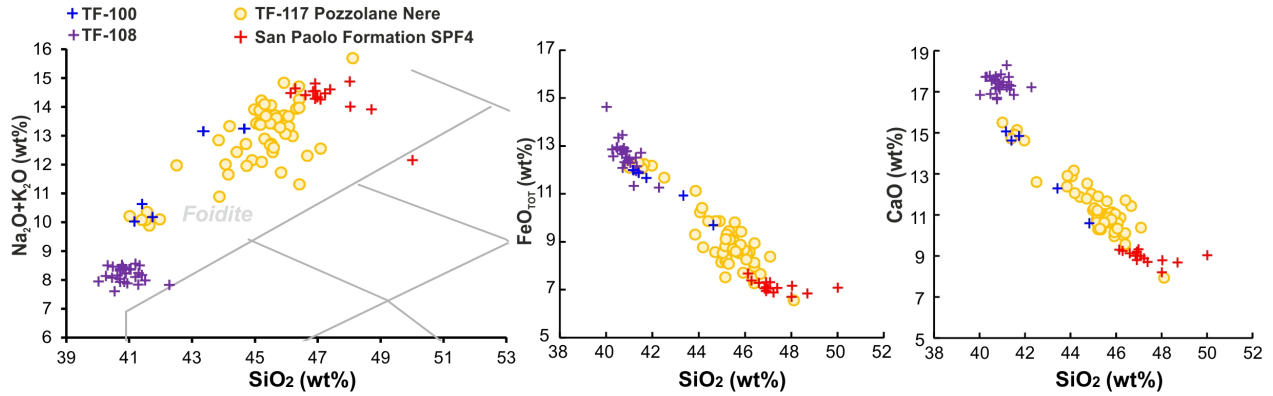
671 Considering the available chronological constraints and its relative proximity to the TF-117/Pozzolane Nere,
672 TF-108 can be attributed to the post-caldera phase of the Pozzolane Nere eruptive cycle (*sensu* Gaeta et al.,
673 2016), which is equivalent to the Centogocce fall succession of Giordano et al. (2006). In proximal settings,
674 the Centogocce deposits consist in a series of scoria-lapilli fall beds and lava flows overlying the Pozzolane
675 Nere deposits, emplaced in the 403.4 ± 5 ka - 396.4 ± 5 ka time interval (recalculated ages from Marra et al.,
676 2009 and Gaeta et al., 2016). Unfortunately, no glass composition is available for this scoria fall succession,
677 and therefore, we used the composition of TF-117/Pozzolane Nere for comparison (Fig. 10a). Furthermore,
678 Pereira et al. (2020) have recently reported the occurrence, within the San Paolo Formation aggradational
679 succession, of a tephra layer (SPF4), with a polymodal rhyolite, K-foidite and phonotephrite composition,
680 interpreted as a reworked volcanoclastic layer containing both Vico and Colli Albani eruption products. Pereira
681 et al. (2020) reported an age of 403.5 ± 4.2 ka for SPF4, which is consistent with the time interval (403.4 ± 5
682 ka - 396.4 ± 5 ka) covered by the Centogocce fall succession, despite a geochemical mismatch of TF-108 with
683 SPF4 (Fig. 10a), which can be expected for multiple explosive and effusive eruptions occurred during a
684 relatively long interval. Based on glass composition and stratigraphic position relatively to the TF-
685 117/Pozzolane Nere, we attribute TF-108 to the Centogocce activity. The stratigraphic position of TF-100,
686 between the TF-117/Pozzolane Nere and the TF-85/Villa Senni (Fig. 2), suggests an age substantially younger
687 than the Centogocce equivalent TF-108. In spite of this, for its composition which partially overlaps the wide
688 composition field of the Pozzolane Nere (Fig. 10a), TF-100 could still be considered as part of the final stage
689 of the Pozzolane Nere eruptive cycle.

690

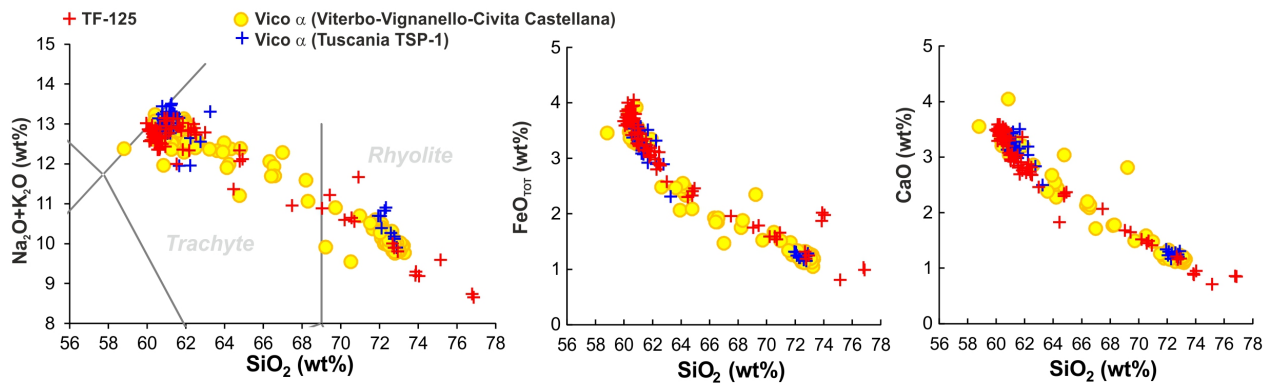
691 5.2.2. Tephra from Vico (CG-3).

692 **TF-125** – This tephra occurs in the lowermost portion of the F4-F5 record, ~50 cm upsection from TF-126 that
693 was directly dated at 424.3 ± 3.2 ka (Giaccio et al., 2019). TF-125 is characterized by a heterogeneous
694 phonolite-trachyte to rhyolite composition, with a silica content ranging from 59 to 77 wt% and an alkali content
695 from 14 to 8 wt%. Recently, Pereira et al. (2020) published new glass geochemical compositions for the early-
696 emplaced volcanics of Vico activity (Vico Period I; Perini et al., 2004), including Vico α and Vico β Plinian fall
697 markers (Cioni et al., 1987), both with a dominant rhyolitic composition, along with the characterization of three
698 minor events (i.e., Vico β_{top} , Vico γ and Vico δ ; Cioni et al., 1987). In addition, Pereira et al. (2020) acquired
699 very precise $^{40}\text{Ar}/^{39}\text{Ar}$ ages for Vico α (414.8 ± 2.2 ka), Vico β (406.5 ± 2.4 ka), Vico β_{top} (406.4 ± 2.0 ka) and
700 Vico δ (399.7 ± 3.0 ka).

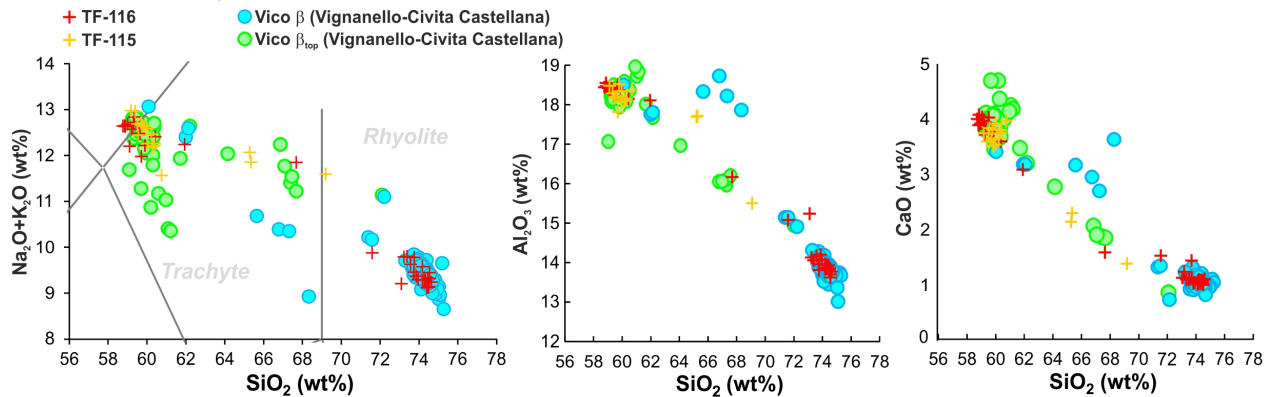
a) **Colli Albani Centogocce (402.7±5.0-396.7±5.0 ka)**



b) **Vico α (414.8±2.2 ka)**



c) **Vico β -Vico β_{top} (406.5±2.4 ka - 406.2±2.0 ka)**



d) **Vico γ (>399.7±3.0, < 406.2±2.0 ka)**

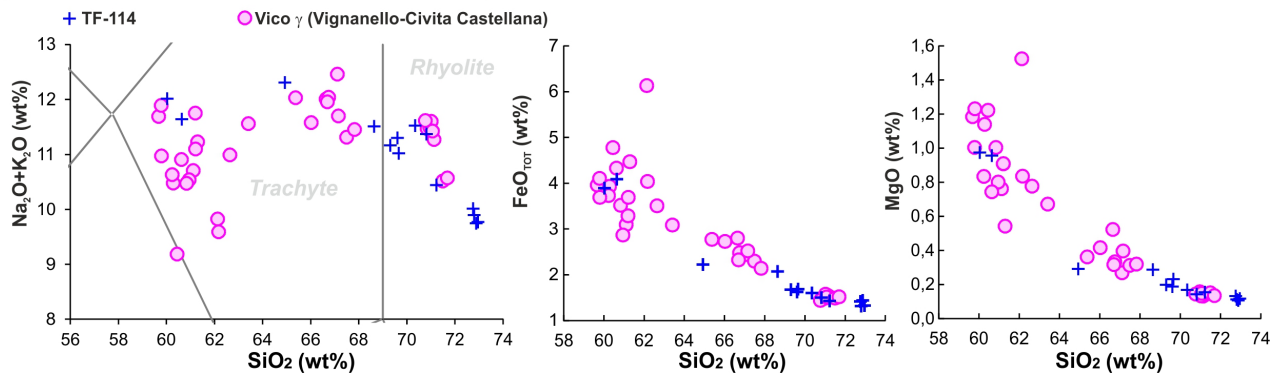


Figure 10. Total alkali versus silica (TAS) classification diagram after [Le Maitre et al. \(2002\)](#) and representative bi-plots for TF-100, TF-108, TF-114, TF-115, TF-116 and TF-125 from the F4-F5 tephra record, compared with SPF4 tephra layer from the San Paolo aggradational succession, Pozzolane Nere (TF-117), proximal Vico α , Vico β , Vico β_{top} and Vico γ units from Vico volcano. Data source: WDS glass composition of TF-100, TF-108, TF-114, TF-115, TF-116, TF-125 and Vico α (TSP-1): this study; WDS glass composition of

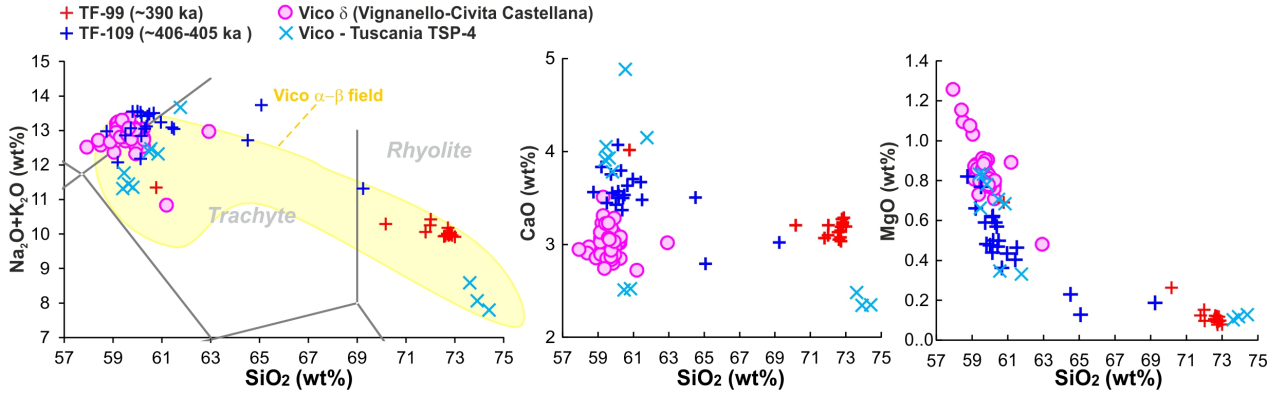
707 TF-117/Pozzolane Nere: [Giaccio et al. \(2017\)](#); WDS glass composition and $^{40}\text{Ar}/^{39}\text{Ar}$ age of tephra SPF4, Vico α , Vico β , Vico β_{top} and
708 Vico γ , sampled at Viterbo (VT), Civita Castellana (CC) and Vignanello (VIG): [Pereira et al. \(2020\)](#). $^{40}\text{Ar}/^{39}\text{Ar}$ ages are recalculated relative
709 to an age of 1.1891 Ma for the Alder Creek sanidine monitor standard ([Niespolo et al., 2017](#)), with the uncertainty expressed at 2σ .
710

711 Using this updated geochemical dataset for the Vico Period I products, we found that TF-125 major element
712 composition matches that of Vico α of [Pereira et al. \(2020\)](#) and of Tuscania-San Pietro TSP-1 (this study; [Fig.](#)
713 [10b](#)), and this correlation is further strengthened by the similarities in the trace element glass compositions
714 obtained here for Vico α and TF-125 ([Fig. 11a](#)). Considering this geochemical affinity and its stratigraphic
715 position between TF-126 (424.3 ± 3.2 ka) and TF-117/Pozzolane Nere (408.5 ± 1.4 ka), consistent with an
716 age of 414.8 ± 2.2 ka, we can confidently correlate TF-125 to the Vico α Plinian eruption.

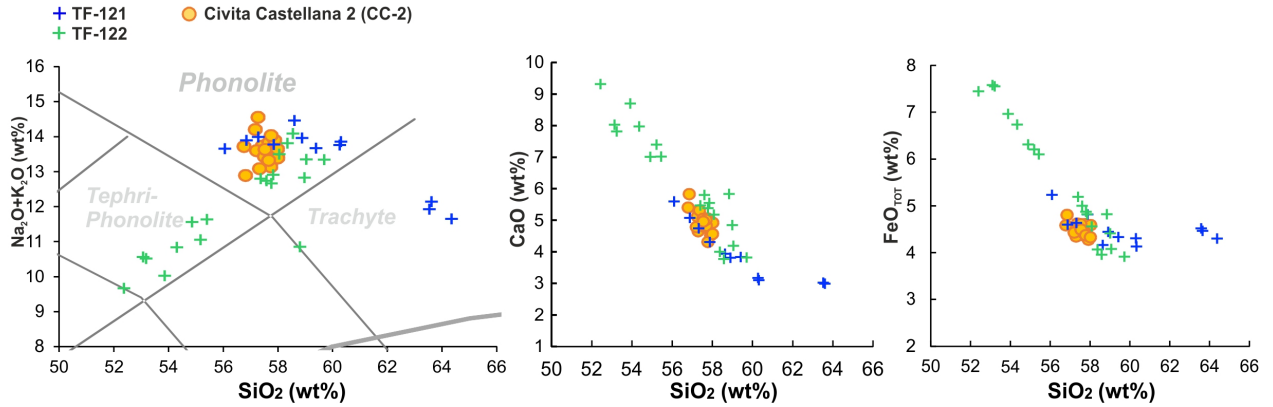
717
718 **TF-116 and TF-115** – TF-116 is located less than 1 m upsection from TF-117, the latter dated at 407.7 ± 4.0
719 ka and correlated to the Pozzolane Nere eruption ([Giaccio et al., 2019](#)), which has been dated here more
720 precisely at 408.5 ± 1.4 ka ([Fig. 9](#)). Like TF-125, this tephra is characterized by a heterogeneous trachytic-
721 rhyolitic composition, with a dominant SiO_2 -rich (>75 wt%) rhyolitic component, and a minor scattered
722 phonolitic-trachytic one (58-68 wt% SiO_2), which is a distinctive, common features of the Vico Period I units
723 ([Pereira et al., 2020](#)). Trace element analyses ([Fig. 7a-b](#)) also support a Latium origin for this tephra.
724 Specifically, the glass rhyolitic composition of TF-116 matches that of Vico β ([Fig. 10c](#)) that, along with its
725 position on top of TF-117/Pozzolane Nere, allows us to correlate TF-116 to Vico β eruption (406.5 ± 2.4 ka;
726 [Pereira et al., 2020](#)). Noteworthy, TF-116 contains a significant trachyte-phonolite component that is poorly
727 represented or documented in proximal settings ([Fig. 10c](#)).

728 TF-115 tephra is found 2 cm above TF-116 and is characterized by a heterogeneous composition, consisting
729 of a main phonolitic-trachytic component (SiO_2 59-66 wt%) and a minor SiO_2 -rich (~ 69 wt%) rhyolitic one.
730 These geochemical features allow unambiguous correlation to Vico β_{top} ([Fig. 10c](#)), consistent with the
731 superposition of the tephra just on top of TF-116/Vico β . Furthermore, consistent with its strict stratigraphic
732 proximity to TF-116/Vico β , the proximal Vico β_{top} has a $^{40}\text{Ar}/^{39}\text{Ar}$ age of 406.5 ± 2.4 ka that is indistinguishable
733 from that of Vico β ([Pereira et al., 2020](#)). Noteworthy, [Pereira et al. \(2020\)](#) also pointed out that the combined
734 glass composition of Vico β and Vico β_{top} is to some extent similar to that of Vico α , so that, in the absence of
735 strong chronological and/or tephrostratigraphic constraints, the geochemical composition of the two units could
736 be potentially confused. However, in the F4-F5 record, the TF-115 and TF-116 couplet occurs on top of the
737 408.5 ± 1.2 ka Pozzolane Nere tephra, well upsection from the Vico α correlative (TF-125). Furthermore, when
738 dealing with sedimentary archives not so well constrained [chronostratigraphically](#) as Fucino, trace element
739 analysis of the Vico eruption products may offer useful means to discriminate the distal equivalents of Vico α
740 and Vico β . In fact, the [phonolite-trachyte](#) end-member glasses of TF-116/Vico β extend to greater levels of
741 incompatible trace element enrichment with respect to TF-125/Vico α ([Fig. 11a-left](#)), whilst the analysis of
742 proximal and distal Vico rhyolitic products reveals greater depletions in Sr associated with the Vico β tephra
743 ([Fig. 11a-right](#)), likely induced by major K-feldspar fractionation. In conclusion, the general stratigraphic,
744 chronological, and geochemical features of TF-116 and TF-115 consistently support their unambiguous
745 attribution to Vico β and Vico β_{top} , respectively.
746

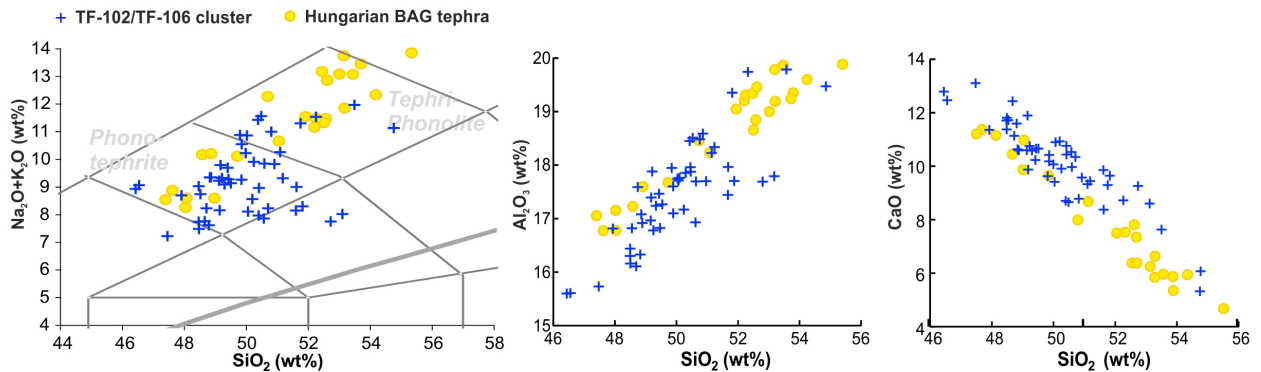
a) Vico unknown (~406-405 ka - ~390 ka)



b) Sabatini Civita Castellana 2 (>408.5, <415 ka)



c) Sabatini unknown (>390 ka, <405 ka)



d) Roccamonfina Mt. Ofelio-Mt. Capitulo (398.5±18.0 ka - 385.6±16.0 ka)

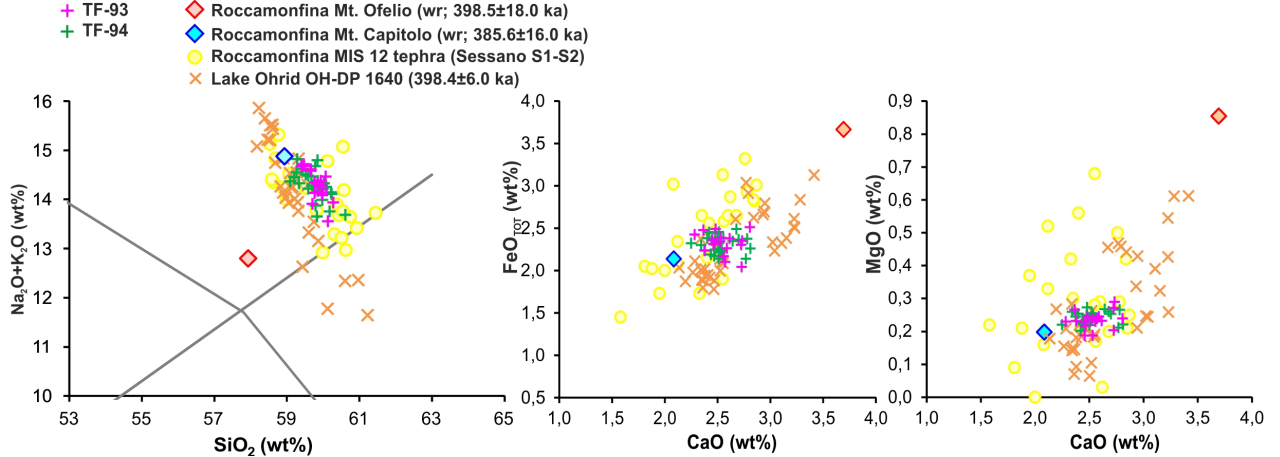


Figure 12. TAS diagram after [Le Maitre et al. \(2002\)](#) and representative bi-plots for the tephra TF-93, TF-94, TF-99, TF-102, TF-103, TF-104, TF-106, TF-109, TF-121 and TF-122 from the F4-F5 record, compared with proximal Vico δ units from Vico volcano, TSP-4 from

769 Tuscania-San Pietro succession, CC-2 from Civita Castellana succession, the distal Bag tephra from the MIS 10 Hungarian loess, tephra
770 OH-DP-1640 from Lake Ohrid and Sessano-1 and 2 (S1-S2) tephra from Sessano basin. For comparison, in panel a), the compositional
771 field of the major Vico α and Vico β Plinian eruptions is also shown. Data source: WDS glass composition of TF-93, TF-94, TF-99, TF-
772 102, TF-103, TF-104, TF-106, TF-109, TF-121, TF-122, TF-123, and TSP-4: this study; WDS glass composition and $^{40}\text{Ar}/^{39}\text{Ar}$ age of Vico
773 δ and CC-2, sampled at Vignanello (VIG) and Civita Castellana (CC), respectively: [Pereira et al., 2020](#); WDS glass composition and
774 modelled age of tephra OH-DP-1640: [Leicher et al. \(2019\)](#); WDS glass composition and of Bag tephra: [Pouclet et al. \(1999\)](#); post-Rio
775 Rava – pre-Brown Leucitic Tuff whole-rock compositions: [Rouchon et al. \(2008\)](#); S1 and S2 SEM-EDS glass composition: [Russo Ermolli
776 et al. \(2010\)](#). $^{40}\text{Ar}/^{39}\text{Ar}$ ages are recalculated relative to an age of 1.1891 Ma for the Alder Creek sanidine monitor standard ([Niespolo et
777 al., 2017](#)), with the uncertainty expressed at 2σ .

778
779 **TF-99 and TF-109** - TF-99 has a predominantly homogeneous rhyolitic composition (70-73 wt% of SiO_2) with
780 a single trachytic shard (60 wt% SiO_2), while TF-109 is characterized by a heterogeneous trachytic composition
781 (59-65 wt% SiO_2) with a minor rhyolitic component (one shard with ~69 wt% SiO_2 ; [Fig. 12a](#)). As stated in
782 section 5.1.3, the occurrence of a rhyolitic component in these tephra makes their attribution to the Vico
783 volcano quite straightforward, because it is the only known Middle Pleistocene peri-Tyrrhenian volcanic source
784 that produced K-rich rhyolitic tephra. Indeed, in the TAS diagram, both tephra plot within the compositional
785 field of the Vico α and Vico β Plinian eruptions ([Fig. 12a](#)).

786 Considering the stratigraphic position of TF-99 and TF-109 within the F4-F5 record, the most plausible
787 candidate for at least one of these tephra layers would be Vico δ , dated at 399.7 ± 3.0 ka ([Pereira et al., 2020](#)).
788 However, neither TF-99 nor TF-109 match Vico δ in composition ([Fig. 12a](#)). Although in the TAS diagram TF-
789 109 would seem compatible with Vico δ , suitable bi-plot diagrams show significant differences on several
790 oxides (e.g., CaO content; [Fig. 12a](#)). On the other hand, the geochemical composition of TF-109 is consistent
791 with the TSP-4 unit of the Tuscania-San Pietro succession ([Fig. 12a](#)). Thus, TF-109/TSP-4 and TF-99 can be
792 only generically attributed to the Vico Period I, their proximal equivalents at Vico not yet identified.

793 794 795 5.2.3. *Tephra of Compositional Group-2 (CG-2)*

796 5.2.3.1. *Sabatini tephra*

797 **TF-102, TF-103, TF-104, TF-106, TF-121, TF-122 and 123** - The geochemical composition of the TF-102/106
798 and TF-121/122 clusters are quite heterogeneous, with a SiO_2 content ranging from 46 wt% to 55 wt% and
799 from 52 wt% to 64 wt%, respectively ([Fig. 12c and 12b](#), respectively). TF-123 shows instead a homogenous
800 high-alkali tephriphonolitic composition ([Fig. 6](#)).

801 The TF-102/106 cluster occurs just on top of TF-108, thus constraining its position close to the Centogocce
802 succession time interval (403.4 ± 5 ka - 396.4 ± 5 ka). TF-121/122 and TF-123 occur instead between TF-125
803 (Vico α , 414.8 ± 2.2 ka; [Pereira et al., 2020](#)) and TF-118 (Fontana Ranuccio, 407.0 ± 4.2 ka; [Pereira et al.,
804 2018](#)), or the more precisely dated TF-117/PN (408.5 ± 1.2 ka), constraining their ages in the narrow time
805 interval between ~415 ka and ~408 ka. Hence, both the TF-102/106 and TF-121/122 clusters and TF-123 can
806 be attributed to the Southern Sabatini activity ([Fig. 3](#); [Sottili et al., 2004, 2010](#)), which was characterized by
807 the emplacement of widespread sub-Plinian to Plinian fall deposits in the time interval ~500-380 kyr ([Marra et
808 al., 2014, Sottili et al., 2019](#)).

809 Though no relevant activity is documented in the ~414-402 ka timespan of TF-121/122 and TF-102/106
810 clusters, recent investigations point to the occurrence of a previously unrecognized Sabatini unit
811 chronologically and geochemically consistent with TF-121/122 ([Pereira et al., 2020](#)). Specifically, at Civita
812 Castellana ([Fig. 1b](#)), [Pereira et al. \(2020\)](#) described a ~1 m-thick pumice fall unit (CC-2), phonolitic in
813 composition and tentatively ascribed it to Sabatini activity, sandwiched between Vico α (CC-1; 414.8 ± 2.2 ka)
814 and Vico β (CC-3; 406.5 ± 2.4 ka), i.e., a similar stratigraphic position of TF-121/122 within the F4-F5

815 succession. This unit was also found at San'Abbondio section (Fig. 1b) immediately on top of Vico α (Pereira
816 et al., 2020). Although more variable, in terms of geochemical composition, both TF-121 and TF-122 are
817 compatible with CC-2 phonolitic glass composition (Fig. 12b). Among the two layers, the thickest TF-121
818 seems to show a higher degree of geochemical similarity, and thus is a good candidate for correlation with
819 CC-2 pumice fall, while the thinner TF-122 could represent a minor eruption slightly preceding CC-2 fall.
820 In contrast, TF-123, whilst sharing a broadly similar chrono-stratigraphic position to the overlying TF-121/122
821 deposits, shows no geochemical similarity to the CC-2 pumice fall and thus must be considered the product of
822 a slightly older, unknown Sabatini eruption.
823 Similarly, the TF-102/106 cluster has no chronological and stratigraphical relative in the currently
824 determined Sabatini proximal eruption record. This cluster would be instead chronologically consistent with
825 the activity of the Volsci volcanic field and specifically with Pofi Scoria cone and Amafi scoria cone, dated at
826 394.4 ± 3.5 ka and 395.8 ± 6.1 ka (Marra et al., 2021), respectively, likely equivalent to the Cava Pompei scoria
827 fall (392.7 ± 3.0 ka) and Isoletta I scoria fall (401.7 ± 3.0 ka) (Pereira et al., 2018). However, the lack of any
828 geochemical glass compositional data currently prevents any possible comparison and correlation with TF-
829 102/106.
830 In contrast, in the ultra-distal setting, the TF-102/106 cluster would be geochemically and chronologically
831 compatible with the so-called Bag Tephra (Fig. 12c), interbedded in Quaternary loess deposits of Hungary and
832 Slovakia (Poulet et al., 1999; Hum, 2005; Sági et al., 2008). In fact, the Bag Tephra has a phonotephritic-
833 tephriphonolitic glass composition (Poulet et al., 1999) very similar to that of the TF-102/106 cluster (Fig.
834 12c). The Bag tephra is commonly found below the so-called Basaharc Lower paleosol of the MIS 9 period
835 (Horváth and Bradák, 2014), thus consistent with the age of TF-102/106. The previous tentative correlation to
836 the Villa Senni eruption (Poulet et al., 1999) is ruled out by glass geochemistry. More recent petrographic
837 investigations (Sági et al., 2008) point out that the Bag tephra likely represents multiple tephra layers.
838 Therefore, the tephra cluster TF-102/106 would be a good candidate for a correlation with such an important
839 marker of the Hungarian loess. However, at present we can only propose a tentative correlation with either an
840 unknown Sabatini eruption cluster or the Pofi Scoria and Amafi centers of the Volsci volcanic field.

841

842 5.2.3.2. Roccamonfina tephra

843 **TF-93 and TF-94** – Both tephra layers are characterized by an almost homogeneous phonolitic composition,
844 with a SiO₂ content of ~59-61 wt% and alkali content ranging between ~13.5 and ~14.5 wt%. Considering their
845 position within the F4-F5 succession, between TF-85 (Villa Senni, 365.8 ± 1.2 ka) and TF-115 (Vico β_{top} , 406.4
846 ± 2.0 ka), the two tephra can be associated with the post-Rio Rava/pre-Brown Leucitic Tuff stage (355-440 ka;
847 Rouchon et al., 2008) of Roccamonfina Volcano, and, more specifically, to the activity of the Monte Ofelio-
848 Monte Capitolo centers, dated to 398.5 ± 18.0 ka and 385.6 ± 16.0 ka (recalculated ages from Rouchon et al.,
849 2008). Although no glass composition is available for these Roccamonfina units, sample RMF6 of Monte
850 Capitolo (398.5 ± 18.0 ka; Rouchon et al., 2008) has a whole rock phonolitic composition, which is consistent
851 with that of the two Fucino tephra (Fig. 12d). The attribution of the two tephra to Roccamonfina is further
852 supported by the analogous composition of two slightly older (i.e., MIS 12) Roccamonfina tephra layers (S1-
853 S2) from the Sessano basin, southern Italy, located immediately east of this volcano (Russo Ermolli et al.,
854 2010). Furthermore, the OH-DP-1640 tephra from Lake Ohrid (modelled age of 398.4 ± 6.0 ka; Leicher et al.,
855 2019), ascribed to Roccamonfina, could be tentatively correlated with TF-93/94 (Fig. 12d), based on a similar

856 age and geochemical composition (besides minor differences). Therefore, TF-93 and TF-94 can be attributed
857 to the Monte Ofelio-Monte Capitolo centers and, based on good geochemical matching, more likely to the
858 latter. Future higher precision $^{40}\text{Ar}/^{39}\text{Ar}$ dating of these volcanic units in proximal setting will be of great interest
859 to strengthen the chronology and attribution proposed here.

860

861 5.2.3.3. *Vulsini tephra*

862 **TF-107, TF-111 and TF-126** – In addition to TF-107 and TF-111, likely attributed to the Vulsini activity based
863 on the Cl vs CaO/FeO diagram (Fig. 7c) as discussed above, here we also re-evaluate the TF-126 layer, in
864 light of the new acquired trace element data. Previously, TF-126 was tentatively correlated to the Castel Broco
865 eruption deposit of Vulsini volcano, as well as geochemically matched to the pumice fall pre-Vico α , found
866 immediately below Vico α in the proximal area of Vico Volcano (Pereira et al., 2020).

867 TF-107 and TF-111 are stratigraphically constrained between the ~365 ka TF-85/Villa Senni tephra and the
868 ~406 ka TF-115/Vico β_{top} . Within the Vulsini volcanic history (e.g., Palladino et al., 2010), the Pumice Fall 0
869 (PF-0) eruption (399.8 ± 18.0 ka; Turbeville, 1992), here tentatively identified with TSP-3 of the Tuscania-
870 San Pietro section, is the only known explosive event geochronologically consistent with both TF-107 and TF-
871 111. Of the two potential distal equivalents of PF-0/TSP-3, TF-111 shows a good geochemical match with
872 TSP-3 (Fig. 13a). Moreover, TSP-3 occurs below TSP-4 that has been here correlated to TF-109 (Fig. 12a),
873 which support the correlation of TF-111 with PF-0/TSP-3, even if $^{87}\text{Sr}/^{86}\text{Sr}$ ratios would seem to discount it
874 (Fig. 7).

875 Regarding the trace element compositions, we notice that both TF-111 and TF-126 share similar levels of
876 incompatible trace element enrichment to the trachytic components of the Vico α deposits, while they strongly
877 differ from Castel Broco (Fig. 11b). This feature, on one hand, would preclude the correlation of TF-126 with
878 Castel Broco and, on the other hand, would also raise doubts over the attribution of TF-111 and TF-126 layers
879 to Vulsini, suggesting instead an origin from Vico. We note, however, that trace element data for Vulsini
880 pyroclastic deposits are currently limited to only one sample from the co-eruptive basal fallout of Castel Broco
881 (Fig. 11b), thus, they may not be fully representative of either the entire compositional spectrum of the Castel
882 Broco eruption products, or even more so, the whole Vulsini eruptive successions. Therefore, to take a
883 conservative approach, while retaining a preferential attribution of TF-111 and TF-126 to the Vulsini district,
884 we cannot fully exclude a Vico source for TF-111/TSP-3 and TF-126/pre-Vico α . Indeed, the unambiguous
885 solution of this issue requires a statistically representative trace element dataset for both Vulsini and Vico
886 products, which is not available yet.

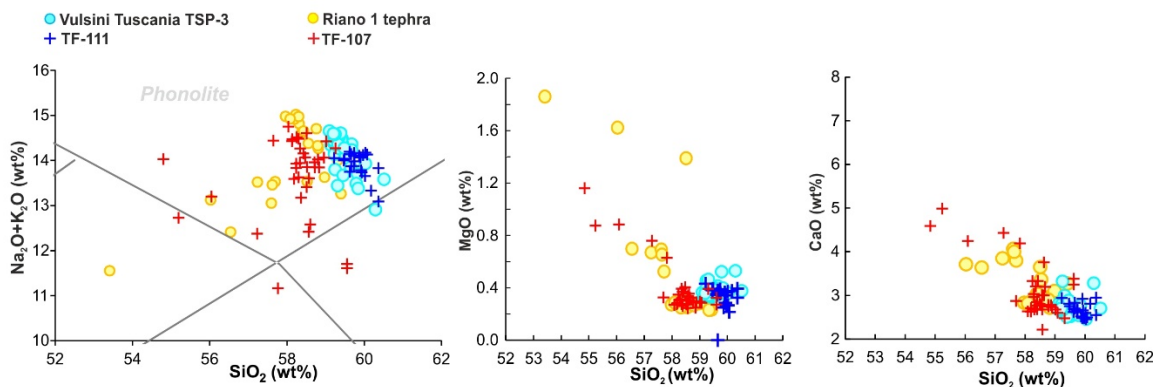
887 TF-107 shares a similar lithology and major element geochemistry with Riano R-1 tephra (Fig. 13a), here
888 tentatively attributed to the activity of the Vulsini volcanic district (Fig. 7c-II) and dated at 404.7 ± 5.0 ka (Marra
889 et al., 2018). While a correlation is further supported by very similar $^{87}\text{Sr}/^{86}\text{Sr}$ values (Fig. 8; Table 4),
890 preliminary trace element glass analyses reveal some inconsistency (Fig. 11b).

891

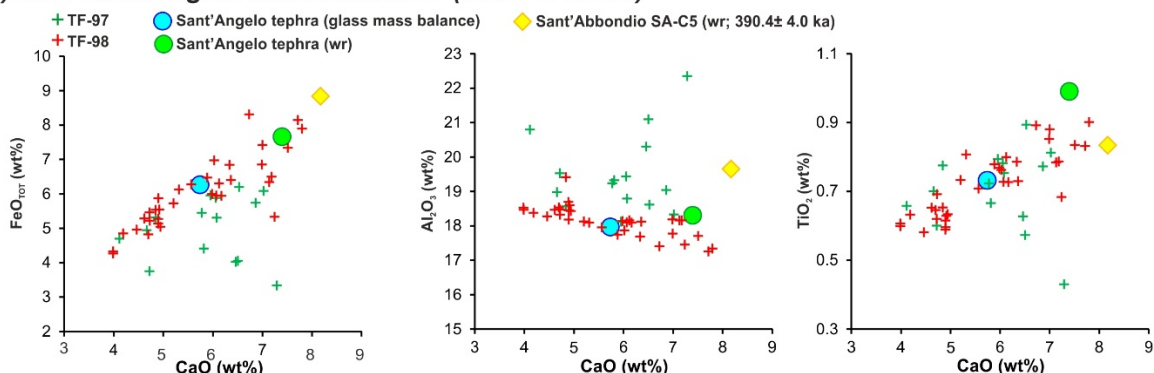
892

893

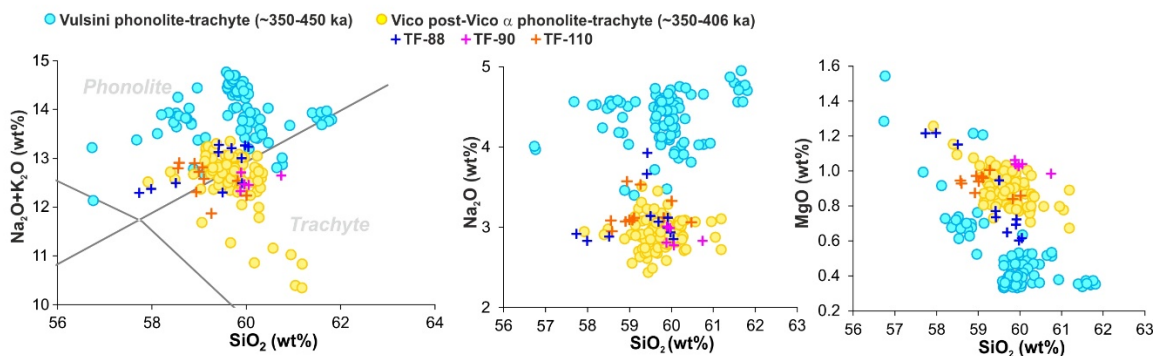
a) Vulsini Pumice Fall 0(?) (~405-406 ka) - Riano 1 (404.7± 5.0 ka)



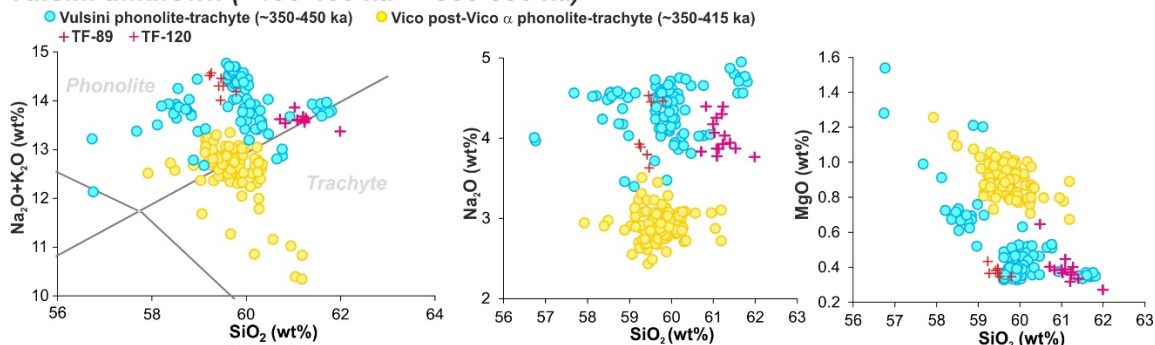
b) Vico Sant'Angelo-Sant'Abbondio (390.4± 4.0 ka)



c) Vico (~415-408 ka - ~366-390 ka)



d) Vulsini unknown (~406-405 ka - ~366-390 ka)



894
895
896
897
898
899
900
901
902
903
904

Figure 13. TAS diagram after [Le Maitre et al. \(2002\)](#) and representative bi-plots for the tephra TF-88, TF-89, TF-90, TF-107, TF110, TF-111, TF-120 and TF-124, compared with the proximal Vulsini unit TSP-3 from Tuscania-San Pietro section and Riano R-1 from the Riano succession (panel a), VCO 163 from Vico area, SA C4 and SA C5 from the Sant'Abbondio Fall succession (panel b) and with the proximal Vulsini (Casale delle Piane, Castel Broco, TSP-2 and TSP-3 from Tuscania-San Pietro section), and Post-Vico α Vico trachyte-phonolites (Vico β, Vico β_{top}, Vico γ) shown as blue and yellow circles in panels c) and d). Data source: WDS glass composition of tephra TF-88, TF-89, TF-90, TF-107, TF-110, TF-111, TF-120, Vulsini (TSP-2, TSP-3) and Riano R-1: this study; VCO 163 whole-rock geochemistry: [Perini et al. \(2004\)](#); SA C4 and SA C5 whole-rock geochemistry and ⁴⁰Ar/³⁹Ar age: [Marra et al. \(2014\)](#); ⁴⁰Ar/³⁹Ar age of R-1: [Marra et al. \(2018\)](#); WDS glass composition of Post-Vico α Vico phonolite-trachytes (Vico β, Vico β_{top}, Vico γ): [Pereira et al. \(2020\)](#). ⁴⁰Ar/³⁹Ar ages are recalculated relative to an age of 1.1891 Ma for the Alder Creek sanidine monitor standard ([Niespolo et al., 2017](#)), with the uncertainties expressed at 2σ.

905
906 **5.2.3.4. Vulsini vs. Vico tephra**

907 **TF-88, TF-89, TF-90, TF-96, TF-97, TF-98, TF-110, TF-120, TF-124** – These nine tephra layers are
908 characterized by Cl contents and CaO/FeO ratios consistent with both Vico and Vulsini volcanic sources (Fig.
909 [7c-III](#)).

910 TF-98 and TF-97 form, together with the rhyolitic tephra TF-99 (unambiguously from Vico; see section 5.2.2.),
911 a stratigraphically strictly related cluster located between TF-85/Villa Senni and TF-116/Vico β . The age of this
912 cluster is therefore bracketed between ~366 ka and ~406 ka. Among the potential Vico equivalents for TF-97
913 and TF-98, [Perini et al. \(2004\)](#) described the so-called Sant'Angelo tephra, which is stratigraphically
914 constrained between Vico β (406.5 ± 2.4 ka; [Pereira et al., 2020](#)) and the Lava di Vico formation (~258 ka),
915 thus chronologically consistent with TF-97 and TF-98, as well as with TF-99, the latter unambiguously
916 attributable to Vico due to its rhyolitic composition (Fig. [12a](#)). However, no glass chemical composition is
917 available for the Sant'Angelo tephra in literature, but only a single whole-rock composition in [Perini et al.](#)
918 [\(2004\)](#). Whilst whole rock compositions only allow very limited comparison with glass data, a relatively good
919 geochemical match can be observed between the least evolved end-member of TF-97/98, and especially
920 of TF-98, and the Sant'Angelo tephra whole-rock composition (Fig. [13b](#)).

921 On the other hand, the whole rock composition of the Sant'Angelo tephra ([Perini et al., 2004](#)) is similar to that
922 of the lowermost unit (i.e., SA-C5) of the Sant'Abbondio lapilli and ash succession of [Marra et al. \(2014; Fig.](#)
923 [13b\)](#), which however yields a quite high loss on ignition, likely reflecting significant alkali loss. Nevertheless,
924 less mobile elements make a tentative correlation of the Sant'Angelo tephra with SA-C5 still tenable (Fig. [13b](#)).

925 The Sant'Abbondio succession, comprising at least six fallout horizons, occurs in the south-eastern sector of
926 the Vico Volcano, at the boundary of the Vico-Sabatini volcanic domains (Fig. [1b](#)). The base and the top of
927 this succession were $^{40}\text{Ar}/^{39}\text{Ar}$ dated at 390.4 ± 4.0 ka (lowermost unit SAAS C5) and 380.4 ± 40.0 ka
928 (uppermost unit SAAS C4; wide error associated with biotite dating), and tentatively attributed to the Sabatini
929 activity ([Marra et al., 2014](#)). However, considering its chemical affinity with the Sant'Angelo tephra, the
930 Sant'Abbondio lapilli and ash succession can be more likely ascribed to the Vico activity and, possibly, to the
931 Sant'Angelo unit. Thus, transitively, also the TF-99/98 should correlate with Sant'Abbondio units.

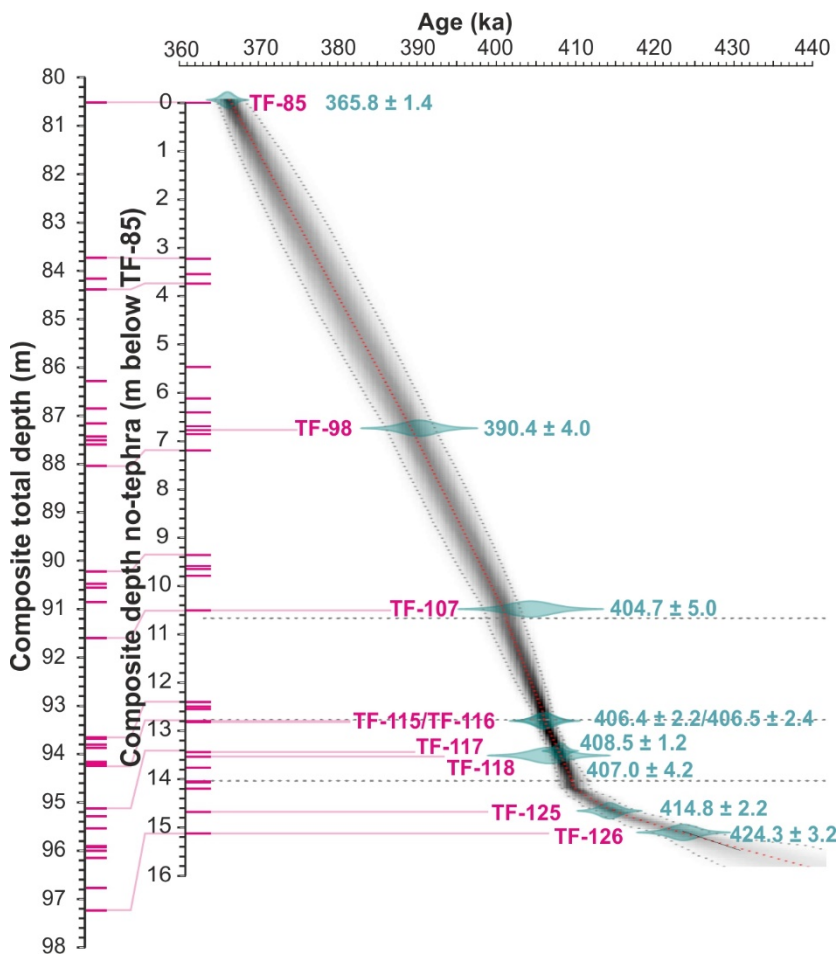
932 Unfortunately, Sant'Abbondio units yielded no fresh glass for direct comparison with the potential Fucino
933 equivalents. Therefore, to get an estimation of the interstitial glass composition of Sant'Abbondio/Sant'Angelo
934 unit, based on literature ([Perini et al., 2004](#)) and new petrographic observations and mineral composition of
935 the Sant'Abbondio and Sant'Angelo juvenile clasts, we performed a mass balance calculation (SD-1). Notably,
936 according to this calculation, the residual melt of juvenile clasts, having bulk composition, petrographic
937 characters, porphyritic degree, and mineral assemblage featuring the Sant'Angelo/Sant'Abbondio tephra,
938 would be fully consistent with the average glass composition of the TF-98 tephra (Fig. [13b](#); see also SD-1).

939 Specifically, we found that the bulk composition of Sant'Angelo/Sant'Abbondio tephra is consistent with the
940 average glass composition of TF-98 (49.3 wt%) + Lct (15.9 wt%) + Cpx (12.4 wt%) + bmca (6.5 wt%) + Plg
941 (12.5 wt%) + Ox (3.4 wt%), which substantially matches the textural features and the mineral assemblage
942 observed in Sant'Angelo/Sant'Abbondio SA-C5 tephra. In conclusion, despite the lack of glass compositional
943 data for the proximal counterpart, the correlation of this Vico unit with TF-97-98, and particularly with TF-98,
944 appears quite convincing. As a preliminary tentative attribution, we thus consider the tephra layers TF-97/98,

945 and likely TF-99, as the distal expression of the Sant'Angelo/Sant'Abbondio succession, which may represent
946 the final explosive activity of the Vico Period I (Perini et al., 2004).
947 TF-88, TF-89, TF-90, TF-96, TF-110, TF-120 and TF-124, though apparently similar in composition and
948 indistinguishable in the CaO/FeO vs diagram (Fig. 7c-III), can be easily attributed either to Vico or Vulsini using
949 the TAS and other simple bivariate diagrams, as shown in Figures 13c-d. Indeed, the glass geochemistry of
950 the post-Vico α phonolite-trachytes (i.e., the phonolite-trachytes component of Vico β , Vico β_{top} and Vico δ) is
951 quite different from that of the Vulsini phonolite-trachytes spanning a similar time-interval (Figs. 13c-d).
952 Specifically, while TF-88, TF-89 and TF-110 systematically plot within the compositional fields of the post-Vico
953 α phonolite-trachytes (Fig. 13c), TF-90, TF-96, TF-120 and the phonolite component of TF-124 plot in the field
954 of the Vulsini phonolites (Fig. 13d).
955 As for their potential proximal equivalents, TF-120 stratigraphically occurs between TF-117/Pozzolane Nere
956 (~408 ka) and TF-125/Vico α (~415 ka), i.e., geochronologically roughly consistent with PF-0 (399.8 ± 18.0 ka;
957 Turbeville, 1992), and thus might be considered as an alternative correlative for this Vulsini eruption, other
958 than the above-proposed TF-111. Finally, based on the available geochronological constraints, no specific
959 correlative deposits have been identified in the proximal records for the other Vico (TF-88, TF-89 and TF-110)
960 and Vulsini (TF-90, TF-96, TF-124) distal tephra layers.

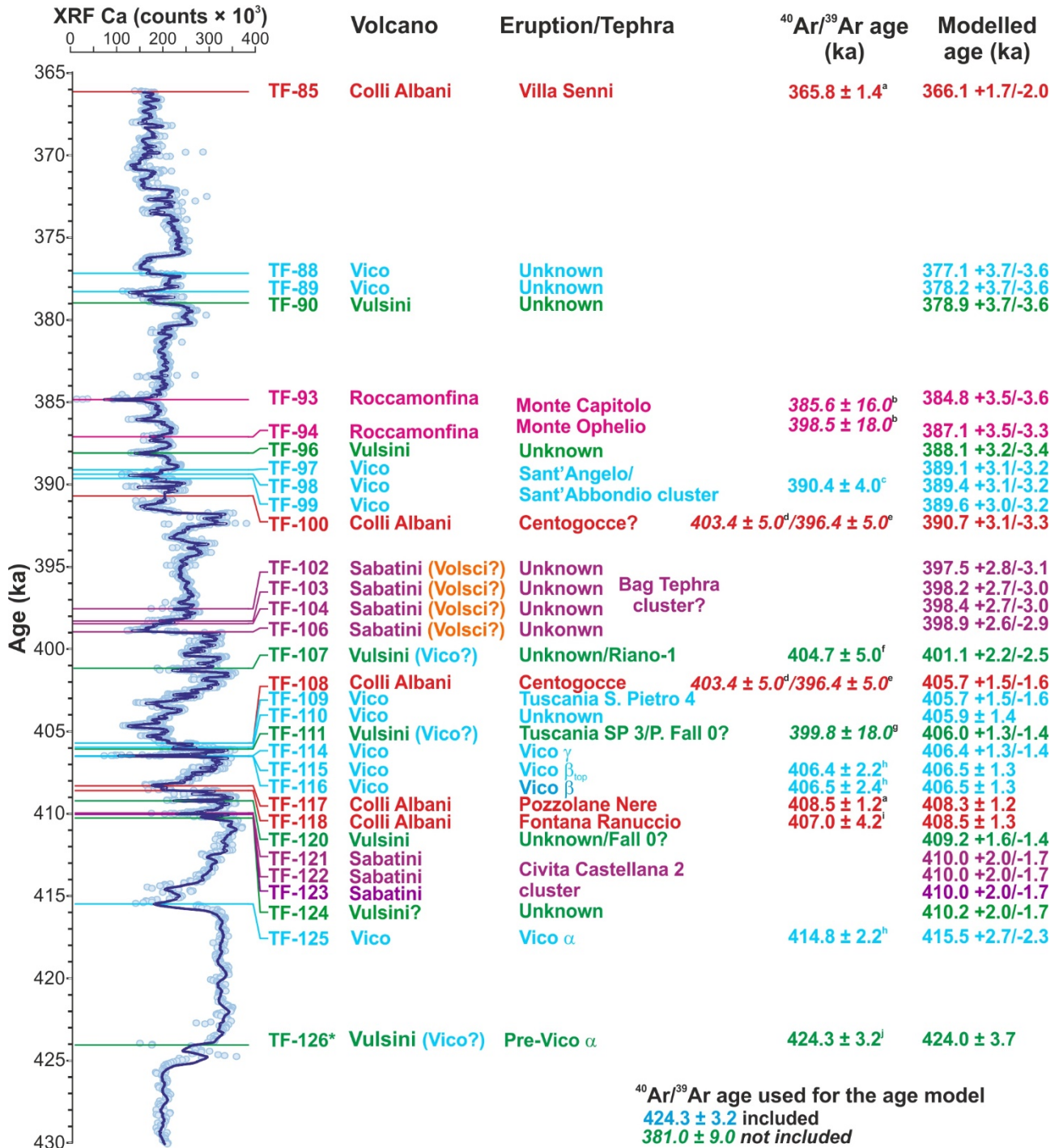
961 962 **5.3. Age model**

963 Based on the direct and indirect (i.e., derived from geochemical fingerprinting) $^{40}\text{Ar}/^{39}\text{Ar}$ dating of the MIS 11
964 tephra record, we have developed a Bayesian age-depth model. Only a sub-set of radioisotopic ages (from
965 direct dating or reliable geochemical and/or stratigraphical correlations) with the necessary requisites of both
966 accuracy and precision were selected for this purpose. Specifically, for the investigated interval we selected
967 nine ages from an equivalent number of tephra layers, as shown in Figure 14. The age-depth curve (Fig. 14)
968 shows a remarkable slope change at ~410 ka, indicating that the sedimentation rate was distinctly lower in the
969 first part of the MIS 11 period (~424-410 ka). While this change in sedimentation rate shows no correlation
970 with primary tephra deposition or volcanoclastic input, that is negligible, it coincides with a shift in Ca, from a
971 relatively long and more stable period with higher Ca to a period characterized by large and rapid, millennial-
972 scale variations of Ca (Fig. 15). Ca was addressed to represent lake primary productivity (Giaccio et al., 2019;
973 Mannella et al., 2019) and thus the marked change in sedimentation rate is likely related to changing
974 environmental conditions, a topic which will be addressed elsewhere. Here, we can only underscore that this
975 change cannot be interpreted as a distortion of the age-depth curve due to age model uncertainty, because it
976 occurs in a stratigraphic interval that is firmly constrained by several radioisotopic ages (Fig. 15).



977
978
979

Figure 14. Bayesian age-depth model for the investigated F4-F5 tephra record of the MIS 11 interval.



981

982

983

984

985

986

987

988

989

990

991

992

Figure 15. Summary of the volcanic sources, individual correlation and chronology ($^{40}\text{Ar}/^{39}\text{Ar}$ and modelled ages) of the investigated Fucino F4-F5 tephra record. The MIS 11 temporal series of the calcium content in Fucino lacustrine sediments from F4-F5 core is also shown (XRF data from Giaccio et al., 2019). Ages not used for the age model are reported in italics. Data source: ^a this study; ^b Rouchon et al. (2008); ^c Perini et al. (2004); ^d Marra et al. (2014); ^e Marra et al. (2009); ^f Turbeville (1992); ^g Pereira et al. (2020); ^h Pereira et al. (2018); ⁱ Giaccio et al. (2019).

The age-depth model allows us to reliably assess the age and climatostratigraphic position of each individual tephra in the F4-F5 MIS 11 section, as shown in Figure 15. Such an integrated paleoenvironmental-tephra record provides a stratigraphically ordered series of tephra within the framework of the sub-millennial scale paleoclimatic variability of the MIS 11 period, which represents one of the most important features of this kind of integrated record. Indeed, while the chronology is susceptible of improvements through time, the

993 climatostratigraphic position of each tephra is firmly and definitively established here. For instance, the TF-126
994 tephra is a valuable marker for the onset of a higher productivity interval, likely driven by higher temperature
995 and enhanced nutrients delivery, i.e., typical of interglacial conditions (i.e., MIS 11c; Fig. 15). This specific
996 climatostratigraphic position is independent of the current geochronological (and source) uncertainties of TF-
997 126 tephra and of any possible future improvement in accuracy and precision of the TF-126 dating itself.

998

999 **5.4. The Fucino MIS 11 tephra record in the framework of central Mediterranean Middle Pleistocene** 1000 **tephrochronology and its relevance for the Quaternary sciences and volcanology**

1001 In the framework of the Mediterranean tephrostratigraphy, few relatively continuous sedimentary records span
1002 through the Middle Pleistocene (Fig. 1a). The on-land marine succession of Montalbano Jonico, southern Italy
1003 (Figs. 1a, 16), records the southern-Italy peri-Tyrrhenian and Vulture volcanic activity at the Early-Middle
1004 Pleistocene transition and provides the first evidence for an early onset of the volcanic activity in the Campania
1005 Area, at the beginning of the Middle Pleistocene (Petrosino et al., 2015). The radioisotopic geochronological
1006 data acquired from Montalbano Jonico also allowed a better constrain of the chronology of the MIS 19
1007 paleoclimatic change (Nomade et al., 2019) and of the cosmogenic nuclide ^{10}Be increase during the
1008 Matuyama-Brunhes geomagnetic reversal (Simon et al., 2018).

1009 The Sulmona Basin lacustrine succession, in central Italy (Figs. 1a, 16), represents another rich tephra archive
1010 encompassing the Early-Middle Pleistocene transition, which records an intense and frequent activity of the
1011 peri-Tyrrhenian volcanism (Giaccio et al., 2013b), poorly documented (or so-far unrecognized) in proximal
1012 settings (Marra et al., 2014; Sottili et al., 2019). The Sulmona succession also provided the basis for
1013 assembling a robust radiometric chronology for both local and extra-regional MIS 19 paleoclimatic records
1014 (Giaccio et al., 2015a; Regattieri et al., 2019) and for constraining the timing of the Matuyama-Brunhes
1015 geomagnetic reversal (e.g., Sagnotti et al., 2014). Furthermore, the Sulmona Basin tephra record spans
1016 discontinuously the MIS 15-MIS 10 period (e.g., Giaccio et al., 2013b, Giaccio et al., 2014; Regattieri et al.,
1017 2016), but a comprehensive tephra study for this interval is still pending. Specifically, among several tephra
1018 spanning the MIS 11 period (Fig. 16), currently only one has been geochemically characterized (Regattieri et
1019 al., 2016). Based on its trachyte-rhyolite composition Regattieri et al. (2016) correlated it to Vico α , but
1020 according to the upgraded geochemical dataset obtained by Pereira et al. (2020) for the Vico Period I units,
1021 this tephra could be either attributed to Vico α or Vico β (Pereira et al., 2020).

1022 The rich tephra record of the river-lagoon stacked aggradational successions of the Tiber River delta, in central
1023 Italy (Figs. 1a, 16), though discontinuous, radioisotopically constrained the timing of the sea-level rise during
1024 the last eleven deglaciations (e.g., Marra et al., 2016b; Luberti et al., 2017), including the MIS 11 period (Fig.
1025 16). However, only few tephra layers have been so far geochemically fully characterized (e.g., Pereira et al.
1026 2020), thus limiting the great potential of this succession for tephrochronological purposes.

1027 The deep-sea core KC01B in the Ionian Sea (Fig. 1a) spans continuously the last 1.1 Ma (Lourens, 2004), but
1028 detailed tephrostratigraphic investigations are currently available only for the last 200 kyr (Insinga et al., 2014;
1029 Fig. 16). A recent detailed tephra and crypto-tephra study of the nearby core ODP Site 964 (Fig. 1) extended
1030 this tephrochronological record back to 625 ka (Fig. 16) and resulted in the first reliable synchronization of the
1031 marine and terrestrial records during specific intervals of MIS 13 and MIS 10 (Vakhrameeva et al., 2021).

1032 The Mercure, Vallo di Diano and Acerno basins in southern Italy (Figs. 1a, 16), in addition to some known
1033 major eruptions from Latium volcanoes, revealed a conspicuous activity of the Roccamonfina Volcano during

1034 the MIS 15-MIS 12 period that is still fragmentarily known or currently not yet identified in the near-source
1035 volcanic area (Karner et al., 1999; Giaccio et al., 2014; Petrosino et al., 2014a, 2014b). Also located in southern
1036 Italy, the San Gregorio Magno lacustrine succession (Fig. 1a) provides a valuable tephra record of the poorly
1037 known Middle Pleistocene activity of the Campanian Volcanic Zone, although not extending beyond 250 ka
1038 (Petrosino et al., 2019; Fig. 16). Similarly, the Adriatic Sea core PRAD 1-2 (Fig. 1a), extends into the late
1039 Middle Pleistocene, reaching ~200 ka (Bourne et al., 2015; Fig. 16).

1040 In the Eastern Mediterranean area, the marine cores KL49, KL51 and LC21 in the Aegean Sea, and the
1041 terrestrial (peatland) tephra record of the Tenaghi Philippon basin (Vakhrameeva et al., 2019) in Greece (Fig.
1042 1a), were used in combination for reconstructing and indirectly dating the explosive activity of the Santorini
1043 Volcano during the last 360 kyr (Wulf et al., 2020; Fig. 16). The Tenaghi Philippon archive also documents a
1044 MIS 12-MIS 10 tephra record, which was dated climatostratigraphically using the high-resolution pollen profile,
1045 allowing a first age estimation of the tephra series of either known or unknown origin (Vakhrameeva et al.,
1046 2018; Fig. 16). Finally, the long and continuous tephra record from Lake Ohrid (Albania-North Macedonia; Fig.
1047 1a), mostly from peri-Tyrrhenian potassic volcanic sources, provided important geochronological constraints
1048 for developing a robust age model for the outstanding 1.36 Ma-long palaeoclimatic succession, but also for
1049 currently unknown volcanic eruptions (Leicher et al., 2019; Wagner et al., 2019; Fig. 16).

1050 In summary, from the above-mentioned Mediterranean Middle Pleistocene tephra records only four long and
1051 relatively continuous successions document in detail the MIS 11 period, i.e., the Sulmona Basin in central Italy,
1052 Lake Ohrid in Albania-Macedonia, the Tenaghi Philippon peatland in Greece and the Ionian Sea core ODP
1053 Site 964 (Figs. 1a, 16). However, except the incompletely explored Sulmona record, due to their remote
1054 location with respect to the peri-Tyrrhenian volcanoes, the remaining three MIS 11 records document none or
1055 only the largest explosive eruptions of the peri-Tyrrhenian potassic volcanic systems, which are the only
1056 sources of the tephra found in Fucino Lake record. Specifically, among the Fucino MIS 11 tephra succession,
1057 only two tephra layers are found at Lake Ohrid, i.e., (i) Vico α /TF-125/OH-DP 1700.6 and (ii) Roccamonfina
1058 Monte Ofelio-Monte Capitolo/TF-96/OH-DP 1640 (Fig. 16), while a third layer, not identified at Fucino, was
1059 correlated to an undefined Roccamonfina eruption occurring at onset of the MIS 11 period (Leicher et al.,
1060 2019). Due to their greater distance from the peri-Tyrrhenian potassic volcanic sources, the MIS 11 records
1061 of Tenaghi Philippon and ODP-964 sites document only few potentially unknown tephra from Neapolitan
1062 volcanoes, while the majority are related to the volcanic sources of Santorini, for Tenaghi Philippon, and
1063 Santorini, Aeolian Islands and South Aegean Volcanic Arc, for ODP-964 (Vakhrameeva et al., 2018, 2019,
1064 2021). None of the MIS 11 tephra from Tenaghi Philippon or ODP-964 are found in the Fucino record.

1065 In conclusion, the general tephrostratigraphic framework for MIS 11 is far from being satisfactorily developed
1066 for a reliable application to Quaternary sciences and volcanology. In this regard, the Fucino MIS 11 record
1067 arises as one of the fundamental reference geochemical and chronological datasets for the future development
1068 and application of the tephrochronology in the Mediterranean Region, especially for the areas closer to the
1069 highly productive tephra sources of peri-Tyrrhenian potassic volcanoes, i.e., that have the potential of capturing
1070 part of the activity recorded at Fucino and thus to benefit from its rich tephrochronological record.

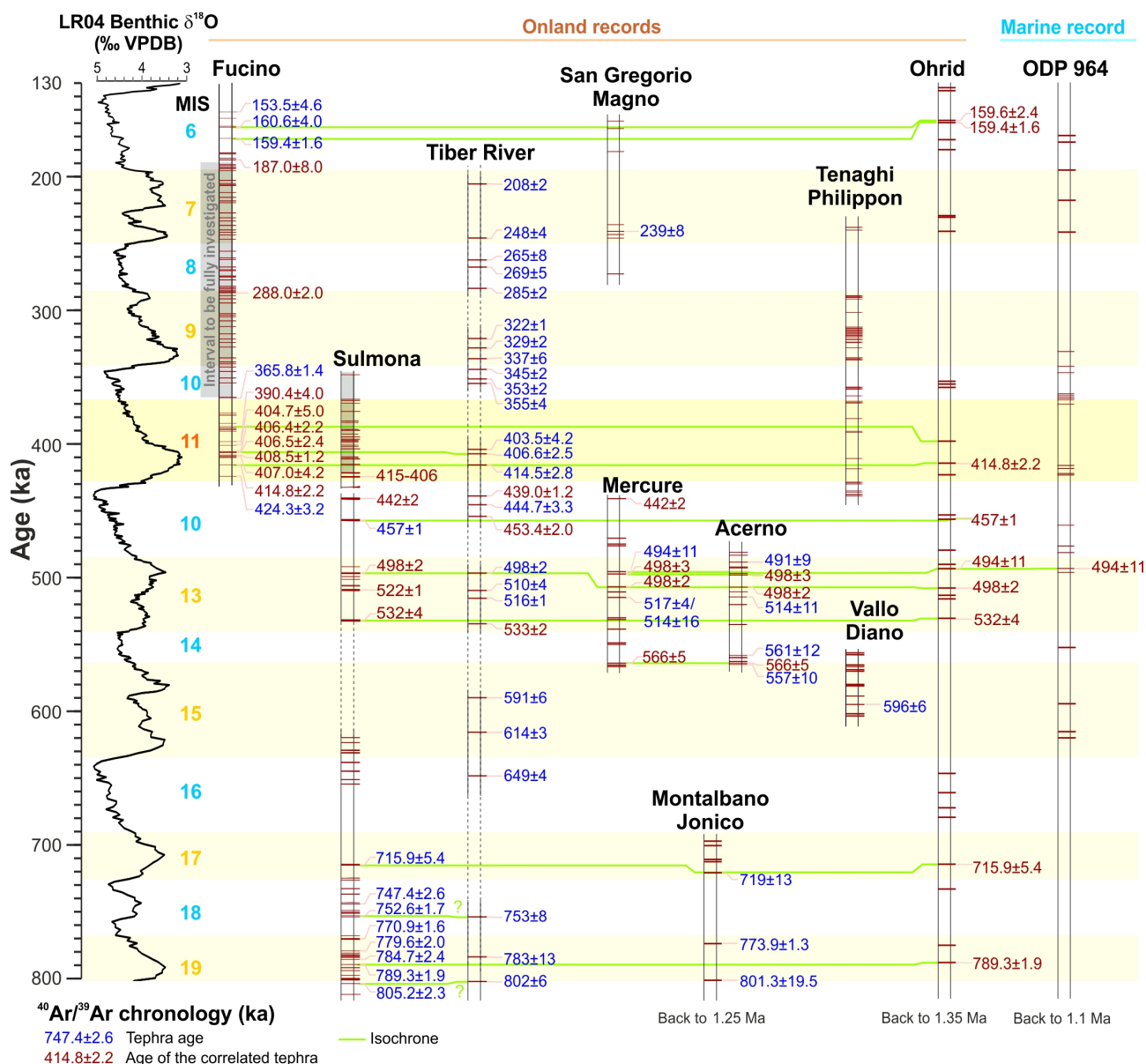
1071

1072 **5.5. Implications for the peri-Tyrrhenian explosive volcanic history**

1073 **5.5.1. Distal tephrostratigraphy for elucidating explosive eruption histories: Advantages and limitations**

1074 Assessing the issue of the explosive volcanism history using distal archives presents a series of advantages,
1075 but also limitations that need to be discussed. The general overview provided in previous sections shows that
1076 distal archives often document explosive activity that is hardly traceable to known eruptions or activity period
1077 of a specific volcanic source. This highlights the great potential of distal tephrostratigraphy for the assessment
1078 of the explosive activity at regional scale (e.g., for the Mediterranean area, [Munno and Petrosino, 2007](#);
1079 [Paterne et al., 2008](#); [Wulf et al., 2008, 2012](#); [Giaccio et al., 2012, 2014](#); [Leicher et al., 2019](#)). However, several
1080 geographical, physical, and time-dependent factors can limit the approach of the distal tephrostratigraphy.
1081 Specifically, the completeness of a distal archive with respect to a given volcano or cluster of volcanoes
1082 depends on the (i) relative distance from the volcanic sources, (ii) position with respect to the dominant winds,
1083 (iii) magnitude and intensity of the events, (iv) direction of the dispersal axis with respect to the volcano and
1084 distal archive location, (v) eruptive dynamics, (vi) variability of the atmospheric circulation pattern during
1085 glacial-interglacial and sub-orbital scale climate change (e.g., [Bursik, 1998](#)). In turn, the impact of all these
1086 factors in limiting the usefulness of the distal tephrostratigraphy depends on the number and geographical
1087 distribution of the distal archives documenting the same temporal interval and, more critical, the activity of the
1088 same volcanic system. Indeed, a dense network of distal archives distributed across a wide region surrounding
1089 a given volcano, sensibly enhances the possibility of capturing the whole activity of that volcanic system,
1090 reducing all the above-mentioned uncertainty and limiting factors, and allowing the construction of a
1091 composite record (e.g., [Blockley et al., 2014](#); [Lowe et al., 2015](#); [Bronk Ramsey et al., 2015a, 2015b](#)).

1092 As stressed throughout the paper, at present only limited tephrostratigraphic records span the interval
1093 documented in this study in detail, and only one (i.e., Lake Ohrid) shares with Fucino some tephra from the
1094 peri-Tyrrhenian potassic volcanic sources ([Fig. 16](#)). Therefore, the framework of the explosive activity of these
1095 volcanic systems obtained using the distal records is likely to be far from complete because of the poorly
1096 developed network of tephra records and correlations. Nevertheless, due to its privileged location, we
1097 demonstrate that the Fucino paleolake captured most of the known major eruptions and many other unknown
1098 explosive events of the peri-Tyrrhenian potassic volcanoes. Therefore, reconstructing the explosive history of
1099 the peri-Tyrrhenian potassic volcanoes during the MIS 11 period using the Fucino record alone is fully justified
1100 and supported by the data gathered which illustrates that Fucino provides an extremely detailed eruptions
1101 record.



1102

1103

1104

1105

1106

1107

1108

1109

1110

1111

1112

Figure 16. The Fucino MIS 11 tephra record within the framework of the Mediterranean Middle Pleistocene tephrochronological records. Data source: **Fucino:** Giaccio et al. (2017, 2019), Mannella et al. (2019), This study; **Sulmona:** Giaccio et al. (2013a, 2013b, 2014, 2015a), Sagnotti et al. (2014), Regattieri et al. (2015, 2019); **Tiber River:** Florindo et al. (2007), Villa et al. (2016), Marra et al. (2016a, 2017, 2019, and references therein), Pereira et al. (2020); **Mercure:** Giaccio et al. (2014), Petrosino et al. (2014a); **San Gregorio Magno:** Munno and Petrosino (2007), Petrosino et al. (2019); **Montalbano Jonico:** Petrosino et al. (2015); **Acerno:** Petrosino et al. (2014b); **Vallo di Diano:** Karner et al. (1999); **Tenaghi Philippon:** Vakhrameeva et al. (2018, 2019), Wulf et al. (2020); **Lake Ohrid:** Leicher et al. (2016, 2019), Wagner et al. (2019); **ODP 964:** Vakhrameeva et al. (2021).

1113 5.5.2. The proximal record

1114 In order to compare the distal (Fucino) and proximal records of the peri-Tyrrhenian explosive volcanism of
 1115 central Italy, we critically review the available geochronological data. The general framework of literature data
 1116 for the peri-Tyrrhenian volcanic activity encompassing the MIS 11 period, or a slightly wider temporal interval,
 1117 is provided in Table 6. Though partially and fragmentarily mentioned in previous sections, i.e., when the
 1118 individual correlations were discussed, in the following section we provide a general overview summarizing
 1119 the state of the art of the knowledge on the history of the peri-Tyrrhenian potassic explosive volcanism.

1120 For the Vulsini Volcanic District, only one direct radioisotopic age determination is available for the studied
 interval, i.e., the already mentioned Pumice Fall 0 dated at 399.8 ± 18.0 ka (Turbeville, 1992; Table 6). Castel

1121 Broco and Casale delle Piane are two others prominent Vulsini eruption units potentially falling in the
 1122 investigated interval, although lacking direct dating. Recently, [Marra et al. \(2020a\)](#) provided a tentative
 1123 reconstruction of the eruptive history in this time span, based on xenocryst populations occurring in primary
 1124 and reworked deposits of the eastern Vulsini (Bolsena-Orvieto and Vulsini Fields activities; [Table 6](#)),
 1125 suggesting that the statistically most significant population age of 425.4 ± 1.6 ka may correspond to that of the
 1126 Castel Broco eruption.

1127 **Table 6.** Summary of the literature geochronological data for the peri-Tyrrhenian potassic volcanism of central Italy during the MIS 11, or
 1128 a slightly wider interval. When possible, i.e., if all the all the required analytical data were published, $^{40}\text{Ar}/^{39}\text{Ar}$ ages are recalculated relative
 1129 to an age of 1.1891 Ma for the Alder Creek sanidine or relative to an age of 28.294 Ma for the Fish Canyon sanidine monitor standards
 1130 ([Niespolo et al., 2017](#)), with the uncertainty expressed at 2σ .
 1131

Volcanic source	Volcanic phase	Unit/sample	Type of activity/product	K/Ar and $^{40}\text{Ar}/^{39}\text{Ar}$ age (ka $\pm 2\sigma$)	References	
Vulsini	Bolsena	Ponticello Pumices	Pumice fall	352.0 \pm 4.0	Nappi et al., 1995 Marra et al., 2020a	
				345.4 \pm 2.1		
	Vulsini Field	Castel Broco Piano della Selva	Pumice fall- pyroclasti flow Pyroclastic flow	399.8 \pm 18.0	Turbeville, 1992 n.d. n.d. 400.5 \pm 3.7 411.4 \pm 2.4 425.4 \pm 1.6 437.6 \pm 2.2	Marra et al., 2020a
				n.d.		
				n.d.		
				400.5 \pm 3.7		
Vico	Period I	SAAS-bottom VICO δ VICO γ VICO β_{top} VICO β VICO α	Pumice fall Pumice fall Pumice fall Pumice fall Pumice fall Pumice fall	390.4 \pm 4.0	Marra et al., 2014 Pereira et al., 2020	
				399.7 \pm 3.0		
				n.d.		
				406.4 \pm 2.0		
				406.5 \pm 2.4		
				414.8 \pm 2.2		
Sabatini	Southern Sabatini	CC-2 La Rosta FALL F	Pumice fall Pumice fall Pumice fall	n.d.	Pereira et al., 2020 Marra et al., 2020b Marra et al., 2014	
				439.1 \pm 1.0		
				448.5 \pm 7.0		
Colli Albani	Villa Senni Eruption Cycle	Madonna degli Angeli succession Pantano Secco hydromagmatic center Madonna degli Angeli succession Tufo Lionato Centogocce succession Pozzolane Nere Corcolle succession Pozzolane Rosse Vallerano Lava	Lava dyke	354.5 \pm 6.0	Gaeta et al., 2006 and references therein Marra et al 2003	
			Lava flow	357.5 \pm 9.0		
			Lava flow	359.5 \pm 6.0		
			Lava flow	359.5 \pm 8.0		
			Scoria fall	367.6 \pm 2.0		
			Scoria fall	368.6 \pm 2.0		
			Lava flow	369.6 \pm 3.0		
			Pyroclastic flow	368.6 \pm 4.0		
			Lava flow	396.0 \pm 5.0		
			Scoria fall	402.3 \pm 5.0		
			Pyroclastic flow	407 \pm 2.0		
			Lava flow	439.5 \pm 5.0		
Scoria	440.5 \pm 3.0					
Pyroclastic flow	455.5 \pm 2.0					
Lava flow	458.0 \pm 8.0					
Volsci volcanic filed		Selva Piana Colle Avarone CA-CGT Isoletta III Isoletta II Valcatara Lademagne II Pofi-Colle La Grotta Giuliano di Roma	Lava Reworked volcanic horizon Scoria fall Scoria fall Lava dyke Reworked volcanic horizon Phreatomagmatic deposit Lava	362.0 \pm 11.0	Boari et al., 2009 Marra et al., 2021 Pereira et al., 2018 Boari et al., 2009 Pereira et al., 2018 Marra et al., 2021 Boari et al., 2009	
				360.8 \pm 6.5		
				363.8 \pm 8.0		
				373.7 \pm 4.0		
				379.0 \pm 8.0		
				387.7 \pm 5.0		
				391.5 \pm 3.6		
				394.6 \pm 6.0		

		Pofi Scoria cone	Scoria fall	394.4±3.5	Marra et al., 2021
		Cava Pompei	Scoria fall	392.7±3.0	Pereira et al., 2018
		Arnara Scoria cone	Scoria fall	395.8±6.1	Marra et al., 2021
		Isoletta I	Scoria fall	401.7±3.0	Pereira et al., 2018
		Lademagne I	Scoria fall	404.0±5.0	
		Supino	Phreatomagmatic deposit	407.7±2.6	Marra et al., 2021
		La Tomacella, upper	Pyroclastic rock	410.0±10.0	Boari et al., 2009
		Tecchiena	Lava	416.1±11.0	Boari et al., 2009
		Celleta	Lava	417.1±6.0	
		La Tomacella, lower	Pyroclastic rock	425.2±13.0	
		Brown Leucititic Tuff	Pyroclastic flow	343.6±6.0	Scaillet et al., 2008
				358.2±10.0	Rouchon et al., 2008
				385.0±23.0	Luhr and Giannetti, 1987
		Scipicciano 89X	Lava flow	361.7±10.0	Rouchon et al., 2008
		Fontana-radina RMF7	Lava flow	363.7±16.0	
		SP/R-30	Lava dome	360.0±42.0 (GM)	Giannetti, 2001
				382.0±3.0 (San)	
				390.0±30.0 (San)	
		SP/R-31	Effusive	370.8±3.0	Rouchon et al., 2008
		La Frascara RMF4	Lava flow	373.9±18.0	
		Galluccio RMF3	Lava flow	375.9±16.0	
		Monte Casi	Lava dome	370.0±9.0	Radicati di Brozolo et al., 1988
		LP/R-247	Effusive	378.9±4.0 (San)	Giannetti, 2001
				399.3±12.0 (San)	
				430.0±6.0 (GM)	
		MLT/R-352	Lava flow	374.0±11.0	Rouchon et al., 2008
		MLP/R-69	Lava dome	376.0±16.0	
		Monte Capitolo RMF6	Pyroclastic	396.2±16.0	Rouchon et al., 2008
		Masseria Robetti	Lava flow	397.0±18.0	Radicati di Brozolo et al., 1988
		MLT/R-290	Lava flow	408.4±9.0	Giannetti, 2001
		Monte Ofelio RMF12	Pyroclastic	409.4±18.0	Rouchon et al., 2008
		MLT/R-351	Lava flow	409.4±10.0	Giannetti, 2001
				415.5±18.0	
		LP/R-104	Lava dome	416.6±32.0	Radicati di Brozolo et al., 1988
		Masseria Robetti	Undefined	421.0±9.0	
		LP/T-247	Lava dome	430.0±6.0	Giannetti, 2001
		Rio Rava RMF14	Lava flow	446.0±12.0	Rouchon et al., 2008

1132 GM, goroundmass; San, sanidine.

1133

1134 At Vico Volcano, multiple explosive eruptions of sub-Plinian to Plinian intensity occurred in the investigated
1135 interval, which roughly matches the Vico Period I stage (Perini et al., 2004), including Vico α , Vico β , Vico β_{top} ,
1136 Vico γ , Vico δ and Sant'Angelo tephra (Cioni et al., 1987; Perini et al., 2004; Pereira et al., 2020) (Table 6).
1137 The chronology of the Vico Period I has recently been improved by Pereira et al. (2020) who reported new
1138 $^{40}\text{Ar}/^{39}\text{Ar}$ ages for 4 out of the 5 main eruption units recognised in proximal settings (Table 6). In addition, we
1139 provided an age constraint for the Sant'Angelo tephra (Perini et al., 2004), based on the proposed correlation
1140 to the Sant'Abbondio lapilli and ash succession (390.4 ± 4.0 ka; Marra et al., 2014).

1141 In contrast, no relevant activity is documented at Sabatini Volcanic District during the MIS 11 period. Indeed,
1142 the intense explosive activity of the Southern Sabatini stage took place between 500 ka ("Fall A" Plinian

1143 eruption) and 439 ka (“La Rosta” Plinian fall; [Sottili et al., 2004](#); [Marra et al., 2020b](#)), while the subsequent
1144 Bracciano stage started at ~325 ka, thus suggesting a long phase of quiescence extending for more than ~100
1145 kyr. However, the recent attribution of CC-2 pumice fall, which is bracketed between Vico α and Vico β , to the
1146 Sabatini activity ([Pereira et al., 2020](#)), would partially fill this seemingly long gap in activity. Moreover, as
1147 already mentioned in section 3.1., the Strombolian lithological features of the R-2 tephra occurring in the MIS
1148 11 lacustrine succession cropping out near Riano ([Fig. 1](#)), laying below the Riano tephra R-1 dated at $404.7 \pm$
1149 5.0 ka ([Marra et al., 2018](#); [Table 6](#)), would also suggest the occurrence of a minor explosive activity of Mts
1150 Sabatini during the MIS 11 period.

1151 The 450-350 ka interval at the Colli Albani Volcanic District was characterized by the occurrence of three main
1152 eruption cycles, all belonging to the Tuscolano-Artemisio phase of activity: Pozzolane Rosse, Pozzolane Nere
1153 and Villa Senni eruption cycles ([Freda et al., 1997, 2011](#); [Giordano et al., 2006](#); [Marra et al., 2009](#); [Gaeta et](#)
1154 [al., 2016](#)) ([Table 6](#)). Each cycle is characterized by large, caldera-forming eruptions, emplacing up to several
1155 tens of km³ of pyroclastic-flow deposits ([De Rita et al., 1988, 1995](#)). The climatic phases were followed by
1156 several kyr-long post-caldera phases of activity, characterized by Strombolian and effusive eruptions revealed
1157 by numerous scoria cones and lava flows along peri-caldera ring faults, namely the Corcolle, Centogocce and
1158 Madonna degli Angeli successions ([Giordano et al., 2006](#)) ([Table 6](#)). The three eruption cycles were separated
1159 from each other by ~50 kyr-long quiescent intervals ([Marra et al., 2009](#); [Gaeta et al., 2016](#)).

1160 The Volsci Volcanic Field was characterized by diffuse, low-scale, magmatic (Strombolian and subordinate
1161 effusive) and phreatomagmatic activities from monogenetic scoria cones and tuff rings (e.g., [Cardello et al.,](#)
1162 [2020](#); [Marra et al., 2021](#)). Several radioisotopic age determinations, encompassing the investigated interval,
1163 have been recently acquired ([Boari et al., 2009](#); [Nomade et al., 2011](#); [Pereira et al., 2018](#); [Marra et al., 2021](#))
1164 ([Table 6](#)). It appears that available ⁴⁰Ar/³⁹Ar ages are often grouped in statistically indistinguishable clusters
1165 ([Table 6](#)), which could be referred to either an individual eruptive event or multiple closely-spaced eruptions.
1166 In reconstructing the eruptive activity, this could lead to overestimate (i.e., multiple dating of the same eruption)
1167 or underestimate (i.e., grouping of statistically indistinguishable datings that refer to multiple events) number,
1168 frequency, and recurrence of the events. Notwithstanding, the quite distinctive compositional features of the
1169 Volsci products ([Marra et al., 2021](#) and references therein), combined with the lack of analyzable glass in the
1170 dated pyroclastic samples prevents their reliable application for tephrochronological purposes. Therefore, the
1171 current data available for the Volsci volcanic field prevent us from assessing the presence of tephra layers
1172 from this volcanic system in distal settings (including Fucino) and thus potentially improving its explosive
1173 history.

1174 Finally, for the Roccamonfina Volcano, despite the large number of dated products, many of the samples
1175 ranging in age from 446 ± 4 ka to 353 ± 5 ka pertain to effusive or poorly defined products ([Luhr and Giannetti,](#)
1176 [1987](#); [Radicati di Brozolo et al., 1988](#); [Giannetti, 2001](#); [Rouchon et al., 2008](#)) ([Table 6](#)). Only the major Brown
1177 Leucitic Tuff eruption, and the minor Mt. Capitolo and Mt. Ofelio eruptions document explosive activity in the
1178 investigated timespan ([Table 6](#)). Moreover, several of these samples were dated by K/Ar method and yielded
1179 low precision age estimates, and therefore are scarcely reliable ([Table 6](#)). For instance, a previous date on
1180 the Brown Leucitic Tuff provided a quite imprecise age of 385 ± 23 ka ([Luhr and Giannetti, 1987](#)), and differs
1181 quite significantly from more recent age determinations obtained for this eruption (e.g., 358.2 ± 10.0 ka,
1182 [Rouchon et al., 2008](#); 343.6 ± 6.0 , [Scaillet et al., 2008](#)). Finally, a large uncertainty, and unreliability, is reflected

1183 by the scattered ages obtained by dating different material from the same sample (e.g., SP/R-30 and LP/R-
1184 247; [Table 6](#)).

1185

1186 **5.5.3. Comparing the proximal and Fucino records of the peri-Tyrrhenian potassic volcanism**

1187 The above critical revision of the available literature data for the peri-Tyrrhenian explosive volcanism of central
1188 Italy allows a suitable comparison with Fucino MIS 11 tephra record. Overall, the history of the peri-Tyrrhenian
1189 explosive volcanism recorded at Fucino appears substantially richer and temporally better resolved with
1190 respect to the proximal settings ([Fig. 17b](#)). Notably, the Fucino record provides direct evidence for some Vulsini
1191 “ghost eruptions” ([Marra et al., 2020a](#)). Indeed, the age distribution of xenocrysts extracted from Vulsini
1192 pyroclastic units younger than MIS 11 ([Marra et al., 2020a](#)) defines three clusters at 425.4 ± 1.6 ka, $411.4 \pm$
1193 2.4 ka and 400.5 ± 3.7 ka ([Table 6](#); [Fig. 17b](#)) that do not correspond to any exposed products dated so far,
1194 which however are in good agreement with the $^{40}\text{Ar}/^{39}\text{Ar}$ and modelled ages of the Fucino tephra TF-126 (424.0
1195 ± 3.7 ka), TF-120 (409.2 ± 1.6 ka) and TF-107 (401.1 ± 2.5 ka), ascribed to Vulsini ([Figs. 15 and 17b](#)). This
1196 provides further evidence for volcanic activity not yet identified in Vulsini proximal settings.

1197 The Fucino record further refines our knowledge of the early explosive history of Vico Volcano ([Pereira et al.,](#)
1198 [2020](#)). Indeed, except for the missing Vico δ , Fucino documents the whole known activity of Vico Period I and
1199 highlights new eruptive events still unrecognised in proximal areas (i.e., TF-99 and TF-109). The age-depth
1200 model of Fucino indicates that the previously undated Vico γ eruption occurred around 406.4 ± 1.4 ka ([Figs.](#)
1201 [15 and 17b](#)), i.e., immediately after the Vico β and Vico β_{top} eruption couplet, both with a modelled age of 406.4
1202 ± 1.3 ka. Fucino provides evidence for three distinct tephra layers (i.e., TF-116, TF-115 and TF-114) within a
1203 very narrow stratigraphic interval of ~ 9 cm ([Table 2](#); [Fig. 5](#)). They represent three distinct eruptive events of
1204 notable intensity occurred in a very short time span and may elude field observations in proximal exposures.
1205 Furthermore, while the uppermost fall deposit of the Sant’Abbondio succession, which is here tentatively
1206 ascribed to the Vico activity (Sant’Angelo tephra), yielded a poorly constrained age of 380 ± 40 ka ([Marra et](#)
1207 [al., 2014](#)), the Fucino record points out that this eruption cluster likely occurred in a short time span between
1208 ~ 389 ka and ~ 390 ka ([Figs. 15 and 17b](#)). Finally, the Fucino record allows us to refine the timing of the early
1209 Vico activity, indicating an age of ~ 377 - 379 ka for the emplacement of at least two additional, previously
1210 unknown, pyroclastic units ([Figs. 15 and 17b](#)).

1211 Regarding the Sabatini volcanic district, the Fucino dataset improves the knowledge on the history and
1212 chronology of the activity, by providing a modelled age of 410.0 ± 2.0 ka for the CC-2 pumice fall ([Pereira et](#)
1213 [al., 2020](#)). Furthermore, Fucino records a cluster of four tephra (TF-102/TF-106) at ~ 397 - 400 ka, which may
1214 represent the equivalent of the Bag Tephra marker(s) of the Middle Pleistocene Hungarian loess, thus
1215 providing the first reliable age and climatostratigraphic position for this stratigraphic marker(s). If confirmed by
1216 future investigations, the recognition of this eruption cluster may shed new light on the Sabatini eruption
1217 frequency. Indeed, during the whole eruptive history (589 ± 4 ka to 70 ± 3 ka) of the district, the longest
1218 dormancy of ~ 90 kyr has been so far documented in the time span 438 ± 1 to 329 ± 4 ka ([Marra et al., 2020b](#)).
1219 The Fucino dataset, showing a previously undetected eruption cluster at $398.9 + 2.6/2.9$ ka - $397.5 + 2.8/-3.1$
1220 ka, allows us to estimate a maximum quiescence of 68.5 ± 4.1 kyr in the district (i.e., same as the time lapse
1221 since the last documented eruption), with implications for hazard assessment in the Roman area. However, at

1222 present we cannot exclude that this cluster of eruptions could originate by the Volsci volcanic field (Fig. 15),
1223 which documents activity in a comparable timespan (Table 6).

1224 With respect to the known stratigraphic and chronological framework of Colli Albani volcano (Marra et al.,
1225 2003, 2009, 2016b; Freda et al., 2006; Giaccio et al., 2009; Gaeta et al., 2011, 2016), the Fucino dataset
1226 integrates the chronology of the post-caldera phase that followed the major Pozzolane Nere eruption.
1227 Specifically, the last documented eruption of this phase (i.e., Centogocce succession; Fig. 15) occurs at 396.4
1228 ± 5 ka in the Fucino record, which confirms the 30.6 ± 6.4 kyr-long dormancy preceding the onset of the Villa
1229 Senni eruption cycle (365.8 ± 1.4 ka), as previously suggested (Gaeta et al., 2016). Such dormancies have
1230 relevance in understanding the relationships between the geodynamic/tectonic and magmatic processes
1231 (Marra et al., 2004), stress-field and eruptive activity (Marra et al., 2009), as well as in assessing the volcanic
1232 hazard in the Roman area (Marra et al., 2016a, 2020b). In particular, the Colli Albani volcano is characterized
1233 by a quasi-periodic eruptive behaviour, with average recurrence times of 41 ± 2 kyr for the onset of the main
1234 eruptive cycles and average dormancies of 38 ± 2 kyr (Marra et al., 2016a). Notably, the last eruptive cycle
1235 started at 41 ± 2 ka and the last eruption occurred at 36 ± 1 ka, thus strongly evidencing a potentially still active
1236 (although quiescent) volcanic system.

1237 Finally, the location of the Fucino paleolake NNW of Roccamonfina volcano is less favourable for intercepting
1238 the distal products of major (Plinian and Sub-Plinian) eruption columns (usually dispersed toward the eastern
1239 quadrants at these latitudes), different from co-ignimbrite ash clouds and eruptive plumes from minor explosive
1240 events subject to lower altitude winds. Nevertheless, the MIS 11 Fucino dataset improves the chronology, both
1241 in term of accuracy and precision, of the post-Rio Rava/pre-Brown Leucitic Tuff stage of the Roccamonfina
1242 activity, through the identification of a possible distal equivalent of the Mt. Ofelio-Mt. Capitolo parasitic centers
1243 (Rouchon et al., 2008).

1244 Overall, based on the updated chronological data for both proximal volcanic areas and Fucino succession, we
1245 obtained the probability density functions for the explosive activity of the peri-Tyrrhenian potassic volcanism
1246 during the MIS 11 period (Fig. 17c). By comparing these statistical expressions of the regional explosive
1247 volcanism, the proximal record would seem to show a single, monotonous increase of the eruptive frequency
1248 between ~ 410 ka and ~ 395 ka, followed by a quite homogenous activity during the following 395-365 ka
1249 interval. Instead, the better-resolved and richer record derived from Fucino shows a much more complex
1250 chronicle. Specifically, the temporal distribution of the peri-Tyrrhenian explosive volcanism is not homogenous
1251 and appears significantly clustered, with at least four (or possibly more) ~ 4 -5 kyr-long periods of frequent
1252 activity separated by similarly long (5 kyr) periods of declining activity or quiescence. Although intriguing as a
1253 feature, here we do not speculate on the possible significance of such cyclicity (e.g., identifying a possible
1254 external forcing such as sea level change (Satow et al., 2021), astronomical factors and/or regional tectonics
1255 (Marra et al., 2004), as the current analysed record of Fucino is still too short for performing a statistically
1256 significant analysis of the frequency distribution of the whole peri-Tyrrhenian potassic explosive activity. We
1257 remark that the shape and fluctuation of the reported curve of the temporal distribution (Fig. 17c) does not
1258 consider the magnitude and intensity of the events, whereas the actual rate of the erupted volume or mass of
1259 magma through time represents an even more important parameter than the mere recurrence interval or
1260 frequency of eruptive events. Therefore, further considerations on this key issue are postponed until the
1261 complete Fucino tephra record covering the last 430 kyr, or even longer, will be retrieved and fully investigated.
1262

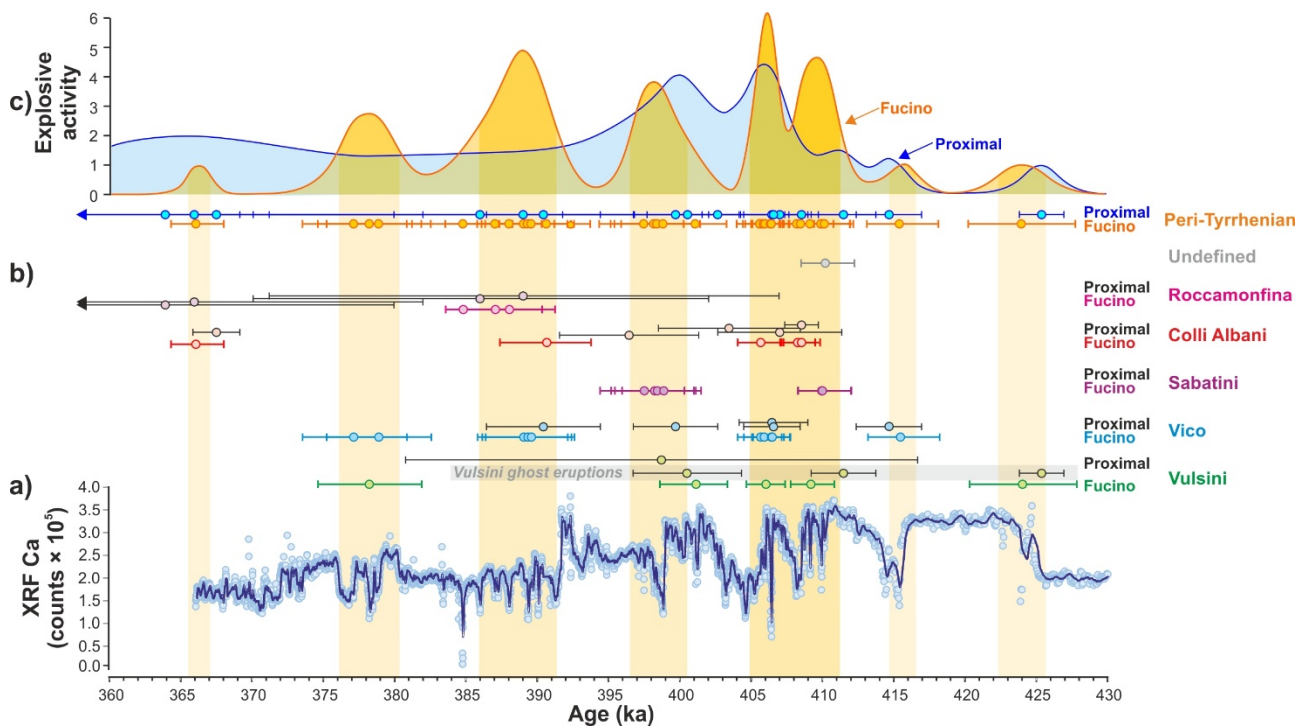


Figure 17. Temporal distribution of the explosive activity of the peri-Tyrrhenian potassic volcanism of central Italy during the 430-360 ka interval, as inferred from the Fucino MIS 11 tephra record and chronological data from proximal volcanic areas. **a)** Temporal series of calcium content of the Fucino lacustrine sediments from F4-F5 core (XRF data from [Giaccio et al., 2019](#)). **b)** Comparison between the Fucino and proximal chronological databases from individual peri-Tyrrhenian volcanoes. **c)** Comparison between the probability density functions of the temporal distribution of the peri-Tyrrhenian explosive activity derived from available chronological data from Fucino and proximal volcanic areas. Source for the $^{40}\text{Ar}/^{39}\text{Ar}$ age of the proximal units: **Vulsini:** [Turbeville \(1992\)](#), [Marra et al. \(2020a\)](#); **Vico:** [Marra et al. \(2014\)](#), [Pereira et al. \(2020\)](#); **Sabatini:** no literature data; **Colli Albani:** [Gaeta et al. \(2016\)](#), [Marra et al. \(2016a\)](#); **Roccamonfina:** [Rouchon et al. \(2008\)](#).

1263
1264
1265
1266
1267
1268
1269
1270
1271
1272
1273
1274
1275
1276
1277
1278
1279
1280
1281
1282
1283
1284
1285
1286
1287
1288
1289
1290
1291
1292

6. Summary and concluding remarks

Here, we have presented a comprehensive review of the state-of-the-art Mediterranean tephrochronology and explosive history of the peri-Tyrrhenian potassic volcanoes during the MIS 11 period. This was achieved in light of new lithostratigraphic, geochemical (major and trace glass composition and multi-phase $^{87}\text{Sr}/^{86}\text{Sr}$ composition) and geochronological ($^{40}\text{Ar}/^{39}\text{Ar}$ dating) characterization of 28 tephra layers from the Fucino F4-F5 succession, as well as of some, potentially equivalent, pyroclastic units collected in proximal areas of the peri-Tyrrhenian potassic volcanoes of central Italy. The integration of these new data with previous investigation from the F4-F5 core, results in a record of 32 tephra layers spanning the 430-365 ka period, thus making Fucino the richest distal archive for this time interval over the entire Mediterranean region. The resulting dataset allowed us to detect the volcanic sources of most of the newly investigated tephra layers and, in many cases, to recognise the specific equivalent eruption or eruptive phase. A Bayesian age-depth model, based on nine, either directly or geochemically correlated, $^{40}\text{Ar}/^{39}\text{Ar}$ dated tephra layers yielded a continuously dated record for the Fucino MIS 11 tephra. A synopsis of all the investigated tephra, along with their volcanic sources, corresponding eruptions and related ages is shown in [Figure 15](#). By combining the updated stratigraphic, geochemical, and chronological datasets, we provide an overview of the MIS 11 tephrochronology for the central Mediterranean area ([Fig. 16](#)) and even beyond, as shown here by the discovering of a possible equivalent of the Hungarian Bag tephra.

Furthermore, regardless of the limitations of using a single location distal tephra archive to reconstruct past volcanism, the Fucino record clearly documents the eruptive history of the peri-Tyrrhenian explosive volcanoes

1293 of central Italy with unprecedented detail and at a higher chronological resolution with respect to available
1294 datasets from proximal areas. The improved knowledge of the activity histories of Vulcini, Vico, Sabatini, Colli
1295 Albani and Roccamonfina volcanoes, in many cases providing new evidence for previously unidentified
1296 eruptions and substantially improving the chronology of the known ones, sets the ground for refining the
1297 eruption timing and frequency as well as duration of intervening quiescence periods. This has key implications
1298 for hazard assessment as well as for identifying cyclic behaviour of the explosive activity (Fig. 17) linked to still
1299 unknown external forcing(s) factors.

1300 Finally, from a wider methodological point of view, the results of this study strengthen and consolidate the
1301 relevance of the distal tephra archives as fundamental, integrative records for better reconstructing the
1302 behaviour of explosive volcanism, which is crucial for understanding the underlying dynamics and the
1303 assessment of the related hazards. This is particularly true in the perspective of future widening of the network
1304 of records throughout the regions surrounding Quaternary volcanic areas. Such network will be most valuable
1305 for extending the lattice of correlations and for tracing individual tephra layers, which in turn are crucial for both
1306 tephrochronological and volcanological purposes. In this perspective, the Fucino Basin, with its long and
1307 continuous sedimentary history and strategic position, arises as a cornerstone for the development and the
1308 application of this approach in the Mediterranean region for the Quaternary sciences and volcanology.

1309

1310 **Acknowledgments**

1311 This article is a contribution of project “Fucino Tephrochronology Unites Quaternary Records (FUTURE)”,
1312 supported by the Italian Ministry of Education, University and Research (MIUR, grant PRIN No.
1313 20177TKBXZ_003; G. Zanchetta, coordinator). The Fucino project is co-funded by DFG (German Research
1314 Foundation) grant WA 2109/16. ⁴⁰Ar/³⁹Ar dating also received complementary contribution from the CNRS
1315 INSU-LEFE 2018-2020 action to S. Nomade. P.G. Albert is supported by a UKRI Future Leaders Fellowship
1316 (MR/S035478/1). INGV, OV laboratories have been also financially supported by the EPOS Research
1317 Infrastructure through the contribution of the Italian Ministry of University and Research (MUR). An earlier
1318 version of the manuscript benefited from useful comments from Roberto Sulpizio and an anonymous reviewer.

1319

1320 **References**

1321

- 1322 Albert, P.G., Giaccio, B., Isaia, R., Costa, A., Niespolo, E.M., Nomade, S., Pereira, A., Renne, P.R., Hinchliffe, A., Mark,
1323 D.F., Brown, R.J., Smith, V.C., 2019. Evidence for a large-magnitude eruption from Campi Flegrei Caldera (Italy) at 29
1324 ka. *Geology*. [Hhttps://doi.org/10.1130/G45805.1](https://doi.org/10.1130/G45805.1).
- 1325 Albert, P.G., Smith, V.C., Suzuki, T., Tomlinson, E.L., Nakagawa, T., McLean, D., Yamada, M., Staff, R.A., Scholout, G.,
1326 Takemura, T., Nagahashi, Y., Kimura, J., Suigetsu 2006 Project Members, 2018. Constraints on the frequency and
1327 dispersal of explosive eruptions at Sambe and Daisen volcanoes (South-West Japan Arc) from the distal Lake Suigetsu
1328 record (SG06 core). *Earth Science Reviews*, 185, 1004-1028.
- 1329 Amato, V., Aucelli, P.P.C., Cesarano, M., Filocamo, F., Leone, N., Petrosino, P., Roskopf, C.M., Valente, E., Casciello,
1330 E., Giralt, S., Jicha, B.R., 2018. Geomorphic response to late Quaternary tectonics in the axial portion of the Southern
1331 Apennines (Italy): A case study from the Calore River valley. *Earth Surface Processes and Landforms*, 43, 2463-2480.
- 1332 Amato, V., Aucelli, P.P.C., Cesarano, M., Jicha, B., Lebreton, V., Orain, R., Pappone, G., Petrosino, P., Russo Ermolli, E.,
1333 2014. Quaternary evolution of the largest intermontane basin of the Molise Apennine (Central Southern Italy).
1334 *Rendiconti Lincei*, 25, 197-216.
- 1335 Belkin, H.E., Rolandi, G., Jackson, J.C., Cannatelli, C., Doherty, A.L., Petrosino, P., De Vivo, B., 2016. Mineralogy and
1336 geochemistry of the older (>40 ka) ignimbrites in the Campanian Plain, southern Italy. *Journal of Volcanology and
1337 Geothermal Research*, 323, 1-18.
- 1338 Bini M., Zanchetta G., Drysdale R.N., Giaccio B., Stocchi P., Vacchi M., Hellstrom J.C., Couchoud I., Monaco L., Ratti A.,
1339 Martini, F., Sarti L., 2020. An end to the Last Interglacial highstand before 120 ka: Relative sea-level evidence from
1340 Infreschi Cave (Southern Italy). *Quaternary Science Reviews* 250, 106658.

- 1341 Blaauw, M. & Christen, J.A., 2011. Flexible paleoclimate age-depth models using an autoregressive gamma process.
 1342 Bayesian Analysis, 6:3, 457-474.
- 1343 Blockley, S.P.E., Bourne, A.J., Brauer, A., Davies, S.M., Hardiman, M., Harding, P.R., Lane, C.S., MacLeod, A., Matthews,
 1344 I.P., Pyne-O'Donnel, S.D.F., Rasmussen, S.O., Wulf, S., Zanchetta, G., 2014. Tephrochronology and the extended
 1345 intimate (integration of ice-core, marine and terrestrial records) event stratigraphy 8-128 ka 2bk. Quaternary Science
 1346 Reviews, 106, 88-100.
- 1347 Boari, E., Tommasini, S., Laurenzi, M.A., Conticelli, S., 2009. Transition from Ultrapotassic Kamafugitic to Sub-Alkaline
 1348 Magmas: Sr, Nd, and Pb Isotope, Trace Element and ^{40}Ar - ^{39}Ar Age Data from the Middle Latin Valley Volcanic Field,
 1349 Roman Magmatic Province, Central Italy. Journal of Petrology, 50, 7, 1327-1357.
- 1350 Boncio, P., Lavecchia, G., Pace, B., 2004. Defining a model of 3D seismogenic sources for seismic hazard assessment
 1351 applications: The case of central Apennines (Italy). Journal of Seismology, 8(3), 407-425.
 1352 <https://doi.org/10.1023/B:JOSE.0000038449.78801.05>.
- 1353 Bourne, A.J., Albert, P.G., Matthews, I.P., Trincardi, F., Wulf, S., Asioli, A., Blockley, S.P.E., Keller, J., Lowe, J.J., 2015.
 1354 Tephrochronology of core PRAD 1-2 from the Adriatic Sea: insights into Italian explosive volcanism for the period 200-
 1355 80 ka. Quaternary Science Reviews, 116, 28-43.
- 1356 Bourne, A.J., Lowe, J.J., Trincardi, F., Asioli, A., Blockley, S.P.E., Wulf, S., Matthews, I.P., Piva, A., Vigliotti, L., 2010.
 1357 Distal tephra record for the last ca 105,000 years from core PRAD 1-2 in the central Adriatic Sea: implications for the
 1358 marine tephrostratigraphy. Quaternary Science Reviews, 29, 3079-3094.
- 1359 Bronk Ramsey, C., Albert, P.G., Blockley, S.P.E., Hardiman, M., Housley, R.A., Lane, C.S., Lee, S., Matthews, I.P., Smith,
 1360 V.C., Lowe, J.J., 2015a. Improved age estimates for key Late Quaternary European tephra horizons in the RESET
 1361 lattice. Quaternary Science Reviews, 118, 18-32.
- 1362 Bronk Ramsey, C., Housley, R.A., Lane, C.S., Smith, V.C., Pollard, A.M., 2015b. The Reset tephra database and
 1363 associated analytical tools. Quaternary Science Reviews, 118, 33-47.
- 1364 Bursik, M., 1998. Tephra dispersal. In: Gilbert, J.S., Sparks, R.S.J. (eds). The physics of explosive volcanic eruptions.
 1365 Geological society of London Special Publication, 145, 115-144.
- 1366 Cardello, G.L., Consorti, L., Palladino, D.M., Carminati, E., Carlini, M., Doglioni, C., 2020. Tectonically controlled
 1367 carbonate-seated maar-diatreme volcanoes: The case of the Volsci Volcanic Field, central Italy. Journals of
 1368 Geodynamics, 139, 101763.
- 1369 Cavinato, G.P., Carusi, C., Dell'Asta, M., Miccadei, E., Piacentini T., 2002. Sedimentary and tectonic evolution of Plio-
 1370 Pleistocene alluvial and lacustrine deposits of Fucino Basin (central Italy). Sedimentary Geology, 148, 29-59.
- 1371 Centamore, E., Dramis, F., Di Manna, P., Fumanti, F., Milli, S., Rossi, D., Palombo, M.R., Palladino, D.M., Triglia, R.,
 1372 Zanon, V., Chiocchini, M., Didaskalou, P., Potetti, M., Nisio, S., 2010. Note illustrative del Foglio 402 Ceccano. Carta
 1373 Geologica d'Italia 1:50000. Servizio Geologico d'Italia, Roma.
- 1374 Cioni, R., Sbrana, A., Bertagnini, A., Buonasorte, G., Landi, P., Rossi, U., Salvati, L., 1987. Tephrostratigraphic correlations
 1375 in the Vulsini, Vico and Sabatini volcanic succession. Periodico di Mineralogia, 56, 137-155.
- 1376 Cross, J.K., Tomlinson, E.L., Giordano, G., Smith, V.S., De Benedetti, A.A., Roberge, J., Manning, C.J., Wulf, S., Menzies,
 1377 M.A., 2014. High level triggers for explosive mafic volcanism: Albano Maar, Italy. Lithos, 190-191, 137-153.
- 1378 D'Antonio, M., Mariconte, R., Arienzo, I., Mazzeo, F.C., Carandente, A., Perugini, D., Petrelli, M., Corselli, C., Orsi, G.,
 1379 Principato, M.S., Civetta, L., 2016. Combined Sr-Nd isotopic and geochemical fingerprinting as a tool for identifying
 1380 tephra layers: Application to deep-sea cores from Eastern Mediterranean Sea. Chemical Geology, 443, 121-136.
- 1381 D'Agostino, N., Jackson, J. A., Dramis, F., Funicello, R., 2001. Interactions between mantle upwelling, drainage evolution
 1382 and active normal faulting: an example from the central Apennines (Italy). Geophysical Journal International, 147(2),
 1383 475-497.
- 1384 de Fontaine, C.S., Kaufman, D.S., Anderson, R.S., Werner, A., Waythomass, C.F., Brown, T.A., 2007. Late Quaternary
 1385 distal-fall deposits in lacustrine sediments, Kenai Peninsula, Alaska. Quaternary Research, 68, 1, 64-78.
- 1386 De Rita, D., Funicello, R., Parotto, M., 1988. Carta geologica del complesso vulcanico dei Colli Albani (Vulcano Laziale).
 1387 C.N.R.-Gruppo Nazionale Vulcanologia.
- 1388 De Rita, D., Giordano, G., Rosa, C., Sheridan, M.F., 1995. Volcanic risk at the Alban Hills volcano and numerical
 1389 simulations. In: Triglia, R. (Ed), The Volcano of the Alban Hills. Tipografia SGS, Rome, pp. 267-283.
- 1390 De Vivo, B., Rolandi, G., Gans, P.B., Calvert, A., Bohrson, W.A., Spera, F.J., Belkin, H.E., 2001. New constraints on the
 1391 pyroclastic eruptive history of Campanian volcanic Plain (Italy). Mineralogy and Petrology, 73, 47-65.
- 1392 Del Carlo, P., Smedile, A., Petrelli, M., Di Roberto, A., 2020. Evidence of an unknown explosive eruption of Mt. Etna
 1393 volcano (Italy) during the Late Glacial. Journal of Volcanology and Geothermal Research. 402, 106992.
- 1394 Di Roberto, A., Smedile, A., Del Carlo, P., De Martini, P.M., Iorio, M., Petrelli, M., Pantosti, P., Pinzi, S., Todrani, A., 2018.
 1395 Tephra and cryptotephra in a ~60,000-year old lacustrine sequence from the Fucino Basin: new insights into the major
 1396 explosive events in Italy. Bulletin of Volcanology, 80:20.
- 1397 Doglioni, C., Harabaglia, P., Martinelli, G., Mongelli, F., Zito, G., 1996. A geodynamic model of the Southern Apennines
 1398 accretionary prism. Terra Nova, 8:6, 540-547.
- 1399 Donato, P., Albert, P.G., Crocitti, M., De Rosa, C., Menzies, M.A., 2016. Tephra layers along the southern Tyrrhenian coast
 1400 of Italy: Links to the X-5 & X-6 using volcanic glass geochemistry. Journal of Volcanology and Geothermal Research,
 1401 317, 30-41.
- 1402 Dugmore, A.J., 1989. Icelandic volcanic ash in Scotland. Scottish Geographical Magazine, 105:3, 168-172, DOI:
 1403 10.1080/14702548908554430.
- 1404 Dugmore, A.J., Newton, A.J., Smith, K.T., Mairs, K.A., 2013. Tephrochronology and the late Holocene volcanic and flood
 1405 history of Eyjafjallajökull, Iceland. (2013). Journal of Quaternary Science, 28:3, 237-247.
- 1406 Florindo, F., Karner, D.B., Marra, F., Renne, P.R., Roberts A.P., Weaver, R., 2007. Radioisotopic age constraints for
 1407 Glacial Terminations IX and VII from aggradational sections of the Tiber River delta in Rome, Italy. Earth and Planetary
 1408 Science Letters 256, 61-80. doi: 10.1016/j.epsl.2007.01.014.

- 1409 Freda, C., Gaeta, M., Giaccio, B., Marra, F., Palladino, D.M., Scarlato, P., Sottili, G., 2011. CO₂-driven large mafic explosive
1410 eruptions: the Pozzolane Rosse case study from the Colli Albani Volcanic District (Italy). *Bulletin of Volcanology*, 73,
1411 241-256.
- 1412 Freda, C., Gaeta, M., Karner, D.B., Marra, F., Renne, P.R., Taddeucci, J., Scarlato, P., Christensen, J.N., Dallai, L., 2006.
1413 Eruptive history and petrologic evolution of the Albano multiple maar (Alban Hills, Central Italy). *Bulletin of Volcanology*,
1414 68, 567-591.
- 1415 Freda, C., Gaeta, M., Palladino, D.M., Trigila, R., 1997. The Villa Senni eruption (Alban Hills, Central Italy): the role of H₂O
1416 and CO₂ on the magma chamber evolution and on the eruptive scenario. *Journal of Volcanology and Geothermal
1417 Research*, 78 (1-2), 103-120.
- 1418 Funciello, R., De Rita, D., Sposato, A., Esposito, A., Fabbri, M., Marsili, P., Mazzini, I., Paccara, P., Trigari, A., Capelli, G.,
1419 Faccenna, C., Fiorentino, A., Mazza, R., Rossetti, F., Sardella, R., Soligo, M., Tuccimei, P., Villa, I.M., 2012. Note
1420 Illustrative della Carta Geologica d'Italia alla scala 1:50.000, Foglio 354 "Tarquinia". Presidenza del Consiglio dei
1421 Ministri, Agenzia per la Protezione dell'Ambiente e per i servizi Tecnici: Roma, Italy, Servizio Geologico d'Italia, scale
1422 1:50,000 (in press).
- 1423 Gaeta, M., Freda, C., Christensen, J.N., Dallai, L., Marra, F., Karner, D.B., Scarlato, P., 2006. Time-dependent
1424 geochemistry of clinopyroxene from the Alban Hills (Central Italy): clues to the source and evolution of ultrapotassic
1425 magmas. *Lithos* 86, 330-346.
- 1426 Gaeta, M., Freda, C., Marra F., Arienzo, I., Gozzi, F., Jicha, B., Di Rocco, T., 2016. Paleozoic metasomatism at the origin
1427 of Mediterranean ultrapotassic magmas: Constraints from time-dependent geochemistry of Colli Albani volcanic
1428 products (Central Italy). *Lithos*, 244, 151-164.
- 1429 Gaeta, M., Freda, C., Marra, F., Di Rocco, T., Gozzi, F., Arienzo, I., Giaccio, B., Scarlato, P., 2011. Petrology of the most
1430 recent ultrapotassic magmas from the Roman Province (Central Italy). *Lithos*, 127, 298-308.
- 1431 Galadini, F. & Galli, P., 2000. Active tectonics in the Central Apennines (Italy) - Input Data for Seismic Hazard Assessment.
1432 *Natural Hazards*, 22, 225-270.
- 1433 Gatta, M., Sinopoli, G., Giardini, M., Giaccio, B., Hajdas, I., Pandolfi, L., Bailey, G., Spikins, P., Rolfo, M.F., Sadori, L.,
1434 2016. Pollen from Late Pleistocene hyena (*Crocota Crocuta spelaea*) coprolites: An interdisciplinary approach from
1435 two Italian sites. *Review of Palaeobotany and Palynology*, 233, 56-66.
- 1436 Gehrels, M.J., Lowe, D.J., Hazell, Z.J., Newnham, R.M., 2006. A continuous 5300-yr Holocene cryptotephrostratigraphic
1437 record from northern New Zealand and implications for tephrochronology and volcanic hazard assessment. *The
1438 Holocene*, 16, 2, 173-187.
- 1439 Giaccio, B., Arienzo, I., Sottili, G., Castorina, F., Gaeta, M., Nomade, S., Galli, P., Messina, P., 2013a. Isotopic (Sr-Nd)
1440 and major element fingerprinting of distal tephra: An application to the Middle-Late Pleistocene markers from the Colli
1441 Albani volcano, central Italy. *Quaternary Science Reviews*, vol. 67, 190-206.
- 1442 Giaccio, B., Castorina, F., Nomade, S., Scardia, G., Voltaggio, M., Sagnotti, L., 2013b. Revised Chronology of the Sulmona
1443 Lacustrine Succession, Central Italy. *Journal of Quaternary Science*, 28, 545-551.
- 1444 Giaccio, B., Galli, P., Messina, P., Peronace, E., Scardia, G., Sottili, G., Sposato, A., Chiarini, E., Jicha, B., Silvestri, S.,
1445 2012b. Fault and basin depocentre migration over the last 2Ma in the L'Aquila 2009 earthquake region, central Italian
1446 Apennines. *Quaternary Science Reviews*, 56, 69-88.
- 1447 Giaccio, B., Galli, P., Peronace, E., Arienzo I., Nomade, S., Cavinato, G.P., Mancini, M., Messina, P., Sottili, G., 2014. A
1448 560-440 ka tephra record from the Mercure Basin, Southern Italy: volcanological and tephrostratigraphic implications.
1449 *Journal of Quaternary Science*, 29, 232-248.
- 1450 Giaccio, B., Leicher, N., Mannella, G., Monaco, L., Regattieri, E., Wagner, B., Zanchetta, G., Gaeta, M., Marra, F., Nomade,
1451 S., Palladino, D.M., Pereira, A., Scheidt, S., Sottili, G., Wonik, T., Wulf, S., Zeeden, C., Ariztegui, D., Cavinato, G.P.,
1452 Dean, R.J., Florindo, F., Leng, M.J., Macri, P., Niespolo, E., Renne, P.R., Rolf, C., Sadori, L., Thomas, C., Tzedakis,
1453 P.C., 2019. Extending the tephra and paleoenvironmental record of the Central Mediterranean back to 430 ka: A new
1454 core from Fucino Basin, central Italy. *Quaternary Science Reviews*, 225, 106003.
- 1455 Giaccio, B., Marra, F., Hajdas, I., Karner, D.B., Renne, P.R., Sposato, A., 2009. ⁴⁰Ar/³⁹Ar and ¹⁴C geochronology of the
1456 Albano maar deposits: Implications for defining the age and eruptive style of the most recent explosive activity at Colli
1457 Albani Volcanic District, Central Italy. *Journal of Volcanology and Geothermal Research*, 185, 203-213.
- 1458 Giaccio, B., Niespolo, E.M., Pereira, A., Nomade, S., Renne, P.R., Albert, P.G., Arienzo, I., Regattieri, E., Wagner, B.,
1459 Zanchetta, G., Gaeta, M., Galli, P., Mannella, G., Peronace, E., Sottili, G., Florindo, F., Leicher, N., Marra, F.,
1460 Tomlinson, E.L., 2017. First integrated tephrochronological record for the last ~190 kyr from the Fucino Quaternary
1461 lacustrine succession, central Italy. *Quaternary Science Reviews*, 158, 211-234.
- 1462 Giaccio, B., Nomade, S., Wulf, S., Isaia, R., Sottili, G., Cuvuoto, G., Galli, P., Messina, P., Sposato, A., Sulpizio, R.,
1463 Zanchetta, G., 2012a. The late MIS 5 Mediterranean tephra markers: a reappraisal from peninsular Italy terrestrial
1464 records. *Quaternary Science Reviews*, 56, 31-45.
- 1465 Giaccio, B., Regattieri, E., Zanchetta, G., Nomade, S., Renne, P.R., Sprain, C.J., Drysdale, R.N., Tzedakis, P.C., Messina,
1466 P., Scardia, G., Sposato, A., Bassinot, F., 2015a. Duration and dynamics of the best orbital analogue to the present
1467 interglacial. *Geology*, 43, 603-606.
- 1468 Giaccio, B., Regattieri, E., Zanchetta, G., Wagner, B., Galli, P., Mannella, G., Niespolo, E., Peronace, E., Renne, P.R.,
1469 Nomade, S., Cavinato, G.P., Messina, P., Sposato, A., Boschi, C., Florindo, F., Marra, F., Sadori, L., 2015b. A key
1470 continental archive for the last 2 Ma of climatic history of the central Mediterranean region: A pilot drilling in the Fucino
1471 Basin, central Italy. *Scientific Drilling*, 20, 13-19.
- 1472 Giannetti, B. & De Casa, G., 2000. Stratigraphy, chronology, and sedimentology of ignimbrites from the white trachytic tuff,
1473 Roccamonfina Volcano, Italy. *Journal of Volcanology and Geothermal Research*, 96, 3-4, 243-295.
- 1474 Giannetti, B., 1996a. The geology of the Yellow Trachytic Tuff, Roccamonfina Volcano. *Journal of Volcanology and
1475 Geothermal Research*, 71, 1, 53-72.

- 1476 Giannetti, B., 1996b. Volcanology of trachytic and associated basaltic pyroclastic deposits at Roccamonfina volcano,
1477 Roman Region, Italy. *Journal of Volcanology and Geothermal Research*, 71, 2-4, 229-248.
- 1478 Giannetti, B., 2001. Origin of the calderas and evolution of Roccamonfina volcano (Roman Region, Italy). *Journal of*
1479 *Volcanology and Geothermal Research*, 106, 301-319.
- 1480 Giordano, G., De Benedetti, A.A., Diana, A., Diano, G., Gaudioso, F., Marasco, F., Miceli, M., Mollo, S., Cas, R.A.F.,
1481 Funicello, R., 2006. The Colli Albani mafic caldera (Roma, Italy): Stratigraphy, structure and petrology. *Journal of*
1482 *Volcanology and Geothermal Research*, 155, 49-80.
- 1483 Goldstein, S.L., Denis, P., Oelkers, E.H., Rudnick, R.L., Walter, L.M., 2003. Standards for publication of isotope ratio and
1484 chemical data in chemical geology. *Chemical Geology*, 202, 1-4.
- 1485 Horváth, E. & Bradák, B., 2014. Sárga föld, lész, lész: Short historical overview of loess research and lithostratigraphy in
1486 Hungary. *Quaternary International*, 319, 1-10.
- 1487 Hum, L., 2005. Középső pleisztocén tufithorizontok megjelenése dunaszekcsői és Mórág környéki löszszelvényekben.
1488 *Malakológiai Tájékoztató*, 23, 131-148 (in Hungarian).
- 1489 Insinga, D.D., Tamburrino, S., Lirer, F., Vezzoli, L., Barra, M., De Lange, G.J., Tiepolo, M., Vallefucio, M., Mazzola, S.,
1490 Sprovieri, M., 2014. Tephrochronology of the astronomically-tuned KC01B deep-sea core, Ionian Sea: insights into the
1491 explosive activity of the Central Mediterranean area during the last 200 ka. *Quaternary Science Reviews*, 85, 63-84.
- 1492 Jochum, K.P., Stoll, B., Herwig, K., Willbold, M., Hofmann, A.W., Amini, M., Aarbug, S., Abouchami, W., Hellebrand, E.,
1493 Mocek, B., Raczek, I., Stracke, A., Alard, O., Bouman, C., Becker, S., Dücking, M., Brätz, H., Klemm, R., de Bruin, D.,
1494 Canil, D., Cornell, D., de Hoog, C.-S., Dalpé, C., Danyushevsky, L., Eisenhauer, A., Gao, Y., Snow, J.E., Groschopf,
1495 N., Günther, D., Latkoczy, C., Guillong, M., Hauri, E.K., Höfer, H.E., Lahaye, Y., Horz, K., Jacob, D.E., Kasemann,
1496 S.A., Kent, A.J.R., Ludwig, T., Zack, T., Mason, P.R.D., Meixner, A., Rosner, M., Kisawa, K., Nash, P.B., Pfänder, J.,
1497 Premo, W.R., Sun, W.D., Tiepolo, M., Vannucci, R., Vennemann, T., Wayne, D., Woodhead, J.D., 2006. MPI-DING
1498 reference glasses for in situ microanalysis: New reference values for element concentrations and isotope ratios.
1499 *Geochemistry, Geophysics, Geosystems*, 7:2.
- 1500 Karner, D.B. & Renne, P.R., 1998. ⁴⁰Ar/³⁹Ar geochronology of Roman volcanic province tephra in the Tiber River valley:
1501 Age calibration of middle Pleistocene sea-level changes. *Geological Society of America Bulletin*, 110, 6, 740-747.
- 1502 Karner, D.B., Juvinge, E., Brancaccio, L., Cinque, A., Russo Ermolli, E., Santangelo, L., Bernasconi, S., Lirer, L., 1999. A
1503 potential early middle Pleistocene tephrostratotype for the Mediterranean basin: the Vallo Di Diano, Campania, Italy.
1504 *Global and Planetary Change*, 21, 1-15.
- 1505 Keller, J., Ryan, W.B.F., Ninkovich, D., Altherr, R., 1978. Explosive volcanic activity in the Mediterranean over the last
1506 200,000 yr as recorded in deep-sea sediments. *Geological Society of America Bulletin*, 89, 591-604.
- 1507 Kousis, I., Koutsodendris, A., Peyron, O., Leicher, N., Francke, A., Wagner, B., Giaccio, B., Knipping, M., Pross, J., 2018.
1508 Centennial-scale vegetation dynamics and climate variability in SE Europe during Marine Isotope Stage 11 based on
1509 a pollen record from Lake Ohrid, *Quaternary Science Reviews*, 190, 20-38.
- 1510 Kuehn, S.C., Froese, D.G., Shane, P.A.R., INTAV Intercomparison Participants, 2011. The INTAV intercomparison of
1511 electron-beam microanalysis of glass by tephrochronology laboratories: Results and recommendations. *Quaternary*
1512 *International*, 246, 19-47.
- 1513 Lane, C.S., Brauer, A., Blockley, S.P.E., Dulski, P., 2013. Volcanic ash reveals time-transgressive abrupt climate change
1514 during the Younger Dryas. *Geology*, 41 (12), 1251-1254.
- 1515 Larsen, G., Róbertsdóttir, B.G., Oladottir, B.A., Eiríksson, J., 2020. A shift in eruption mode of Hekla volcano, Iceland, 3000
1516 years ago: two-coloured Hekla tephra series, characteristics, dispersal and age. *Journal of Quaternary Science*, 35,
1517 *Special Issue 1-2*, 143-154.
- 1518 Le Maitre, R.W., Streckeisen, A., Zanettin, B., Le Bas, M.J., Bonin, B., Bateman, P., Bellieni, G., Dudek, A., Efremova, S.,
1519 Keller, J., Lameyre, J., Sabine, P.A., Schmid, R., Sørensen, H., Woolley, A.R., 2002. *Igneous Rocks: A Classification*
1520 *and Glossary of Terms. Recommendation of the International Union of Geological Sciences Subcommittee on the*
1521 *Systematics of Igneous Rocks, 2nd Edition. Cambridge University Press, Cambridge. 236 pages.*
- 1522 Lee, J.Y., Marti, K., Severinghaus, J.P., Kawamura, K., Yoo, H.S., Lee, J.B., Kim, J.S., 2006. A redetermination of the
1523 isotopic abundances of atmospheric Ar. *Geochimica and Cosmochimica Acta*, 70, 4507-4512.
- 1524 Leicher, N., Giaccio, B., Zanchetta, G., Wagner, B., Francke, A., Palladino, D.M., Sulpizio, R., Albert, P.G., Tomlinson,
1525 E.L., 2019. Central Mediterranean explosive volcanism and tephrochronology during the last 630 ka based on the
1526 sediment record from Lake Ohrid. *Quaternary Science Reviews*, 226, 106021.
- 1527 Leicher, N., Zanchetta, G., Sulpizio, R., Giaccio, B., Wagner, B., Nomade, S., Francke, A., Del Carlo, P., 2016. First
1528 tephrostratigraphic results of the DEEP site record from Lake Ohrid (Macedonia and Albania). *Biogeosciences*, 13, 2151-
1529 2178.
- 1530 Lisiecki, L.E. & Raymo, M.E., 2005. A Pliocene-Pleistocene stack of 57 globally distributed benthic $\delta^{18}\text{O}$ records.
1531 *Paleoceanography*, 20, doi:10.1029/2004PA001071.
- 1532 Lourens, L.J., 2004. Revised tuning of Ocean Drilling Program Site 964 and KC01B (Mediterranean) and implications for
1533 the $\delta^{18}\text{O}$, tephra, calcareous nannofossil, and geomagnetic reversal chronologies of the past 1.1 Myr.
1534 *Paleoceanography and Paleoclimatology*, 19, PA3010.
- 1535 Lowe, D.J., Bronk Ramsey, C., Housley, R.A., Lane, C.S., Tomlinson, E.L., RESET Team, RESET Associates, 2015. The
1536 RESET project: constructing a European tephra lattice refined synchronisation of environmental and archaeological
1537 events during the last c. 100 ka. *Quaternary Science Reviews*, 118, 1-17.
- 1538 Lowe, D.J., 2011. Tephrochronology and its application: A review. *Quaternary Geochronology*, 6, 107-153.
- 1539 Luberti, G.M., Marra, F., Florindo, F., 2017. A review of the stratigraphy of Rome (Italy) according to geochronologically
1540 and paleomagnetically constrained aggradational successions, glacio-eustatic forcing and volcano-tectonic processes.
1541 *Quaternary International*, 438, Part B, 40-67.
- 1542 Luhr, J.F. & Giannetti, B., 1987. The Brown Leucitic Tuff of Roccamonfina Volcano (Roman Region, Italy). *Contributions*
1543 *to Mineralogy and Petrology*, 95, 420-436.

- 1544 Lustrino, M., Duggen, S., Rosenberg, C.L., 2011. The Central-Western Mediterranean: Anomalous igneous activity in an
1545 anomalous collisional tectonic setting. *Earth-Science Reviews*, 104, 1-3, 1-40.
- 1546 Mannella, G., Giaccio, B., Zanchetta, G., Regattieri, E., Niespolo, E.M., Pereira, A., Renne, P.R., Nomade, S., Leicher, N.,
1547 Perchiazzi, N., Wagner, B., 2019. Paleoenvironmental and paleohydrological variability of mountain areas in the central
1548 Mediterranean region: A 190-ka-long chronicle from the independently dated Fucino paleolake record (central Italy).
1549 *Quaternary Science Reviews*, 210, 190-210.
- 1550 Marra, F., Cardello, G.L., Gaeta, M., Jicha, B.R., Montone, P., Niespolo, E.M., Nomade, S., Palladino, D.M., Pereira, A.,
1551 De Luca, G., Florindo, F., Frepoli, A., Renne, P.R., Sottili, G., 2021. The Volsci Volcanic Field (central Italy): eruptive
1552 history, magma system and implications on continental subduction processes. *International Journal of Earth Sciences*.
1553 <https://doi.org/10.1007/s00531-021-01981-6>.
- 1554 Marra, F., Castellano, C., Cucci, L., Florindo, F., Gaeta, M., Jicha, B., Palladino, D.M., Sottili, G., Tertulliani, A., Tolomei,
1555 C., 2020b. Monti Sabatini and Colli Albani: the dormant twin volcanoes at the gates of Rome. *Scientific Reports*
1556 10:8666. <https://doi.org/10.1038/s41598-02-65394-2>.
- 1557 Marra, F., Costantini, L., Di Buduo, G.M., Florindo, F., Jicha, B.R., Monaco, L., Palladino, D.M., Sottili, G., 2019. Combined
1558 glacio-eustatic forcing and volcano-tectonic uplift: geomorphological and geochronological constraints on the Tiber
1559 River terraces in the eastern Vulsini Volcanic District (central Italy). *Global and Planetary Change*, 182, 103009.
1560 doi:10.1016/j.gloplacha.2019.103009.
- 1561 Marra, F., Freda, C., Scarlato, P., Taddeucci, J., Karner, D.B., Renne, P.R., Gaeta, M., Palladino, D.M., Triglia, R.,
1562 Cavaretta, G., 2003. Post-caldera activity in the Alban Hills volcanic district (Italy): $^{40}\text{Ar}/^{39}\text{Ar}$ geochronology and insights
1563 into magma evolution. *Bulletin of Volcanology*, 65, 227-247.
- 1564 Marra, F., Gaeta, M., Giaccio, B., Jicha, B.R., Palladino, D.M., Polcari, M., Sottili, G., Taddeucci, J., Florindo, F.,
1565 Stramondo, S., 2016a. Assessing the volcanic hazard for Rome: $^{40}\text{Ar}/^{39}\text{Ar}$ and In-SAR constraints on the most recent
1566 eruptive activity and present-day uplift at Colli Albani Volcanic District. *Geophysical Research Letters*, 43, 6898-6906.
- 1567 Marra, F., Jicha, B., Florindo, F., 2017. $^{40}\text{Ar}/^{39}\text{Ar}$ dating of Glacial Termination VI: constraints to the duration of Marine
1568 Isotopic Stage 13. *Scientific Reports*, 7, 8908. doi:10.1038/s41598-017-08614-6
- 1569 Marra, F., Jicha, B., Palladino, D.M., Gaeta, M., Costantini, L., Di Buduo, G.M., 2020a. $^{40}\text{Ar}/^{39}\text{Ar}$ single crystal dates from
1570 pyroclastic deposits provide a detailed record of the 590-240 ka eruptive period at the Vulsini Volcanic District (central
1571 Italy). *Journal of Volcanology and Geothermal Research*, 398, 106904.
- 1572 Marra, F., Karner, D.B., Freda, C., Gaeta, M., Renne, P., 2009. Large mafic eruptions at Alban Hills Volcanic District
1573 (Central Italy): chronostratigraphy, petrography and eruptive behavior. *Journal of Volcanology and Geothermal
1574 Research*, 179, 217-232.
- 1575 Marra, F., Nomade, S., Pereira, A., Petronio, C., Salari, L., Sottili, G., Bahain, J.J., Boschian, G., Di Stefano, G., Falguères,
1576 C., Florindo, F., Gaeta, M., Giaccio, B., Masotta, M., 2018. A review of the geological sections and the faunal
1577 assemblages of Aurelian Mammal Age of Latium (Italy) in the light of a new chronostratigraphic framework. *Quaternary
1578 Science Reviews*, 181, 173-199.
- 1579 Marra, F., Rohling, E.J., Florindo, F., Jicha, B., Nomade, S., Pereira, A., Renne, P.R., 2016b. Independent $^{40}\text{Ar}/^{39}\text{Ar}$ and
1580 ^{14}C age constraints on the last five glacial terminations from the aggradational successions of the Tiber River, Rome
1581 (Italy). *Earth and Planetary Science Letters*, 449, 105-117.
- 1582 Marra, F., Sottili, G., Gaeta, M., Giaccio, B., Jicha, B., Masotta, M., Palladino, D.M., Deocampo, D.M., 2014. Major
1583 explosive activity in the Monti Sabatini Volcanic District (central Italy) over the 800-390 ka interval: geochronological-
1584 geochemical overview and tephrostratigraphic implications. *Quaternary Science Reviews*, 94, 74-101.
- 1585 Marra, F., Taddeucci, J., Freda, C., Marzocchi, W., Scarlato, P., 2004. Recurrence of volcanic activity along the Roman
1586 Comagmatic Province (Tyrrhenian margin of Italy) and its tectonic significance. *Tectonics*, 23, TC4013.
- 1587 Matthews, I.P., Trincardi, F., Lowe, J.J., Bourne, A.J., MacLeod, A., Abbott, P.M., Andersen, N., Asioli, A., Blockley, S.P.E.,
1588 Lane, C.S., Oh, Y.A., Satow, C.S., Staff, R.A., Wulf, S., 2015. Developing a robust tephrochronological framework for
1589 Late Quaternary marine records in the Southern Adriatic Sea: new data from core station SA03-11. *Quaternary Science
1590 Reviews*, 118, 84-104.
- 1591 Mcmanus, J., Oppo, D., Cullen, J., & Healey, S. 2003. Marine isotope stage 11 (MIS 11): analog for Holocene and future
1592 Climate? Earth's climate and orbital eccentricity: the marine isotope stage 11 question, 137, 69-85.
- 1593 Morabito, S., Petrosino, P., Milia, A., Sprovieri, M., Tamburrino, S., 2014. A multidisciplinary approach for reconstructing
1594 the stratigraphic framework of the last 40 ka in a bathyal area of eastern Tyrrhenian Sea. *Global and Planetary Change*,
1595 123, Part A, 121-138.
- 1596 Munno, R. & Petrosino, P., 2007. The late Quaternary tephrostratigraphical record of the San Gregorio Magno basin
1597 (southern Italy). *Journal of Quaternary Science*, 22, 247-266.
- 1598 Nappi, G., Renzulli, A., Santi, P., Gillot, Y.P., 1995. Geological evolution and geochronology of the Vulsini volcanic district
1599 (central Italy): *Bollettino della Società Geologica Italiana*, v. 114, p. 599-613.
- 1600 Narcisi, B. & Vezzoli, L., 1999. Quaternary stratigraphy of distal tephra layers in the Mediterranean - an overview. *Global
1601 and Planetary Change*, 21, 31-50.
- 1602 Newnham, R.M., Lowe, D.J., Alloway, B.V., 1999. Volcanic hazards in Auckland, New Zealand: a preliminary assessment
1603 of the threat posed by central North Island silicic volcanism based on the Quaternary tephrostratigraphical record.
1604 Geological Society, London, Special Publications, 161, 27-45.
- 1605 Niespolo, E.M., Rutte, D., Deino, A.L., Renne, P.R., 2017. Intercalibration and age of the Alder Creek Sanidine $^{40}\text{Ar}/^{39}\text{Ar}$
1606 standard. *Quaternary Geochronology*, 39, 205-213.
- 1607 Nomade, S., Bassinot, F., Mariano, M., Simon, Q., Dewilde, F., Maiorano, P., Isguder, G., Blamart, D., Girone, A., Scao,
1608 V., Pereira, A., Toti, F., Bertini, A., Combourieu-Nebout, N., Peral, M., Bourlès, D.L., Petrosino, P., Gallicchio, S.,
1609 Ciaranfi, N., 2019. High-resolution foraminifer stable isotope record of MIS 19 at Montalbano Jonico, southern Italy: A
1610 window into Mediterranean climatic variability during a low-eccentricity interglacial. *Quaternary Science Reviews*, 205,
1611 106-125.

- 1612 Nomade, S., Gauthier, A., Guillou, H., Pastre, J.-F., 2010. $^{40}\text{Ar}/^{39}\text{Ar}$ temporal framework for the Alleret maar lacustrine
1613 sequence (French Massif-Central): Volcanological and paleoclimatic implications. *Quaternary Geochronology*, 5:1, 20-
1614 27.
- 1615 Nomade, S., Muttoni, G., Guillou, H., Robin, E., Scardia, G., 2011. First $^{40}\text{Ar}/^{39}\text{Ar}$ age of the Ceprano man (central Italy).
1616 *Quaternary Geochronology*, 6, 453-457.
- 1617 Palladino, D.M., Agosta, E., Freda, C., Spaziani, S., Trigila, R., 1994. Geo-petrographic and volcanological study of
1618 Southern Vulcini: the Valentano–Marta–La Rocca sector. *Memorie Descrittive della Carta Geologica d'Italia*, 49, 255–
1619 276.
- 1620 Palladino, D.M., Simeì, S., Sottili, G., Trigila, R., 2010. Integrated approach for the reconstruction of stratigraphy and
1621 geology of Quaternary volcanic terrains: an application to the Vulcini Volcanoes (central Italy). In: Groppelli, G., Viereck,
1622 e L. (Eds.), *Stratigraphy and Geology in Volcanic Areas*. Geological Society of America Special Paper, 464, 66–84.
- 1623 Patacca, E., Scandone, P., Di Luzio, E., Cavinato, G.P., Parotto, M., 2008. Structural architecture of the central Apennines:
1624 Interpretation of the CROP 11 seismic profile from the Adriatic coast to the orographic divide. *Tectonics*, 27, TC3006,
1625 doi:10.1029/2005TC001917.
- 1626 Paterne, M., Guichard, F., Duplessy, J.C., Siani, G., Sulpizio, R., Labeyrie, J., 2008. A 90,000-200,000 yrs marine tephra
1627 record of Italian volcanic activity in the Central Mediterranean Sea. *Journal of Volcanology and Geothermal Research*,
1628 177, 187-196.
- 1629 Paterne, M., Guichard, F., Labeyrie, J., 1988. Explosive activity of the south Italian volcanoes during the past 80,000 years
1630 as determined by marine tephrochronology. *Journal of Volcanology and Geothermal Research*, 34, 153-172.
- 1631 Paterne, M., Guichard, F., Labeyrie, J., Gillot, P.Y., Duplessy, J.C., 1986. Tyrrhenian Sea tephrochronology of the oxygen
1632 isotope record for the past 60,000 years. *Marine Geology*, 72, 259-285.
- 1633 Peccerillo, A., 2017. Cenozoic Volcanism in the Tyrrhenian Sea Region. In: *IAVCEI, Advances in Volcanology*, 2 ed.
1634 Springer, p. 400.
- 1635 Pereira, A., Monaco, L., Marra, F., Sébastien, N., Gaeta, M., Leicher, N., Palladino, D.M., Sottili, G., Guillou, H., Scao, V.,
1636 Giaccio, B., 2020. Tephrochronology of the central Mediterranean MIS 11c interglacial (~425-395 ka): New constraints
1637 from the Vico volcano and the Tiber delta, central Italy. *Quaternary Science Reviews*, 243, 106-470.
- 1638 Pereira, A., Nomade, S., Moncel, M.H., Voinchet, P., Bahain, J.J., Biddittu, I., Falgueres, C., Giaccio, B., Manzi, G., Parenti,
1639 F., Scardia, G., Scao, V., Sottili, G., Vietti, A., 2018. Integrated geochronology of Acheulian sites from the southern
1640 Latium (central Italy): insights on human-environment interaction and the technological innovations during the MIS 11-
1641 MIS 10 period. *Quaternary Science Reviews*, 187, 112-129.
- 1642 Perini, G. & Conticelli, S., 2002. Crystallization conditions of leucite-bearing magmas and their implications on the
1643 magmatological evolution of ultrapotassic magmas: the Vico Volcano, central Italy. *Mineralogy and petrology*, 74, 253-
1644 276.
- 1645 Perini, G., Conticelli, S., Francalanci, L., 1997. Inferences on the volcanic history of the Vico volcano, Roman Magmatic
1646 Province, central Italy: stratigraphic, petrographic and geochemical data. *Mineralogica et Petrographica Acta*, 40, 67-
1647 93.
- 1648 Perini, G., Conticelli, S., Francalanci, L., Davidson, J. P., 2000. The relationship between potassic and calc-alkaline post-
1649 orogenic magmatism at Vico volcano, central Italy. *Journal of Volcanology and Geothermal Research*, 95, 243-268.
- 1650 Perini, G., Francalanci, L., Davidson, J.P., Conticelli, S., 2004. Evolution and Genesis of Magmas from Vico Volcano,
1651 Central Italy: Multiple Differentiation Pathways and Variable Parental Magmas. *Journal of Petrology*, 45:1, 139-182.
- 1652 Perini, G., Teplei III, F.-J., Davidson, J.P., Conticelli, S., 2003. The origin of K-feldspar megacrysts hosted in alkaline
1653 potassic rocks from central Italy: a track for low-pressure processes in mafic magmas. *Lithos*, 66, 223-240.
- 1654 Petrosino, P., Arienzo, I., Mazzeo, F.C., Natale, J., Petrelli, M., Milia, A., Perugini, D., D'Antonio, M., 2019. The San
1655 Gregorio Magno lacustrine basin (Campania, southern Italy): improved characterization of the tephrostratigraphic
1656 markers based on trace elements and isotopic data. *Journal of Quaternary Science*, 34, 393-404.
- 1657 Petrosino, P., Jicha, B.R., Mazzeo, F.C., Ciaranfi, N., Girone, A., Maiorano, P., 2015. The Montalbano Jonico marine
1658 succession: An archive for distal tephra layers at the Early-Middle Pleistocene boundary in southern Italy. *Quaternary
1659 International*, 383, 89-103.
- 1660 Petrosino, P., Jicha, B.R., Mazzeo, F.C., Russo Ermolli, E., 2014b. A high-resolution tephrochronological record of MIS
1661 14-12 in the Southern Apennines (Acerno Basin, Italy). *Journal of Volcanology and Geothermal Research*, 274, 34-50.
- 1662 Petrosino, P., Morabito, S., Jicha, B.R., Milia, A., Sprovieri, M., Tamburrino, S., 2016. Multidisciplinary tephrochronological
1663 correlation of marker events in the eastern Tyrrhenian Sea between 48 and 105 ka. *Journal of Volcanology and
1664 Geothermal Research*, 315, 79-99.
- 1665 Petrosino, P., Russo Ermolli, E., Donato, P., Jich, B., Robustelli, G., Sardella, R., 2014a. Using tephrochronology and
1666 palynology to date the MIS 13 lacustrine sediments of the Mercure basin (Southern Apennines - Italy). *Italian Journal
1667 of Geosciences*, 133, 169-186.
- 1668 Ponomareva, V.V., Portnyagin, M., Davies, S.M., 2015. Tephra without borders: far-reaching clues into past explosive
1669 eruptions. *Front. Earth Sci.* 3 (83). <https://doi.org/10.3389/feart.2015.00083>
- 1670 Poucllet, A., Horvat, E., Gabris, G., Juvigné, E., 1999. The Bag tephra, a widespread tephrochronological marker in Middle
1671 Europe: chemical and mineralogical investigations. *Bulletin of Volcanology*, 60, 265-272.
- 1672 R Core Team (2017). R: A Language and Environment for Statistical Computing.
- 1673 Radicati di Brozolo, F., Di Girolamo, P., Turi, B., Oddone, M., 1988. $^{40}\text{Ar}/^{39}\text{Ar}$ and K-Ar dating of K-rich rocks from the
1674 Roccamonfina Volcano, Roman Comagmatic Region, Italy. *Geochimica et Cosmochimica Acta*, 52, 1435-1441.
- 1675 Regattieri, E., Giaccio, B., Galli, P., Nomade, S., Peronace, E., Messina, P., Sposato, A., Boschi, C., Gemelli, M., 2016. A
1676 multi-proxy record of MIS 11-12 deglaciation and glacial MIS 12 instability from the Sulmona Basin (central Italy).
1677 *Quaternary Science Reviews*, 132, 129-145.
- 1678 Regattieri, E., Giaccio, B., Mannella, G., Zanchetta, G., Nomade, S., Tognarelli, A., Perchiazzi, N., Vogel, H., Boschi, C.,
1679 Drysdale, R.N., Wagner, B., Gemelli, M., Tzedakis, P., 2019. Frequency and dynamics of millennial-scale variability

- 1680 during marine isotope stage 19: insights from the Sulmona Basin (central Italy). *Quaternary Science Reviews*, 214, 28-
 1681 43.
- 1682 Regattieri, E., Giaccio, B., Zanchetta, G., Drysdale, R.N., Galli, P., Nomade, S., Peronace, E., Wulf, S., 2015. Hydrological
 1683 variability over the Apennines during the Early Last Glacial precession minimum, as revealed by a stable isotope
 1684 record from Sulmona basin, Central Italy. *Journal of Quaternary Science*, 30, 19-31.
- 1685 Renne, P.R., Balco, G., Ludwig, K.R., Mundil, R., Min, K., 2011. Response to the comment by WH Schwarz et al. on “Joint
 1686 determination of 40 K decay constants and $^{40}\text{Ar}/^{40}\text{K}$ for the Fish Canyon sanidine standard, and improved accuracy
 1687 for $^{40}\text{Ar}/^{39}\text{Ar}$ geochronology” by PR Renne et al. (2010). *Geochimica and Cosmochimica Acta*, 75, 5097-5100.
- 1688 Renne, P.R., Sprain, C.J., Richards, M.A., Self, S., Vanderkluysen, L., Pande, K., 2015. State shift in Deccan volcanism
 1689 at the Cretaceous Paleogene boundary, possibly induced by impact. *Science*, 350, 76-78.
- 1690 Rolandi, G., Bellucci, F., Heizler, M.T., Belkin, H.E., De Vivo, B., 2003. Tectonic controls on the genesis of ignimbrite from
 1691 the Campanian Volcanic Zone, southern Italy. *Mineralogy and Petrology*, 79, 3-31.
- 1692 Rouchon, V., Gillot, P.Y., Quidelleur, X., Chiesa, S., Floris, B., 2008. Temporal evolution of the Roccamonfina volcanic
 1693 complex (Pleistocene), Central Italy. *Journal of Volcanology and Geothermal Research*, 177, 500-514.
- 1694 Russo Ermolli, E., Aucelli, P.P.C., Di Rollo, A., Mattei, M., Petrosino, P., Porreca, M., Roskopf, C.M., 2010. An integrated
 1695 stratigraphical approach to the Middle Pleistocene succession of the Sessano Basin (Molise, Italy). *Quaternary
 1696 International*, 225, 114-127.
- 1697 Sági, T., Kiss, B., Bradák, B., Harangi, S., 2008. Középső-pleisztocén löszben előforduló vulkáni képződmények
 1698 Magyarországon: terepi és petrográfiai jellemzők (Middle Pleistocene volcanic sediments in loess in Hungary: field and
 1699 petrographical characteristics). *Földtani Közlöny*, 138, 297-310 (in Hungarian with English abstract).
- 1700 Sagnotti, L., Scardia, G., Giaccio, B., Liddicoat, J.C., Nomade, S., Renne, P.R., Sprain, C.J., 2014. Extremely rapid
 1701 directional change during Matuyama-Brunhes geomagnetic polarity reversal. *Geophysical Journal International*, 199,
 1702 1110-1124.
- 1703 Satow, C., Gudmundsson, A., Gertisser, R., Ramsey, C. B., Bazargan, M., Pyle, D., Wulf, S., Miles, A., Hardiman, M.,
 1704 2021. A sea-level control on the eruptive activity of Santorini volcano, Greece. *Nature Geoscience*.
- 1705 Sbrana, A., Marianelli, P., Pasquini, G., 2018. Volcanology of Ischia (Italy). *Journal of Maps*, 14, 2.
- 1706 Scaillet, S., Vita-Scaillet, G., Guillou, H., 2008. Oldest human footprints dated by Ar/Ar. *Earth and Planetary Science
 1707 Letters*, 275, 320-325.
- 1708 Simon, Q., Bourlès, D.L., Thouveny, N., Horng, C.-S., Valet, J.-P., Bassinot, F., Choy, S., 2018. Cosmogenic signature of
 1709 geomagnetic reversals and excursions from the Réunion event to the Matuyama-Brunhes transition (0.7-2.14 Ma
 1710 interval). *Earth and Planetary Science Letters*, 482, 510-524.
- 1711 Smith, V.C., Isaia, R., Pearce, N.J.G., 2011. Tephrostratigraphy and glass compositions of post-15 kyr Campi Flegrei
 1712 eruptions: implications for eruption history and chronostratigraphic markers. *Quaternary Science Reviews*, 30, 3638-
 1713 3660.
- 1714 Soligo, M. & Tuccimei, P., 2010. Geochronology of Colli Albani volcano. In: Funicello, R., Giordano, G. (eds). *The Colli
 1715 Albani Volcano*. Geological Society of London, Special IAVCEI Publication, 3:99-106.
- 1716 Sottili, G., Arienzo, I., Castorina, F., Gaeta, M., Giaccio, B., Marra, F., Palladino, D.M., 2019. Time-dependent Sr and Nd
 1717 isotope variations during the evolution of ultrapotassic Sabatini Volcanic District (Roman Province, Central Italy).
 1718 *Bulletin of Volcanology*, 81:67.
- 1719 Sottili, G., Palladino, D.M., Marra, F., Jicha, B., Karner, D.B., Renne, P., 2010. Geochronology of the most recent activity
 1720 in the Sabatini volcanic district, Roman Province, central Italy. *Journal of Volcanology and Geothermal Research*, 196,
 1721 20-30.
- 1722 Sottili, G., Palladino, D.M., Zanon, V., 2004. Plinian activity during the early eruptive history of the Sabatini volcanic district,
 1723 central Italy. *Journal of Volcanology and Geothermal Research*, 135, 361-379.
- 1724 Tamburrino, S., Insinga, D.D., Sprovieri, M., Petrosino, P., Tiepolo, M., 2012. Major and trace element characterization of
 1725 tephra layers offshore Pantelleria Island: insights into the last 200 ka of volcanic activity and contribution to the Med-
 1726 iterranean tephrochronology. *Journal of Quaternary Science*, 27, 129-140.
- 1727 Thirlwall, M.F., 1991. Long-term reproducibility of multicollector Sr and Nd isotope ratio analysis. *Chemical Geology*, 94:85-
 1728 104.
- 1729 Thorarinnsson, 1981a. Greetings from Iceland. *Geografiska Annaler: Series A, Physical Geography*, 63:3-4, 109-118, DOI:
 1730 10.1080/04353676.1981.11880024.
- 1731 Thorarinnsson, 1981b. Tephra studies and tephrochronology: a historical review with special reference to Iceland. In: S.
 1732 Self, R.S.J., Sparks (Eds.), *Tephra Studies*, Reidel, Dordrecht (1981), pp. 1-12.
- 1733 Tomlinson, E.L., Albet, P.G., Wulf, S., Brown, R.J., Smith, V.C., Keller, J., Orsi, G., Bourne, A., Menzes, M.A., 2014. Age
 1734 and geochemistry of tephra layers from Ischia, Italy: constraints from proximal-distal correlations with Lago Grande di
 1735 Monticchio. *Journal of Volcanology and Geothermal Research*, 287, 22-39.
- 1736 Tomlinson, E.L., Arienzo, I., Civetta, L., Wulf, S., Smith, V.C., Hardiman, M., Lane, C.S., Carandente, A., Orsi, G., Rosi,
 1737 M., Müller, W., Menzies, M.A., 2012. Geochemistry of the Phlegrean Fields (Italy) proximal sources for major
 1738 Mediterranean tephra: Implications for the dispersal of Plinian and co-ignimbritic components of explosive eruptions.
 1739 *Geochimica et Cosmochimica Acta*, 93, 102-128.
- 1740 Tomlinson, E.L., Smith, V.C., Albet, P.G., Aydar, E., Civetta, L., Cioni, R., Çubukçu, E., Gertisser, R., Isaia, R., Menzies,
 1741 M.A., Orsi, G., Rosi, M., Zanchetta, G., 2015. The major and trace element glass compositions of the productive
 1742 Mediterranean volcanic sources: tools for correlating distal tephra layers in and around Europe. *Quaternary Science
 1743 Reviews*, 118, 48-66.
- 1744 Tomlinson, E.L., Thordarson, T., Muller, W., Thirlwall, M.T., Menzies, M.A., 2010. Microanalysis of tephra by LA-ICP-MS -
 1745 strategies, advantages and limitations assessed using the Thorsmork ignimbrite (Southern Iceland). *Chemical Geology*,
 1746 279, 73-89.

- 1747 Turbeville, B.N., 1992. $^{40}\text{Ar}/^{39}\text{Ar}$ ages and Stratigraphy of the Latera caldera, Italy. *Bulletin of Volcanology*, 55, 110-118.
- 1748 Turbeville, B.N., 1993. Petrology and Petrogenesis of the Latera Caldera, Central Italy. *Journal of Petrology*, 34:1, 77-123.
- 1749 Tzedakis, P.C. 2010. The MIS 11–MIS 1 analogy, southern European vegetation, atmospheric methane and the "early anthropogenic hypothesis". *Climate of the Past*, 6(2), 131-144.
- 1750 Vakhrameeva, P., Koutsodendris, A., Wulf, S., Fletcher, W.J., Appelt, O., Knipping, M., Gertisser, R., Trieloff, M., Pross, J., 2018. The cryptotephra record of the Marine Isotope Stage 12 to 10 interval (460-335 ka) at Tenaghi Philippon, Greece: Exploring chronological markers for the Middle Pleistocene of the Mediterranean reion. *Quaternary Science Reviews*, 200, 313-333.
- 1751 Vakhrameeva, P., Koutsodendris, A., Wulf, S., Portnyagin, M., Appelt, O., Ludwig, T., Trieloff, M., Pross, J., 2021. Land-sea correlations in the Eastern Mediterranean region over the past c. 800 kyr based on macro- and cryptotephtras from ODP Site 964 (Ionian Basin). *Quaternary Science Reviews*, 255, 106811.
- 1752 Vakhrameeva, P., Wulf, S., Koutsodendris, A., Tjallingii, R., Fletcher, W.J., Appelt, O., Ludwig, T., Knipping, M., Trieloff, M., Pross, J., 2019. Eastern Mediterranean volcanism during Marine isotope stages 9 to 7e (335-235 ka): Insights based on cryptotephra layers at Tenaghi Philippon, Greece. *Journal of Volcanology and Geothermal Research*, 380, 31-47.
- 1753 Villa, P., Soriano, S., Grün, R., Marra, F., Nomade, S., Pereira, A., Boschian, G., Pollarolo, L., Fang, F., Bahain, J.J., 2016. The Acheulian and early Middle Paleolithic in Central Italy: Stability and Innovation. *PLoS ONE* 11, e0160516. doi:10.1371/journal.pone.0160516.
- 1754 Wagner, B., Vogel, H., Francke, A., Friederich, T., Donders, T., Lacey, J.H., Leng, M.J., Regattieri, E., Sadori, L., Wilke, T., Zanchetta, G., Albrecht, C., Bertini, A., Combourieu-Nebout, N., Cvetkoska, A., Giaccio, B., Grazhdani, A., Haufler, T., Holtvoeth, J., Joannin, S., Lagoos, M., Leicher, N., Levkov, Z., Lindhorst, K., Masi, A., Melles, M., Mercuri, A.M., Nomade, S., Nowaczyk, N., Panagiotopoulos, K., Peyron, O., Reed, J.M., Sagnotti, L., Sinopoli, G., Stellbrink, B., Sulpizio, R., Timmermann, A., Tofilovska, S., Torri, P., Wagner-Cremer, F., Wonik, T., Zhang, X., 2019. Mediterranean winter rainfall in phase with African monsoons during the past 1.36 million years. *Nature*, 573, 256-260.
- 1755 Washington, H.S., 1906. The Roman comagmatic region. *Carnegie Institution of Washington, Publication* 57, 199 pp.
- 1756 Wastergård, S., 2002. Early to middle Holocene silicic tephra horizons from Katlavolcanic system, Iceland: new results from the Faroe Islands. *Journal of Quaternary Science*, 17:8, 723-730.
- 1757 Wulf, S., Keller, J., Paterne, M., Mingram, J., Lauterbach, S., Opitz, S., Sottili, G., Giaccio, B., Albert, P.G., Satow, C., Tomlinson, E.L., Viccaro, M., Brauer, A., 2012. The 100-133 ka record of Italian explosive volcanism and revised tephrochronology of Lago Grande di Monticchio. *Quaternary Sciences Reviews*, 58, 104-123.
- 1758 Wulf, S., Keller, J., Satow, C., Gertisser, R., Kraml, M., Grant, K.M., Appelt, O., Vakhrameeva, P., Koutsodendris, A., Hardiman, M., Schulz, H., Pross, J., 2020. Advancing Santorini's tephrostratigraphy: New glass geochemical data and improved marine-terrestrial tephra correlations for the past ~360 kyrs. *Earth-Science Reviews*, 200, 102964.
- 1759 Wulf, S., Kraml, M., Keller, J., 2008. Towards a detailed tephrostratigraphy in the Central Mediterranean: The last 20,000 yrs record of Lago Grande di Monticchio. *Journal of Volcanology and Geothermal Research*, 177, 118-132.
- 1760 Wulf, S., Kraml, M., Brauer, A., Keller, J., Negendank, J.F.W., 2004. Tephrochronology of the 100 ka lacustrine sediment record of Lago Grande di Monticchio (Southern Italy). *Quaternary International*, 122, 7-30.
- 1761 Zanchetta, G., Giaccio, B., Bini, M., Sarti, L., 2018. Tephrostratigraphy of Grotta del Cavallo, Southern Italy: insights of the chronology of Middle to Upper Paleolithic transition in the Mediterranean. *Quaternary Science Reviews*, 182, 65-77.
- 1762
- 1763
- 1764
- 1765
- 1766
- 1767
- 1768
- 1769
- 1770
- 1771
- 1772
- 1773
- 1774
- 1775
- 1776
- 1777
- 1778
- 1779
- 1780
- 1781
- 1782
- 1783
- 1784
- 1785
- 1786